VLÁKNA a TEXTIL

FIBRES AND TEXTILES

STU FCHPT

TECHNICAL UNIVERSITY OF LIBEREC
Faculty of Textile Engineering

Trenčianska univerzita Alexandra Dubčeka v Trenčíne
Fakulta priemyselných technológií v Púchove

VÚCHV

VÚTCH CHEMITEX

Spoločnosť priemyselnej chémie ZSVTS

CHEMOSVIT FIBROCHEM

1

Volume 26.
March
2019

Indexed in:
SCOPUS
Chemical Abstracts
World Textiles

ISSN 1335-0617
print version

ISSN 2585-8890
online version

Fibres and Textiles
Vlákna a textil

Published by | *Vydáva*

- Slovak University of Technology in Bratislava, Faculty of Chemical and Food Technology
- Technical University of Liberec, Faculty of Textile Engineering
- Alexander Dubček University of Trenčín, Faculty of Industrial Technologies
- Slovak Society of Industrial Chemistry, Bratislava
- Research Institute of Man-Made Fibres, JSC, Svit
- VÚTCH – CHEMITEX, Ltd., Žilina
- Chemosvit Fibrochem, JSC, Svit

- Slovenská technická univerzita v Bratislave, Fakulta chemickej a potravinárskej technológie
- Technická univerzita v Liberci, Fakulta textilní
- Trenčianska univerzita Alexandra Dubčeka v Trenčíne, Fakulta priemyselných technológií
- Slovenská spoločnosť priemyselnej chémie, Bratislava
- Výskumný ústav chemických vlákien, a.s. Svit
- VÚTCH – CHEMITEX, spol. s r.o., Žilina
- Chemosvit Fibrochem, a.s., Svit

Editor in chief *(Šéfredaktor)*: Anna Ujhelyiová

Executive editor *(Výkonný redaktor)*: Marcela Hricová

http://www.vat.ft.tul.cz

Editorial office and distribution of the journal
(Redakcia a distribúcia časopisu)

Ústav prírodných a syntetických polymérov
Fakulta chemickej a potravinárskej technológie
Slovenská technická univerzita v Bratislave
Radlinského 9, 812 37 Bratislava, SK
Tel: 00 421 2 59 325 575
e-mail: marcela.hricova@stuba.sk

Order and advertisement of the journal
(Objednávka a inzercia časopisu)

Slovenská spoločnosť priemyselnej chémie,
člen Zväzu vedecko-technických spoločností
Radlinského 9, 812 37 Bratislava, SK
Tel: 00 421 2 59 325 575
e-mail: marcela.hricova@stuba.sk

Order of the journal from abroad – excepting Czech Republic
Objednávka časopisu zo zahraničia – okrem Českej Republiky

SLOVART G.T.G, s.r.o. EXPORT-IMPORT
Krupinská 4, P.O.Box 152, 852 99 Bratislava, SK
Tel: 00421 2 839 471-3, Fax: 00421 2 839 485
e-mail: info@slovart-gtg.sk

Typeset and printing *(Sadzba a tlač)*

FOART, s.r.o., Bratislava

Journal is published 4x per year
Subscription 60 EUR

Časopis vychádza 4x ročne
Ročné predplatné 60 EUR

Evidenčné číslo MKCR SR Bratislava EV 4006/10

PARTNERS / SPONSORS

We greatly appreciate Technical University of Liberec for education of students in the field of textile. Without next generation textile experts we can not keep working and would be not able to develop new products.

with thanks

Caledon textile

Fibres and Textiles (1) 2019
Vlákna a textil (1) 2019
March 2019

Special issue venue the 22nd International Conference STRUTEX 2018
"Structure and Structural Mechanics of Textiles"
held on December 5.- 7. 2018 in Liberec, Czech Republic

Content

Předložená publikace je souhrnem odborných prací předních textilních odborníků z celého světa, Fakulty textilní a také studentů doktorských studijních programů na Fakultě textilní Technické univerzity v Liberci.
Práce jsou tematicky rozděleny do dvou kapitol dle sekcí konference. Kapitola první obsahuje práce k tématu Struktura a strukturní mechanika textilií. Kapitola druhá se týká inovací a aplikací textilního výzkumu.
Všechny příspěvky byly vybrány odbornou komisí, která zajistila jejich vysokou odbornou úroveň.

prof. Ing. Bohuslav Neckář, DrSc.

Príspevky boli prijaté do tlače bez recenzie. Za odbornú a jazykovú úroveň príspevkov zodpovedajú autori a prekladatelia.
Contributions were received without review process. The authors are responsible for professional and language level of contributions.

FORMATION OF THE TEXTILE STRUCTURES FOR A SPECIFIED PURPOSE

Marcin Barburski

Lodz University of Technology, Faculty of Material Technologies and Textile Design, Institute of Architecture of Textile, 116 Zeromskiego Street, 90-924 Lodz, Poland
marcin.barburski@p.lodz.pl

Abstract: *Woven fabrics are the most common example of flat textile materials used in the manufacturing of clothing, decorative, technical, and special purpose products. Increasing expectations regarding the variety of fabric uses have prompted researchers to seek the optimal applied properties of fabrics as well as their internal structure. Woven fabric as a complex textile product, with advantages and disadvantages of the fibres and yarns on one side as well as of the way of manufacturing and finishing on the other, is an interesting, however not thoroughly acquainted, study case. The article presents the possibility of modelling mechanical properties of a dedicated woven product, shaping the bending stiffness of technical woven structures intended for pipe conveyor belts, structures as sound-absorbing barriers and multi-axis woven structures used to reinforce composites. These are a few examples of developed, dedicated woven structures of specific purpose.*

Keywords: *Textile structures, pipe conveyor belts, sound-absorbing barriers, multi-axis woven structures.*

1 INTRODUCTION

Woven fabrics are the most common example of flat textile materials used in the manufacturing of clothing and decorative, technical and special purposes products. Increasing expectations of the variety of fabrics' uses incline to the search of optimal applied properties of fabrics and, following, their internal structure. Woven fabric as a complex textile product consisting of advantages and disadvantages of fibres and yarns on one side, as well as of the way of manufacturing and finishing on the other one, is an interesting, however not thoroughly acquainted, study case.

Parameters of fabric structure are used for its identification, that is, to characterize it so that it can be accurately and precisely reproduced at any time. The more accurate the characteristics of structural parameters of the reference fabric, the more fabric being reproduced is similar to the original. In addition, almost all fabric properties can be shaped as functions of many factors.

In the case of textile design, the endeavour is to make the finished product as similar as possible to the designed one. The designer must be careful in choice of parameters of the fibre, yarn and fabric structure so that the functional properties of the finished product are consistent with the earlier assumptions.

The construction of models of textile products aims at setting the basis for discussion on mechanical and applied properties of these products as well as providing the technologists with the information on the extreme parameters of the products possible to manufacturing from certain materials and on machines available.

2 MODELING OF THE FABRICS

Large number of solutions when it comes to construction of fabrics differing in the raw material used, thickness, structure and filing, weave and finishing, makes it difficult to empirically find the dependence between the product structure parameters and the mechanical properties of its finished form. There are many parameters of the fabric structure, which the designer should choose optimally when modelling the characteristics of the product. This is core for giving fabrics the basic functions that a product should achieve for given needs. Thorough knowledge of rule and structural and utilitarian relations in fabrics is the basis needed in their conscious analysis. For many years, scientists have been introducing mechanical and geometric models for structural analysis of fabrics to characterize their internal geometry.

The textile structure changes under small deforming strengths. There are two consequences of these changes: the first is a significant difference in the barrier of deformed products, and the second – a difference in mechanical properties such as resistance and stiffness.

When considering the properties of fabrics, certain models of their construction can be used [1, 2]. There are two basic types of these models:

- mechanical models (e.g. according to Olofsson, Nosek), based on the analysis of the conditions of fabric creation and the properties of its threads,
- geometrical models (e.g. Peirce, Kemp), not concentrating on tension of threads, or not taking into account the external forces, but, relatively, most precisely reflecting the actual structure of the fabric.

In the literature on the fabric structure various descriptions are always based on simplified models.

Peirce’s geometric model is widely used to describe the structure of fabrics. However, structural changes of fabrics during stretching are characterized using Painter’s nomogram.

In order to specify and more accurately describe the structure of fabric subjected to static load, it seems important to look for new methods in this field of research so that they could describe the fabric architecture as precisely as possible, with the possibility of predicting its mechanical properties.

There are many parameters of the fabric structure that the designer should choose optimally when modelling the product features. This is the basis in providing fabrics with the most important functions needed during the use of the finished product. Thorough knowledge of laws and relations between structural and utilitarian features of fabrics makes up the basis for conscious analysis of many aspects of fabrics. This knowledge also serves as an indispensable tool for fabric design.

Experimental and scientific research, as well as fabrics modelling enables determining the principles of changes in the fabric structure subjected to static forces. By modelling changes in the fabric structure subjected to static forces with the use of new modified nomograms, it is possible to more accurately describe the structure of real fabrics subjected to static strengths, eliminating generalizations of analysis while using Painter's nomogram [9].

All real fabrics can be specified by the deformation of circular cross section of warp and weft threads. The scale of the deformation depends on the kind of thread, material used, the way of weaving, the weave, the weaving strengths and the susceptibility of thread to cross deformation. The shape of cross section of threads in fabric can only be approached by different plane geometric figures, such as: a circle (Peirce) [3-6], an ellipse, a hippodrome shape (Kemp) [3], a convex lens (Milasius) [7]. The shape of cross -section in real fabrics is diverse, which is the result of pressing and bending strengths effecting in the areas of contact of crossing warp and weft threads.

Fabric modelling using Painter’s nomogram was compared with three new nomograms created as a result of research carried out at the Institute of Textile Architecture, Lodz University of Technology [8]. The experiment showed that depending on the designer's approach and expectations, various forms of the internal structure of fabrics may be created. In addition, changes in the internal geometry of the fabric, subjected to static loads, can also be modelled in a different way. Thus, using these nomograms, each designer has the opportunity to achieve whatever they expect as far as the fabric structure is concerned.

Taking the elliptical cross-section of the yarn into account, it is possible to more accurately model the internal structure of fabrics and go through different stages of their changes when subjected to deforming strengths.

3 CONVEYOR BELTS DESIGN

The knowledge about structure and modelling of woven fabrics was used to shape technical woven products intended for pipe conveyor belts. Conveyor belts are designed for the technological transport of all kinds of bulk materials and damp which do not cause permanent adherence to the belt and conveyor construction elements. These conveyors are applicable wherever it is necessary to quickly and accurately transport materials on the distance specified by the range of one or more coupled conveyors.

The textile conveyor belt is made of fabric-rubber carcass and rubber covers. The carcass may consist of 2 to 6 spacers made of synthetic polyamide-polyester fabrics impregnated with a solution of latex which provides an intermediate layer preventing from delamination of fabric and rubber. Conveyor belt at the point of contact with the drive and reverse drums is flat. Pipe conveyor belt is closed in the work field or return and maintained by a set of four or six rollers on its circuit.

The main problem occurs when the conveyor closes, as previous construction of the pipe conveyor system makes the edges collapse inwards and the conveyor spin, causing unsealing of the belt, which may result in a loss of material transported. In addition, the unsealing causes that the material transported is not sufficiently protected against weather conditions such as rain and wind.

One of the most important elements before designing a new product is to identify and clarify the purpose of the textile product as well as to determine the problem to solve. Precise determination of the characteristics to be fulfilled by a textile product determines the properties of the product through the refinement of the structure of the product.

Formation of bending stiffness of technical woven structures differing in weave and internal geometry allowed designing the innovative pipe conveyor belt that is able to close while eliminating the tendency of collapsing its edges inward and minimizing the stresses generated in the structure during the return of the conveyor belt. Based on the first test summaries, it was stated that depending on the weave, belts differently press against the rollers, have different stiffness and that the layer of rubber did not largely eliminate the differences in fabric properties [9-11].

The preliminary research opened the way for further research on the optimization of the production process of conveyor belts so that the mechanical properties of the fabric as reinforcement could be used in a controlled manner and as far as possible. The action was taken to optimize bending stiffness of fabric used in pipe conveyor belt.

The analysis of measurement results enabled designing a new woven structure, symmetric to its longitudinal axis but different in bending stiffness on its width. These differences were possible by using three different weaves paired with each other on the fabric width (Table 1).

In order to verify the validity of the application of the selected three weaves, a new woven structure was produced and then covered with latex and vulcanized (Figure 1). The measurements were done of structure parameters of the new fabric, as well as of mechanical properties of the belt and its pressure on the set of rollers [9, 10].

Table 1 Weaves applied in a new woven structure [10]

Satin weave	Back weft weave	Warp rep weave
$\frac{1}{7}(3)$	On the basis of twill weaves 1/3 and 3/1	$\frac{1}{1}(0,0,0,1,0,0,0)$
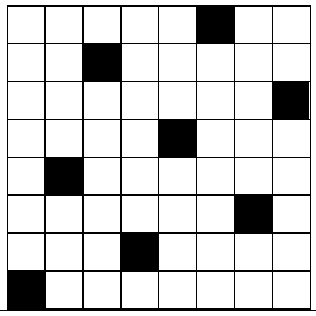	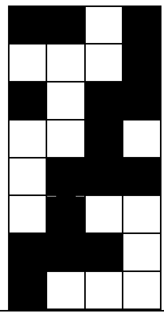	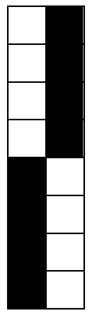

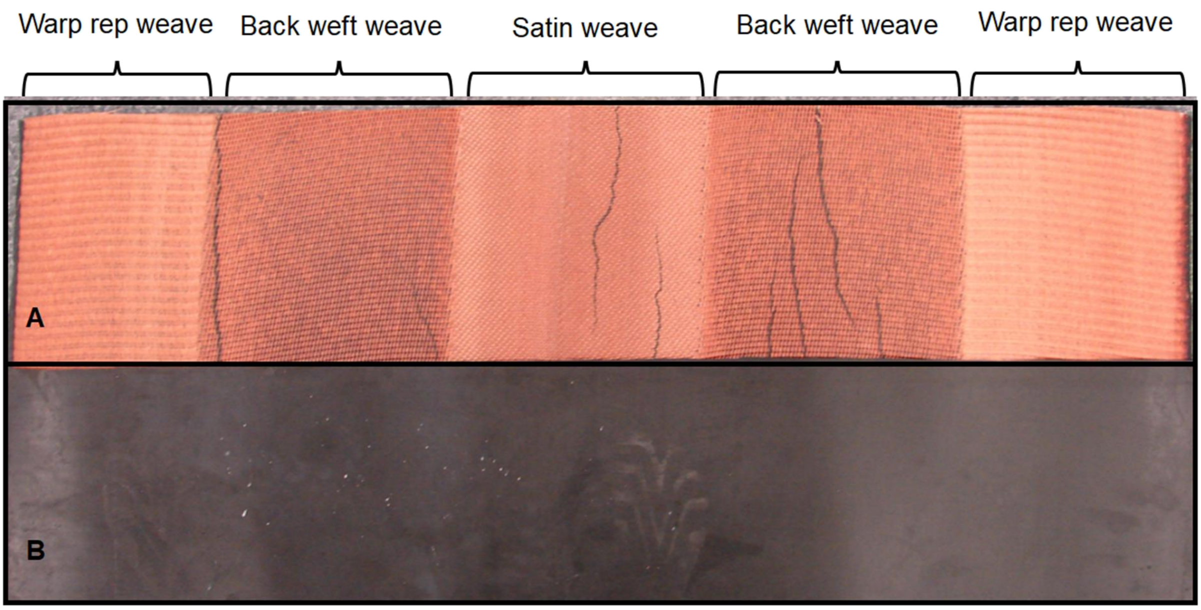

Figure 1 New woven structure with zones of different weaves symmetrically arranged along the longitudinal axis of the belt. A) covered with latex, B) vulcanized [10]

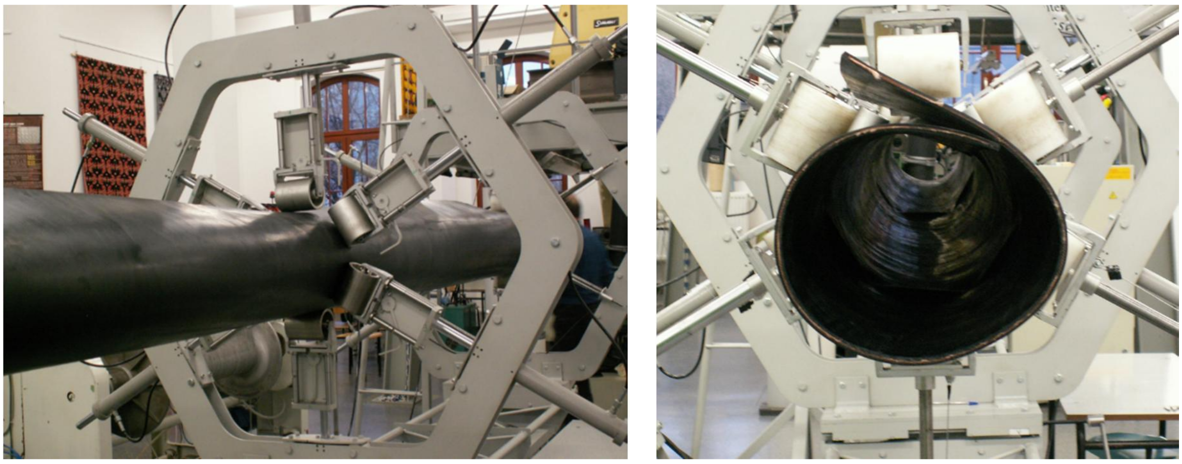

Figure 2 Pipe conveyor belt with the new fabric carcass of different weaves [10]

In line with the project assumptions the fabrics were made as reinforcement of one-spacer conveyor belts. The conveyor belt was made with the possibility of piping and closing but without a tendency of its edges to collapse inward (Figure 2). The construction of the belt made it possible to minimize the stresses generated in the structure at the stage of the belt return eliminating multiple layers of spacers and gaining high transverse flexibility. One-spacer belt has minimized thickness, which reduces its weight, which in turn minimizes the resistance movement during rewinding the belt through the drums [12].

This original solution puts a step forward in the conveyor belt industry. The new woven structure will also better protect the carried material from weather conditions such as rain and wind. Implementation of the project allowed the introduction of innovative solutions for the production of conveyor belts produced, inter alia, in the FTT Wolbrom SA.

4 THE TEXTILE SOUND ABSORPTION BARRIERS

Other dedicated textile structures may be used as acoustic absorption barriers. The problem of noise is one of the fundamental issues that have a very significant impact on the comfort and safety of people [13]. Currently, noise is a common occurrence in the human environment. It is presented in all types of human environment and has adverse effects on human health, including hindering rest and regeneration. It reduces the efficiency of human work and also increases the likelihood of accidents at work. Long-term exposure to noise on the human body is also accompanied by deterioration of hearing or, in extreme cases, total deafness [14].

Fibrous materials have been widely used in noise reduction due to their porous structures [15]. Researchers are still developing new materials that can absorb sound energy. They comprise experimental studies on acoustic properties improvements of rigid polyurethane closed-cell foams, by incorporating various quantities of textile wastes into the matrix [16]. Various fibrous materials including inorganic and metallic fibres, synthetic fibres, natural fibres, and nanofibrous membranes for noise reduction are reviewed. The tailored cross-sections of synthetic fibres such as circle, hollow and triangle are beneficial to improve acoustic absorption properties. The use of material wastes, coming from the fibres of fluffs, when manufacturing the sound absorber products, can help to combat two different kinds of problems: the disposal of this kind of waste and the noise control [17].

The main aim of research work was to present the acoustic transmission losses of 10 different structures of woven fabrics and to investigate the influence of weaving on the acoustic attenuation of the fabrics under the presented tests. The patterns of weaves and their structures influence mechanical properties. The internal structures give different effects, for example of abrasion resistance and air permeability, deformability and complex shape forming including shearing properties. It is interesting how the structures of fabrics influence acoustic attenuation.

10 specimens of 150 x 150 cm fabrics of different structures and patterns were used for the study. The raw material for the weaving was the textured Polyester 167 dtex x 2 as the warp material. In eight samples, as the weft, the acrylic yarn 64 tex was used. Cotton and Trevira weft of similar linear density were used in other samples. The fabrics were made on the Picanol Gamma loom with Jacquard machine in the Institute of Architecture of Textiles, Lodz University of Technology. The textiles were especially prepared to specific purposes as acoustic absorption barrier. All fabrics were made on the same loom with constant

densities 30 warp/cm but the internal stresses changed it during 24-hour relaxations. The individual fabrics were subjected to sound absorption tests in the aeroacoustic anechoic chamber in the Laboratory of Aeroacoustics of the Institute of Turbomachinery (Lodz University of Technology) to achieve free-field anechoic environment.

As it was expected, all tested fabrics have low sound absorbing properties at low frequencies. The presented studies also showed that all fabrics with honeycomb weaves have much less attenuation than other fabrics. Low attenuation of these fabrics is likely due to their similarity to fabrics with lower number of threads per centimeter, resulting in less dense structures at higher thicknesses. Other woven fabrics are more compact and much thinner, which results in good sound absorbing properties. The research proved that the best absorbing properties were in the cases of satin, double cloth and back weft weaves. At higher frequencies thickness also had an insignificant effect on sound absorption. It can then be concluded that if there is air space inside and behind a fabric, sound absorption possibilities move through the frequency range. Similar results were obtained by other researchers using different testing method (inside a reverberation room) for cases of coated and uncoated textiles [18].

The proposed honeycomb fabrics can be used in combination with other acoustic adaptations, such as partially blocking and transmitting the sound to a deeper sound damping installations that, due to different reasons, must be otherwise hidden. They can also be used, for example, as covers for voice or loudspeakers systems. The honeycomb fabrics could protect the loudspeaker against the wind or other severe weather conditions without negatively affecting the good quality of the sound. In such cases, modern printing techniques allow creating interesting artistic decorative motifs, for example in concert halls, where acoustic performance is critical, and fabric's job is not only to absorb sound itself, but also to allow other acoustic sound adaptations behind the fabric to absorb sound in more predictive manner. In such cases the main task of a fabric is not to hinder or reflect the sound but to control the hall or room environment and act as additional finishing protective layer. The presented results can also be useful for interior designers and architects as the experiments were performed for the first time on such materials and compared to standard fabrics [19].

5 TEXTILE REINFORCEMENT COMPOSITE

The search for new materials of better properties than those traditionally used in techniques (metal alloys, wood, construction ceramics, etc.) resulted in creating the group of materials referred to as composites. Today, technological progress is inseparable from material engineering which deals with the creation of new materials. Engineers constructing innovative materials base on designing conditioned by the operating conditions and loads they will be subjected. Composite materials can meet these demands. Composites are now a rapidly expanding field linking issues of textiles, metallurgy, mechanics and polymer chemistry as well as plastics processing [20, 21].

The main components of the construction composite are matrix and reinforcement. The matrix is more or less homogeneous material filling the space between the reinforcing elements. The matrix volume fraction *Vm* is usually 20-80%. The reinforcement can be a different material arranged to increase the strength and stiffness of the composite. Due to the properties of textiles, they are the most common type of reinforcement in the composites. They may be woven, braided or knitted fabrics, non-wovens or parallel-arranged fibres. The composite resulting from wearing several layers of fabric in a "pile" is not suitable for any application because of its deformability, even under its own weight and the lack of permanent connection of layers. Both of these effects are eliminated in the second stage of producing the composite - lamination step i.e. creating a permanent connection of layers in the stiff construction element. The process involves hardening a sequence of layers arranged complying with the appropriate parameters of temperature, pressure and holding time.

In connection with the development of flat textile structures and the expansion of the area of their applications there is a need to assess the isotropy of their mechanical properties. Classical orthogonally built fabrics (weft threads arranged perpendicular to the warp threads) and less those of the orthogonal structure are one of the types of the sandwich composites reinforcement. They are characterized by isotropic properties only in the directions designated by the systems of threads which may be the same when the threads of both systems have the same mechanical parameters.

In order to provide the layered composite materials with suitable isotropic properties, the fabrics being next layers of the reinforcement are placed at different angles to the main axis of the composite. The number of layers and their layout angles are a result of mechanical requirements for composite construction. In the aeronautics the composites of carbon fibre reinforcement have on average six times higher tensile strength and three times higher modulus of elasticity than steel although they have four times lower weight.

When human safety conditions are not needed to be ensured, glass, aramid or natural fibres are often used as the reinforcement. One of the natural fibres are flax fibres that have mechanical properties similar to glass fibres and significantly better than iron and aluminium. The flax fibres show the new direction of work of the new quality and new product.

The challenge is to create such composite of natural fibres which would compete with composites of glass reinforcement as well as aluminium and iron [22, 23].

During the research work at international cooperation with Politecnico di Milano and KU Leuven the research focused on analysing the flax fabric used as a reinforcement of the composite. The fabric was subjected to biaxial tensile, bending and shearing in order to determine formability and mechanical properties of the product. The second part of the experiment focused on the analysis of flax fabric structure deformation at the tetrahedral form. During the formation of complex shaped composites the important parameter characterising the textile product is its drape. Among other things, this parameter determines the mechanical properties of the finished product.

The obtained results of the study are the complete set of data needed to characterize the deformation capacity of this flax product during the formation of the complex shapes of the finished composite product. These results also provide a reference data for numerical modelling. On the basis of the analysis it was found that this type of flax fabric has good deformability at low shear angles when forming on complex moulds and has better quality in this respect than other fabrics used as reinforcement of composites [24, 25].

This is mainly textile isotropy that, together with raw material and finish, decides of the textile product capabilities, hence the necessity for its insightful analysis. Finished products have mostly dimensional structure, which results in that the internal structure of the woven product is not homogeneous. These changes can result in differences in the mechanical, performance and filtration properties and in the finished product manufacturing processes.

Properties of the individual components are different from the properties of the composite but significantly influence it; hence the need for analysis of the composites components.

Traditional textiles are characterized by, depending on their structure, different degrees of anisotropy of physical and mechanical properties. Meanwhile, the new, non-classical applications of textiles not only require materials with high strength, but also of higher and higher isotropy of its properties. The alternative to classical fabrics having large anisotropy are the multiaxial fabrics. The Institute of Textile Architecture, Lodz University of Technology for many years conducted research on innovative multiaxial woven structures under the guidance of prof. Marek Snycerski. Among other things, globally innovative technologies producing 3, 4, 5 and even 6-axis textiles were developed [26-29].

Multiaxial woven structure is the name of the flat textile product, formed from at least three sets of threads connected by interlaces. Design of such structure is the formation of a grid where the nodes represent intersections of no more than two threads, and then the introduction of interlaces. The grid only shows the mutual layout of the threads (geometry), presenting them in as straight lines with directions consistent with the directions of the axis structure.

Triaxial fabrics have long been known and described in the literature [30-35]. There is significantly less information published about fouraxial fabrics and it mainly relates to methods of their production [36-40].

The main criterion used to classify the multiaxial structures is the number of thread sets (axes), another is the type of grid and the manner of thread interlacing, i.e. the weave. Theoretically, it is possible to create many types of such fabrics weaves. Multiaxial fabric structures can actually be oriented to any thread sets. Due to the shed method of producing classical fabrics, it was agreed that multiaxial fabrics will be oriented to the set which can stand for weft (threads arranged horizontally).

Fouraxial fabrics can be created from three warp sets and one weft set. Spans arise between the threads of these sets. Their shape and regularity depend on the weave and the values of thread scales. The sixaxial fabrics are formed by six sets of threads: five warp and one weft [Figure 3]. Their grids can be modelled by combining respectively mutually rotated classical fabrics [26]. The sixaxial fabric of plain weave was formed in the Institute of Textile Architecture. The fabric has large spans and the largest of them take the dodecagon shape. Structurally the fabric belongs to the group of heterogeneous scale.

An alternative to the parallel-arranged fibres or classical fabrics are multiaxial fabrics of increased isotropy.

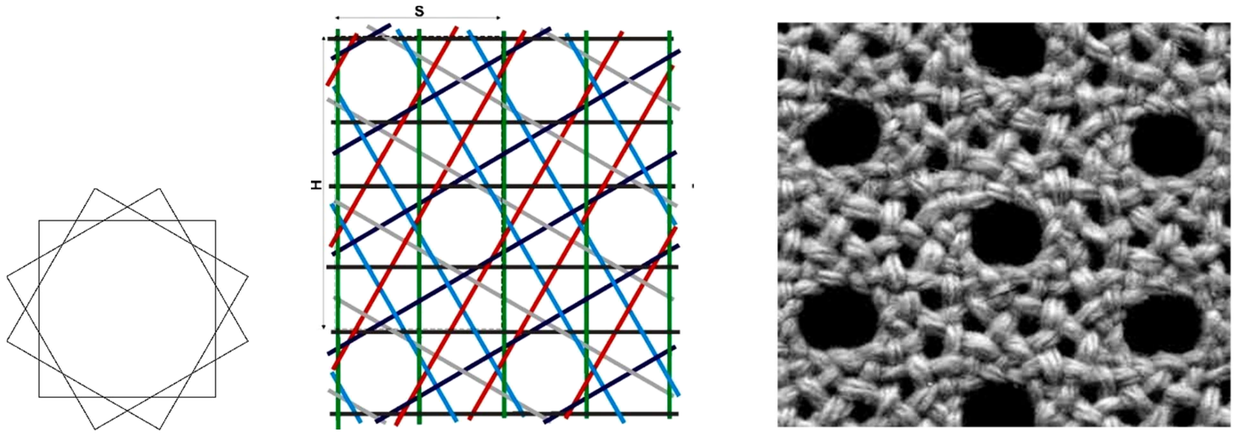

Figure 3 Base for modelling sixaxial grid, report of sixaxial fabric of plain weave and heterogeneous grid, picture of the sixaxial fabric sample [31]

6 SUMMARY

This article presents selected issues regarding designing and formation of woven structures for a specified purpose. Scientific research is focused on formation new woven structures of complex, modified, multi-axial, and spatial, for a specified purpose, which can be used, among others, as textile reinforcements of various composites or acoustic barriers. A wide spectrum of technical application possibilities of textile products has been presented. The manuscript indicates the need for further actions regarding new applications of textile products not yet fully recognized.

7 REFERENCES

1. Masajtis J.: Structural analysis of fabrics, Lodz 1999, (in Polisch)
2. Janusz T.: Weaving, part. III, Warsaw 1963, (in Polisch)
3. Peirce F.T.: 5 - The geometry of cloth structure, Journal Textiles Institute Transaction 28(3), 1937, pp. T45-T96, https://doi.org/10.1080/19447023708658809
4. Szosland J.: Laboratory of the fabric construction and technology, Lodz 1984, (in Polisch)
5. Szosland J.: Basics of fabric construction and technology, Warsaw, 1991, (in Polish)
6. Frontczak-Wasiak I.: Laboratory of the basics of mechanical fiber technology - weaving, Lodz, 1987, (in Polish)
7. Milašius V.: Woven fabric's cross-section: problems, theory, and experimental data, Fibres and Textiles in Eastern Europe 4(23), 1998, pp. 48-50
8. Barburski M., Masajtis J.: Modelling of the change of structure of woven fabric under mechanical loading, Fibres and Textiles Easter Europe 1(72), 2009, pp. 39-45
9. Barburski M.: Analysis of the mechanical properties of conveyor belts on the three main stages of production, Journal of Industrial Textiles 45(6), 2016, pp. 1322-1334, https://doi.org/10.1177/1528083714559567
10. Barburski M.: Analysis of the pipe conveyor belt pressure on the rollers on its circuit, Journal of Industrial Textiles 45(6), 2016, pp. 1619-1634, https://doi.org/10.1177/1528083714567242
11. Barburski M., Goralczyk M., Snycerski M.: Analysis of Changes in the internal structure of PA6.6/PET fabrics of different weave patterns under heat treatment, Fibres and Textiles Easter Europe 23(4), 2015, pp. 46-51, DOI: 10.5604/12303666.1152722
12. P.404943 Barburski M. Snycerski M.: The method for producing the reinforcing fabrics, particular carcass in pipe conveyors belt and reinforcement fabric, particular carcass in the pipe conveyor belt UPRP 2013-08-01
13. EU Commission: Directive 2002/49/EC of the European Parliament and of the Council of 25 June 2002 relating to the assessment and management of environmental noise
14. WHO, 2011: Burden of disease from environmental noise. The WHO European Centre for Environment and Health, Bonn
15. Tang X., Yan X.: Acoustic energy absorption properties of fibrous materials: a review, Composites Part A: Applied Science and Manufacturing Vol. 101, 2017, pp. 360-380, DOI: 10.1016/j.compositesa.2017.07.002
16. Tiuc A., Vermeşan H., Gabor T., Vasile O.: Improved sound absorption properties of polyurethane foam mixed with textile waste, Energy Procedia 85, 2016, pp. 559-565, https://doi.org/10.1016/j.egypro.2015.12.245
17. Maderuelo-Sanz R., Nadal-Gisbert A.V., Crespo-Amorós J. E., Parres-García F.: A novel sound absorber with recycled fibers coming from end of life tires (ELTs), Applied Acoustics 73(4), 2012, pp. 402-408, https://doi.org/10.1016/j.apacoust.2011.12.001
18. Memon H., Wang N, Zhu C.: Study on sound insulation properties of different coated woven fabrics, Journal of Fiber Bioengineering and Informatics 8(4), 2015, pp. 645-656, DOI: 10.3993/jfbim00170
19. Barburski M, Blaszczak J.R., Pawliczak Z.: Influence of designs of weaves on acoustic attenuation of fabrics, Journal of Industrial Textiles, 2018, DOI: 10.1177/1528083718769945

20. German J.: Introduction of basic information about materials, Kraków 2005, passim
21. Oczoś K.E.: Fiber composites - properties, application, machining; Mechanic - Monthly of Scientific and technical 7, 2008, pp. 1-9
22. Wang Wei, Huang Gu: Characterisation and utilization of natural coconut fibers composites, Materials and Design 30(7), 2009, pp. 2741-2744, https://doi.org/10.1016/j.matdes.2008.11.002
23. Boisse P., Buet K., Gasser A. Launay J.: Meso/macro-mechanical behaviour of textile reinforcements for thin composites, Composites Science and Technology 61(3), 2001, pp. 395-401, https://doi.org/10.1016/S0266-3538(00)00096-8
24. Vanleeuw B, Carvelli V, Lomov S.V, Barburski M, Vuure A.W.: Deformability of a flax reinforcement for composite materials, Key Engineering Materials 611-612, 2014, pp. 257-264; Trans Tech Publications, Switzerland, https://doi.org/10.4028/www.scientific.net/KEM.611-612.257
25. Vanleeuw B., Carvelli V., Barburski M., Lomov S.V., Aart W. van Vuure: Quasi-unidirectional flax composite reinforcement: deformability and complex shape forming, Composites Science and Technology 110, 2015, s. 76-86, http://dx.doi.org/10.1016/j.compscitech.2015.01.024
26. Balcerzak M., Frontczak-Wasiak I., Snycerski M.: Four-axis fabric without clearances, The patent application P-392601 from 07.10.2010; Owner: Technical University of Lodz 07.10.2010
27. Snycerski M., Cybulska M, Frontczak-Wasiak I., Suszek H.: Patent PL Six axis fabric (in print), the application P-383907 from 07.08.2007; Owner: Technical University of Lodz
28. Frontczak-Wasiak I., Snycerski M., Stempień Z., Suszek H.: Patent No. 209689, Method and device for evaluating the isotropy of the mechanical properties of flat textile Owner: Technical University of Lodz
29. Frontczak-Wasiak I, Snycerski M.: Characteristics of multi-axial woven structures, Fibres & Textiles in Eastern Europe 13(4), 2005, pp. 27-33
30. Cybulska M., Frontczak-Wasiak I.: Modeling and properties of multiaxial woven structures, 2nd Autex Conference, Ghent, Belgium, 2002
31. Dow N.F., Tranfield G.: Preliminary investigations of feasibility of weaving triaxial fabrics (doweave), Textile Research Journal 40(11), 1970, pp. 986-998, https://doi.org/10.1177/004051757004001106
32. Schwartz P., Fornes R., Mohamed M.: An analysis of the mechanical behavior of triaxial fabrics and the equivalency of conventional fabrics, Textile Research Journal 52(6), 1982, pp. 388-394, https://doi.org/10.1177/004051758205200606
33. Schwartz P., Fornes R.E., Mohamed M.H.: Tensile properties of triaxially woven fabrics under biaxial loading, Journal of Engineering for Industry 102(4), 1980, pp. 327-332
34. Boisse P. Zouari B, Daniel J.L.: Importance of in-plane shear rigidity in finite element analyses of woven fabric composite performing, Composites Part A 37(12), 2006, pp. 2201-2212, DOI: 10.1016/j.compositesa.2005.09.018
35. Xue P. Cao J. Chen J.: Integrated micro/macro-mechanical model of woven fabric composites under large deformation, Composite Structures 70(1), 2005, pp. 69-80, https://doi.org/10.1016/j.compstruct.2004.08.013
36. Araujo M., Lima M. Costa N.: New weaving concept for multiaxial fabric, TECNITEX 2001, Technical Textilies: "Designing Textiles for Technical Applications", 1st Autex Conference, Minho, Portugal, 2001
37. Iliej M, Jais T., Czu W.: Termouprugij analiz triechaprwlennych tkanych kompozitow Tkanye konstrukcionnyje kompozity Izdatielstwo „MIR" 1991 g s.302-314, red. Czu T.W, Ko F.
38. Skelton J.: Triaxially Woven Fabrics: their structure and properties, Textile Research Journal 41(8), 1971, pp. 637-647, https://doi.org/10.1177/004051757104100801
39. Trost W.C., Le tissage triaxial: la machine TW 2000, Industrie Textile 1068, 1977, pp. 339-343; Chemiefasern/Textil-Industrie 5, 1977, pp. 444-446
40. Shigenobu I.: Multiaxial fabric with triaxial and quartaxial portions, pat. No 5,472,020, Dec. 5, 1995

VARIATION BRAIDING TECHNOLOGY BY THE EXAMPLE OF NOVEL STENT STRUCTURES

Marielies Becker[1], Frank Ficker[2] and Roxana Miksch[2]

[1]Fraunhofer Application Center for Textile Fiber Ceramics TFK, Kulmbacher Straße 76, 95213 Münchberg, Germany
[2]Institute for Material Sciences at Hof University, Kulmbacher Straße 76, 95213 Münchberg, Germany
marielies.becker@isc.fraunhofer.de, frank.ficker@hof-university.de, roxana.miksch@hof-university.de

Abstract: *Coronary stents are commercially available in many different types and are already successfully used. In case of a stenosis in a bifurcated coronary region, the otherwise usually uncomplicated and safe treatment still causes some problems [1]. In the introduced research project different tubular and bifurcated stent structures have been implemented, using a variation braiding machine, which enables the fully automatic production of complex, if required bifurcated braided structures. Additionally an implanting concept for bifurcated areas has been devised to enable a safe and quick interventional therapy.*

Keywords: *Braiding, stents, bifurcations, complex tubular structures, shape memory.*

1 INTRODUCTION

Technical textiles become more and more important in a wide range of medical applications. From well known simple bandaging, and surgical sewing materials to complex high technical textile structures, which are neccessary to construct functional artifical ligaments, tendons and cartilages [2, 3].

A material construction based on textile technique is especially suitable for products that require a high flexibility and at the same time a suitable amount of stability, such as needed for medical stents [4].

To re-open a morbid narrowed vessel, for a sufficient blood circulation, an interventional treatment is possible. In this case the vessel gets expanded and is additionally supported by an endoluminal vascular implant, a stent [5]. Coronary stents are commercially available in many different types and are already successfully used, but in case of a stenosis in a bifurcated coronary region, the otherwise usually uncomplicated and safe treatment still causes some problems [1].To enable tailor-made solutions, the novel variation braiding technolog has been used to develop new, innovative structures and bifurcations, which have the potential to improve the interventional results.

2 EXPERIMENTAL

2.1 Materials

Stents, especially for the coronary usage require a strong, but at the same time flexible and compressible material [6]. Nowadays there is a big variety of materials in use, from metal-alloys to bioresorbable polymers that dissolves after a certain time. In the here presented research project metal-alloys have been in the focus [7]. Platinum/chromium alloy is a quite new, but already very important material for coronary stents. Caused by its high amount of platinum it is very tough and enables a delicate, but still stable stent construction, which reduces the occurrence frequency of restenosis, but at the same time requires high pressure while implanting the material into the vessel [6].

To increase the material flexibility the super elastic nickel/titanium alloy, so called Nitinol, has been selected for the here introduced research project. Nitinol is a popular material for a big number of different stent systems from several manufacturers, especially because of its shape memorizing effect and its super-elastic properties, combined with a good biocompatibility [8, 9]. While most metallic alloys show a plastic deformation when compressed, Nitinol has the temperature-dependent ability to deform elastic and get back to its original shape, even after a significant deformation. This effect can be explained by different crystal structures in different temperature fields [9].

2.2 Methods

2.2.1 The variation braider

For the research activities a novel variation braiding machine has been used to develop various complex tubular structures. The braiding machine is constructed with 4x4 horn gears arranged in a square and a maximum of 32 carriers. To enable a high structural braiding flexibility the machine is equipped with 24 selectable pneumatic cross sections, 9 core yarn feeders and 16 filler yarn feeders. With this technical features a fully automated pattern change and even the production of a bifurcation is possible without an interruption of the braiding process.

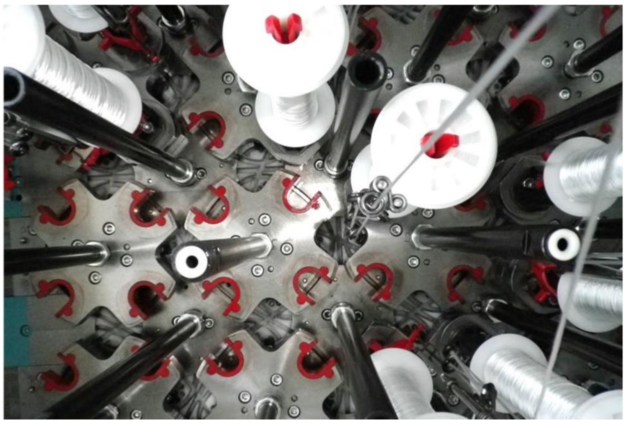

Figure 1 Variation braiding machine with selectable cross sections

2.2.2 Braiding of technical materials

The braiding of technical materials like metal or brittle fibers requires a couple of adjustments during the braiding process. The yarn feeding for example has to be as linear as possible to avoid material kinks and the carriers have to be overturned to eliminate material twists and so enable a uniform, intact braid.

By using metallic wires in the production, increased abrasion of the corresponding machine parts might accrue. To reduce this effect, all yarn feeding elements have to be sufficiently adapted.

Figure 2 Multi-branched braids

2.2.3 Pattern variations

The used braiding machine has diverse possibilities to create custom structures, which can vary in their pattern, density and overall structure. The technical possibilities enable the production of tubular-square- or flat braids, spiral braids, core/shell braids and combinations of all types. For stent structures different types of tubular braids and interlocking structures can be suitable.

By changing the design of the pattern cycle, carrier movement and the speed of the takedown-wheel, different material densities with varying supporting effects can be achieved. To make the technique even more multifarious, it is possible to bifurcate all types of braids and herby be able to create stent solutions for complex human vessel architectures.

3 RESULTS AND DISCUSSION

Based on the research of human anatomic tube structures and in collaboration with different surgeons, several concepts for customized self-expanding stents have been developed.

In a first step a number of braided tubular net structures have been designed. Caused by the different structures and densities, varying strong supportive effects have been achieved, which made it possible to reinforce different sectors in a disparate degree.

Enhancing these results, bifurcated structures as seen in Figure 3 have been realized to produce a pattern, which might be suitable for bifurcated vessels. A simple bifurcated braided tube usually shows a varying density and even holes in the transition area. These unwanted effects reduce the supportive force in the affected area and might increase the risk of a re-stenosis. To avoid this problem an adjusted pattern has been developed, which creates a homogeneous structure, even in the transition area.

Beside the customized construction of a bifurcated braid, the possible difficulties during the implantation of such a complex stent system have been investigated. The longer the intervention takes to re-open a stenosed vessel, the higher the risk for the patient gets. This made it necessary to think about a suitable and fast implantation technique.

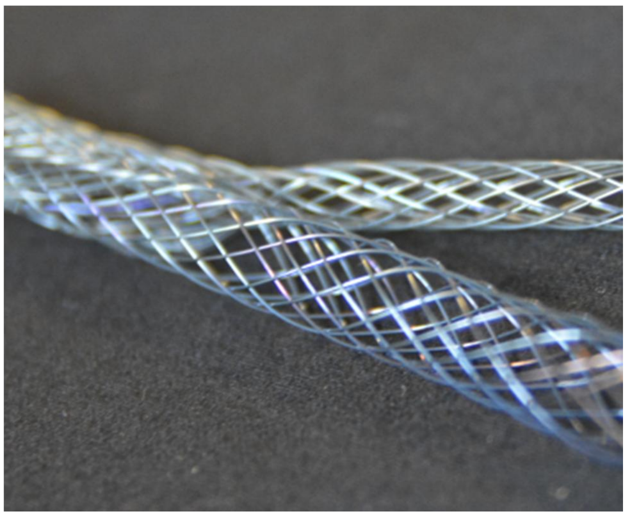

Figure 3 Example for a bifurcated braid

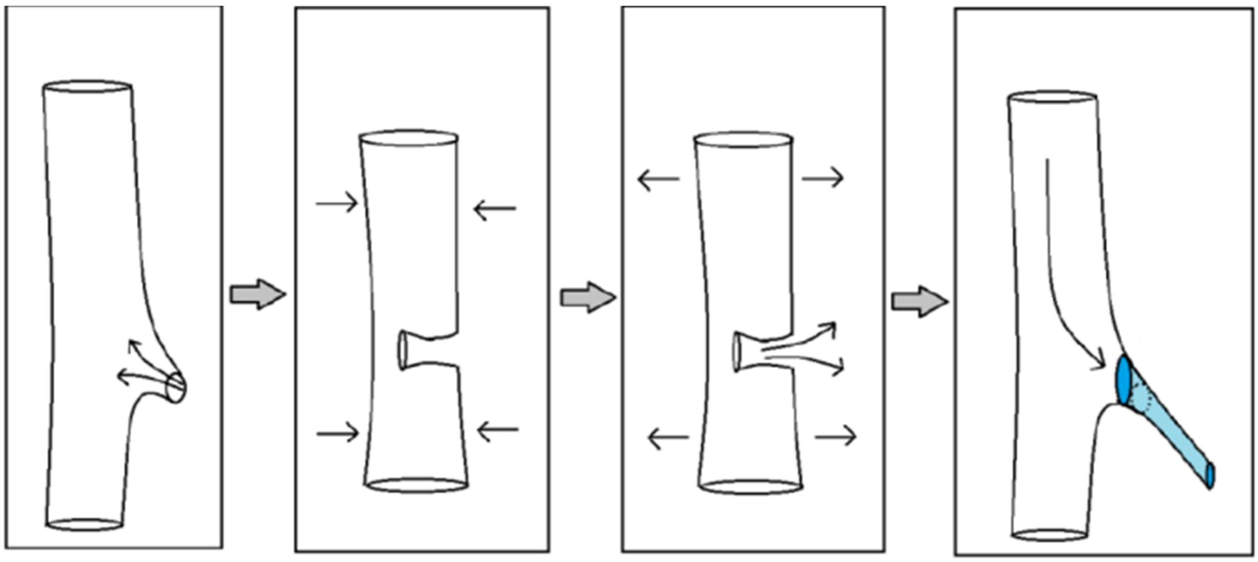

Figure 4 Concept for implantable bifurcated stent

Following these requirement a Y-shaped bifurcated stent structure with one long main stent and a short side stent has been constructed.

Before implanting the stent, the manufactured short side arm can be pulled into the main arm, similar to a bud. Following, the stent gets compressed and implanted into the stenosed area in the vessel. There the stent expands and re-opens the main vessel. Finally the pulled-in side arm gets inflated, to open and support the crossover to the side vessel. To support the side vessel a second simple tube stent gets implanted through the already opened transition area (see Figure 4). This technique might be an applicable solution for complex stenosis, but has still to be tested conscientiously.

4 CONCLUSIONS

Variation braiding technology is highly innovative when it comes to flexible tubular structures. It offers the technical possibilities to create various different bifurcated forms and is so suitable for the development of complex stent structures. In combination with the use of the super elastic nickel/titanium alloy Nitinol, customizable stent solutions have the potential to generate new features for complex anatomical circumstances and should be followed up in future development projects.

5 REFERENCES

1. Pause B.: Komplex interventions at coronary bifurcations in a bench model, Saarbrücken: Academy Publishing House, 2012 (in German)
2. Wintermantel E.: Medical Technology, Life Science Engineering 5., Springer Publishing House, 2009 (in German)
3. Chellamani J.: Medical textiles using Braiding Technology, Journal of Academia and Industrial Research (JAIR), 2013
4. Berglund T.: Interview and Memo, Oslo, 2016
5. Erdmann E.: Clinical Cardiology; Deseases of the heart, the neural circulatory and of vessels around the heart 8, Heidelberg: Springer Medicine Publishing House, 2011 (in German)
6. Erbel R.: Cardic Catheder-Manual, Diagnosis and Interventional Therapy, Cologne: German Medical Publishers, 2010 (in German)
7. Leibniz University Hannover, Bioresorbable Implantats, 2016, [Online], https://www.analytik.uni-hannover.de/forschung_implantate.html; (in German)
8. White R., Fogarty T.: Peripheral Endovascular Interventions, 2 Hrsg., New York: Springer Science + Business Media, 1996
9. Keller T.: Osseointegration of a Plasma-Immersions-Ions-Implantation treated Auto-compression-chamber made of Nitinol, Munich: Technical University Munich, 2004 (in German)

THE STRUCTURE OF ARCHAEOLOGICAL TEXTILES FROM THE EARLY AND HIGH MIDDLE AGES IN FINDS FROM THE CZECH REPUBLIC (PART 1)

Helena Březinová, Milena Bravermanová and Jana Bureš Víchová

Institute of Archaeology of the Czech Academy of Sciences, Prague, Czech Republic
www.arup.cas.cz, brezinova@arup.cas.cz, milena.bravermanova@seznam.cz, JVichova@seznam.cz

Abstract: *Textile production has deep roots in the past, and knowledge of the processing and use of textile fibres can be assumed since the Stone Age. Over the centuries, textile production has constantly improved and a range of raw materials and textile bindings have been used. In archaeological finds we rarely encounter the remains of fragile textile material; however, it is possible to reconstruct the level, maturity and variety of textile structures in the past, above all from small discovered fragments, most often from burial or waste features. The article provides an overview of weaves, their characteristics and specific examples identified in preserved textiles from archaeological finds in the Czech Republic dating to the period from the Early to the Late Middle Ages.*

Keywords: *archaeological textiles, weave, Early Middle Ages, High Middle Ages, Prague Castle*

1 INTRODUCTION

The investigation and professional processing of textile preserved in archaeological contexts provides an unique opportunity for learning about the method, level and diversity of textile production in the past. Although the Czech Republic lacks ideal conditions for the preservation of organic archaeological material, find units, mainly grave and waste situations, occasionally provide textiles from various time periods. A major part of the investigation of textiles is the study of weaves and the method of their creation. The following article provides a summary of all weaves documented on textiles obtained from archaeological finds in the Czech Republic in the period between the Early and Late Middle Ages. The work presents basic weaves such as tabby, twill, satin and their extended versions, as well as more intricate and very complicated weaves such as those with floating weft threads, damask, weft-faced compound twill, proto-lampas, lampas and velvet[1]. The selection of specific examples includes both classic variants of individual weaves and variants with certain differences or interesting aspects in their execution. The presented fabrics produced with simple or very complicated weaves are part of the broad spectrum of medieval textile production that achieved, especially in the production of silk fabrics, a high utility, economic and artistic value.

2 SOURCE INVENTORY

The remains of medieval textiles appear in archaeological finds from various environments, with the most frequent being waste pits and features from medieval urban environments where higher moisture and a lack of air create ideal conditions for the preservation of organic material and which generate remnants of common material culture used in medieval households. An important group of textile finds that has been particularly useful for the study of more complicated weaves, period fashion, styles, patterns and trade with luxury fabrics is grave textiles preserved in enclosed graves and tombs connected most frequently with the royal, aristocratic and Church environment, in many cases with a concrete historical figure. Also offering good conditions for the preservation of textiles are find environments supported by the regular circulation of air, including the backfill of vaults and floors in historical buildings. Another source for studying textiles is small fragments preserved in the corrosion surface layers of metal artefacts; these finds, especially those from the Early Medieval period, provide a unique opportunity for the investigation of textile structures [1].

Specific fabrics representing individual weaves were selected in three types of find environments significant for archaeological textile finds in the Czech Republic. Medieval textiles from waste features and layers make up an assemblage of more than 1500 textile fragments from the thick waste layers from the 14th and 15th centuries in the centre of Prague [2]. Funeral textiles were chosen from a unique collection from archaeological excavations at Prague Castle, especially from St. Vitus Cathedral, the resting place of the Bohemian rulers, their family members and Church dignitaries [3, 4]. An example of Early Medieval textiles preserved in the corrosion layers of metal artefacts is finds from Great Moravian inhumation graves in Mikulčice [5].

The study of weaves is connected with the development of individual types of looms of various constructions. We focus exclusively on those that were used to make the fabrics documented in Czech territory. The simplest type was the warp-weighted loom, the use of which appears in prehistoric times and in Europe is regarded as the main weaving device up until the Early Medieval period. The loom was composed of two uprights, a warp beam with tied warp threads and the cloth beam. The warp threads were typically tightened by a set of weights. The shedding device was composed of a certain number of shed rods with heddles that raised the warp threads, and by moving the individual shed rods forwards and backwards, a shed was created for passing the weft through. The weaver operated the loom from the front while standing. The simplest fabrics with tabby and twill weaves were woven on this type of loom.

During the course of the 13rd century, the warp-weighted loom was gradually replaced in the Czech environment by the more technically advanced horizontal treadle loom. The invention of this type of loom is attributed to China in the 2nd century BC. Its use then expanded westward, and by the Early Middle Ages, the horizontal treadle loom could also be found in Europe. The loom was composed of a wooden frame with four uprights and cross beams. Two rollers were attached to the front and back uprights – in the front by the weaver was a cloth roller onto which the finished fabric was wound. In the back was the warp roller to which the warp threads were attached and wound. The most important part of the loom was the shedding mechanism composed of two or more heddle bars, two or more treadles, the heddle harness and the beater. The bottom of each heddle bar was attached by rope to the treadle, which the weaver operated by foot. The shed was created by alternately pushing and releasing the treadles. A two-person horizontal loom operated by two weavers was used to weave exceptionally wide fabrics. This type of loom was used to produce tabby, twill and satin weaves.

The use of the most complicated weaving device in period textile production, the drawloom, began roughly in the 3rd century in the eastern Mediterranean. It was used to produce patterned fabrics, mainly from silk. It developed as a refinement of the horizontal loom and was equipped with a special type of figure harness consisting of lashes controlled by lifting cords. This device was operated by a drawboy sitting opposite the weaver on a raised seat. The drawloom permitted the continual repetition of a pattern in the width and length of the textile. Decorative motifs stood out more because it was possible to work better with the pattern wefts. Drawlooms were used to produce, for example, more complicated weft-faced compound twill, proto-lampas and lampas [6].

Velvet without a pattern was woven on a horizontal loom, and thin metal rods were inserted in the fabric a certain intervals. Loops formed above the ground fabric once the rods were removed. If these rods had a longitudinal channel along which a sharp tool could be run, the loops were cut to create cut velvet. In the case of patterned velvet, pile warps were controlled by a special type of figure harness. If another pattern occurred in the fabric, e.g. woven with metal wefts, a second figure harness was required for work with the warp threads [7].

3 TABBY

Tabby (plain weave) is a weave based on a unit of two ends and two picks in which each end passes over and under one pick, with the points of binding being set over one end on successive picks. It is the simplest and densest weave and has the same appearance on the obverse and reverse sides of the fabric. The tabby weave is the most commonly documented weave, from the earliest prehistoric textile finds in Europe, including in the Czech Lands [9], up to the studied medieval period, where, in all investigated find units with the exception of assemblages of luxury silk textiles from Prague Castle, it significantly exceeds the occurrence of all other weaves [2, pp. 66-68].

3.1 Wool fabric [2, p. 318]

Find circumstances: Prague 1 – New Town, waste layer
Storage; inventory number: The City of Prague Museum; 25_A11E_347
Dating: 14th – 15th century
Provenance: Bohemia
Technical analysis (Figure 1)

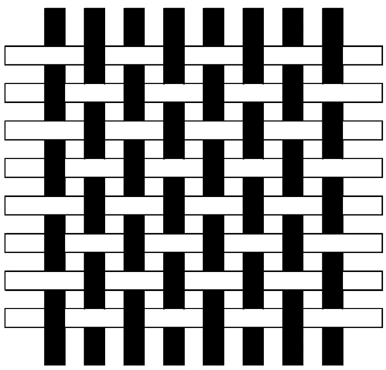

Figure 1 Wool fabric: weave diagram

Weave: tabby
Warp wool, z-twist, light brown colour[2]
count: 13 threads per cm
Weft wool, s-twist, light brown colour
count: 13 threads per cm
Characteristics of the weave: regular
Pattern: unpatterned
Original use: indeterminable

3.2 Crepe fabric [10]

Find circumstances: Prague Castle, St. Vitus Cathedral, Royal crypt, originally the separate coffin of one of the following queens: Blanka of Valois (†1348), Anne of Bavaria (†1353), Anna of Schweidnitz (†1362), Joanna of Bavaria (†1386), Elizabeth of Pomerania (†1393), as of 1611 a common coffin for all the queens
Storage; inventory number: Prague Castle collection; PHA 4/04, HS 25802
Dating: 14th century
Provenance: Spain (?)
Technical analysis (Figure 2)

Figure 2 Crepe fabric: detail of fabric with hem © Prague Castle Administration, photo: J. Gloc

Weave: tabby
Warp silk, z-twist, ochre-brown colour
count: c. 60 threads per cm
Weft silk, z-twist, ochre-brown colour
count: c. 60 threads per cm
Characteristics of the weave: warp and weft threats are very wavy (crepe), an effect achieved by means of a relatively high identical z-twist in the warp and weft threads; both edges of the strip of fabric have a decorated waviness, the result of the use of thicker, mostly paired, and weakly spun warp threads in the hem
Pattern: unpatterned
Original use: a typical medieval woman's veil, a so-call 'kruseler'

4 TWILL

Twill is a weave based on a unit of three or more ends and three or more picks, in which each end passes over two or more adjacent picks and under the next one or more, or under two or more adjacent picks and over the next one or more. The points of binding are set over by one end, always in the same direction, on successive picks forming diagonal lines. The repetition of a twill may be expressed as a numerical ratio, with the first figure indicating the number of picks over which an end passes, the second the number of picks under which it passes.

Like the tabby weave, the twill weave is documented in finds dating back to prehistoric times. Both weaves appear in great numbers in assemblages connected with the common textile material culture of the medieval population [2, pp. 66-67].

4.1 Worsted fabric [2, p. 305]

Find circumstances: Prague 1 – New Town, waste layer
Storage; inventory number: The City of Prague Museum; 10_V31_83
Dating: 14th – 15th century
Provenance: western Europe (?), Bohemia (?)
Technical analysis (Figure 3a, b)

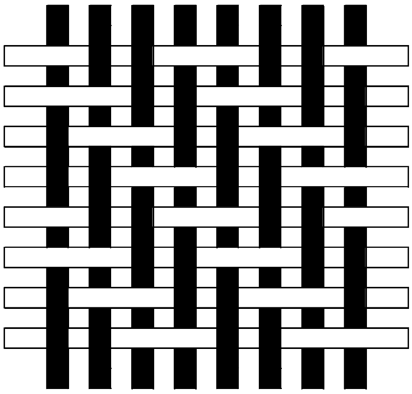

a)

b)

Figure 3 Worsted fabric: a) weave diagram; b) fabric detail © Z. Kačerová

Weave: 2.2 twill
Warp worsted wool, z-twist, light brown colour
count: 22 threads per cm
Weft worsted wool, z-twist, light brown colour
count: 16 threads per cm
Characteristics of the weave: regular
Pattern: unpatterned
Original use: indeterminable

5 EXTENDED TABBY AND TWILL

An extended weave is created from a ground tabby, twill or satin weave by adding or removing certain binding points or through another arrangement of threads, thus producing a new binding of the ground weave.

5.1 Chequered fabric [11]

Find circumstances: Prague Castle, St. Vitus Cathedral, Royal crypt, perhaps the Romanesque chest apparently used to transport the remains of Conrad II Oto, Duke of Bohemia (†1191)
Storage; inventory number: Prague Castle collection; PHA 95/02, HS 25829
Dating: 12th century (?)
Provenance: Spain, southern Europe (?)
Technical analysis (Figure 4a, b)

Weave: 2.2 extended tabby (louisine), 2.2.3. extended tabby (louisine), 3.1.1.1.1.1. weft-faced twill S, 3.1.1.1.1.1. weft-faced chevron twill in the warp direction, 3.1.1.1.1.1. weft-faced chevron twill in the weft direction, 3.1.1.1.1.1. weft-faced lozenge twill

Warp silk, z-twist, ochre-brown colour
count: c. 50-77 threads per cm

Weft *latté*, silk, without visible twist, light brown and green colour
count: c. 20-35 threads per cm

Characteristics of the weave: combination of several simple weaves that continually alternate

Pattern: the fabric (*etoffe à carreaux*) is decorated across the entire preserved width with a small geometric pattern of diamonds, zigzags and crosswise and lengthwise stripes achieved with a combination of several simple weaves; the chequered pattern is further enhanced by the use of different colours of weft threads

Pattern rapport: indeterminable

Original use: possible wrap for the relics of Conrad II Oto, Duke of Bohemia

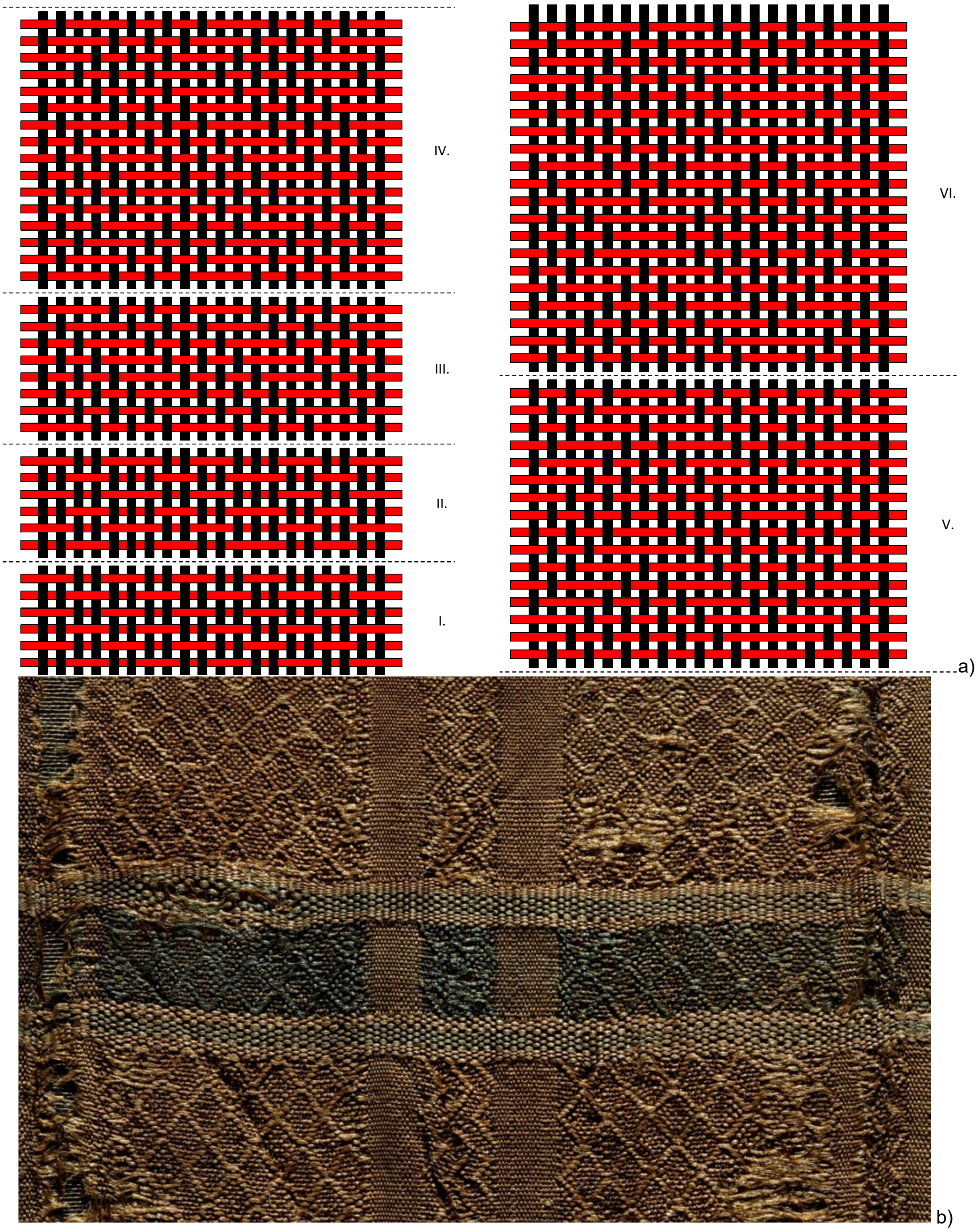

Figure 4 Chequered fabric: a) weave diagram: I. – 2.2 extended tabby; II. – 2.2.3 extended tabby; III. – 3.1.1.1.1.1 weft-faced twill S; IV. – 3.1.1.1.1.1 weft-faced chevron twill in the warp direction; V. – 3.1.1.1.1.1 weft-faced chevron twill in the weft direction; VI. – 3.1.1.1.1.1 weft-faced lozenge twill; b) fabric detail © Prague Castle Administration, photo: J. Gloc

5.2 Fabric with stylised diamond mesh [12]

Find circumstances: Prague Castle, St. Vitus Cathedral, Royal crypt, lining of the Romanesque chest apparently used to transport the remains of Conrad II Oto, Duke of Bohemia (†1191)
Storage; inventory number: chest – National Museum; fabric sample – Prague Castle collection; PHA 95/03
Dating: second half of the 12th century (?)
Provenance: Spain (?)
Technical analysis (Figure 5)

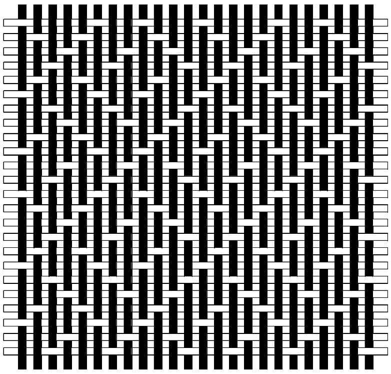

Figure 5 Fabric with stylised diamond mesh: weave diagram

Weave: interconnection of 3.1 twill S and 3.1 twill Z
Warp flax, z-twist, brown-red colour
count: 23 threads per cm
Weft cotton, without apparent twist, brown-red colour
count: 13 threads per cm
Characteristics of the weave: patterned twill; several binding points not realised; weave unit 12/12
Pattern: stylised diamond mesh in which stripes falling obliquely from the right to the left are divided by double bars into rectangular fields containing small rectangles
Pattern rapport: height 2 cm, width 2 cm
Original use: lining of Romanesque chest

6 WEAVES WITH FLOATING WEFT THREADS

The pattern of this type of fabric is composed of either a floating ground weft or one of the weft threads in a standard weave (double-faced weave; see 6.1.), or a supplementary floating weft is added to the weft thread – pattern or brocading – regularly bound by the warp (see 6.2.).

6.1 Fabric with diamonds [12]

Find circumstances: Prague Castle, St. Vitus Cathedral, graves of the Prague bishops, probably Bishop Nikolaus (†1258)
Storage; inventory number: Church treasury at St. Vitus (held by the Prague Castle Administration); K 434
Dating: first half of 13th century
Provenance: Spain, southern Europe (?)
Technical analysis (Figure 6a, b)
Weave: tabby with floating weft (double-faced weave)
Warp silk, z-twist, light brown colour
count: c. 27-28 threads per cm
Weft silk, without visible twist, light brown colour
count: c. 19-21 threads per cm
Characteristics of the weave: even wefts float on the face, odd wefts on the reverse; floating wefts over 3-13 warps
Pattern: small, constantly repeating diamonds, with each larger diamond containing another smaller diamond
Pattern rapport: height 1.8 cm, width 5.7 cm
Original use: remnant of burial gown, possibly a dalmatic

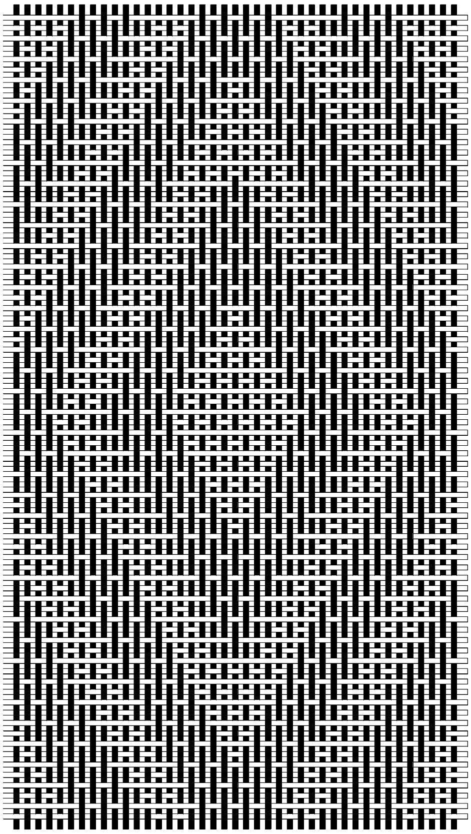

a)

b)

Figure 6 Fabric with diamonds: a) weave diagram; b) fabric detail © Prague Castle Administration, photo J. Gloc

6.2 Fabric with a supplemental pattern weft [13]

Find circumstances: Mikulčice-Kostelisko, grave no. 2041, small fabric fragments preserved in the corrosion layer of an iron sword in its scabbard
Storage; inventory number: Institute of Archaeology of the Czech Academy of Sciences, Brno; 266/114
Dating: 9th century
Provenance: ?
Technical analysis (Figure 7a, b)
Weave: tabby with a supplemental pattern weft
Warp flax, z-twist, brown colour
count: c. 25 threads per cm
Weft proportion (pass): 1 ground weft to 1 pattern weft
- ground: flax, z-twist, brown colour
- pattern: flax, S/2z, brown colour
count: 20 threads per cm (ground weft),
20 threads per cm (pattern weft)
Characteristics of the weave: a tabby weave with one supplementary floating pattern weft whose short floats, always across two warp threads, create a small geometric pattern on the fabric obverse; weave unit 20/16 (8+8)
Pattern: diagonal rows of disarrayed diamonds
Pattern rapport: height 0.4 cm, width 0.8 cm
Original use: part of the inner lining of a wooden sword scabbard

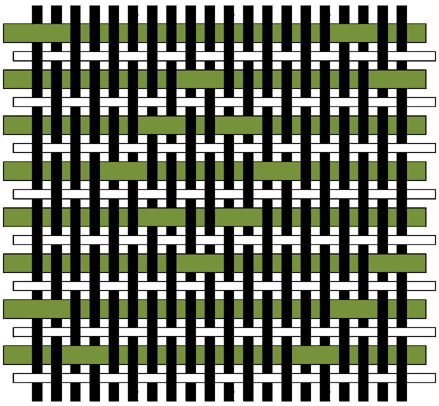
a)


b)

Figure 7 Fabric with supplemental patterning weft: a) weave diagram; b) reverse of mineralised fabric © Institute of Archaeology of the Czech Academy of Sciences, Brno

7 SATIN

Satin is a weave based on a unit of five or more ends and a number of picks equal to, or a multiple of, the number of ends. Each end either passes over four or more adjacent picks and under the next one, or passes under four or more adjacent picks and over the next one. The points of binding are set over two or more ends on successive picks.

This weave appeared in China in the 9th century and later also gained popularity in central Asia, the Near East and in Egypt, where it was used in the ground of lampas fabrics. It doesn't appear in European silk production until the end of the 13th century, and the use of this weave increases in the following century. Satin's occurrence on wool fabrics in European assemblages from the 14th century is very rare, and it isn’t until the 15th century that the weave appears more frequently [2, pp. 88, 91].

7.1 Silk fabric [2, p. 333]

Find circumstances: Prague 1 – New Town, waste layer
Storage; inventory number: The City of Prague Museum; 40_B5_69
Dating: 14th – 15th century
Provenance: western, southern Europe (?)
Technical analysis (Figure 8a, b)
Weave: 5-end warp-faced satin
Warp silk, z-twist, brown colour
count: 95 threads per cm
Weft silk, without visible twist, brown colour
count: 36 threads per cm
Characteristics of the weave: interruption 2
Pattern: unpatterned
Original use: indeterminable

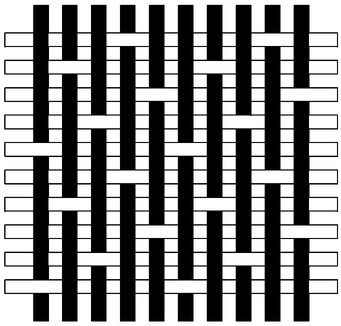
a)

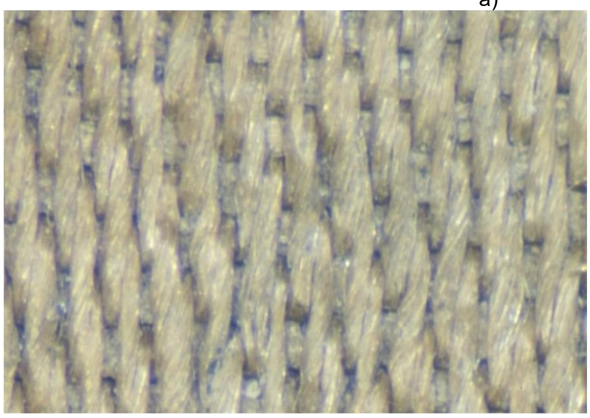
b)

Figure 8 Silk fabric: a) weave diagram; b) fabric detail © Z. Kačerová

8 DAMASK

Damask is a figured textile with one warp and one weft in which the pattern is formed by a contrast of binding systems. In its classic form, it is reversible, and the contrast is produced by the use of the warp and weft faces of the same weave.

Damask in twill weaves appeared in the east Mediterranean and the Near East sometime in the 3rd-4th century, in China much earlier. From sometime in the 7th century the production of this type of damask became very important in China, whereas its popularity in the west declined. Thanks to trade on the renewed Silk Road, damask expanded westward again from the end of the 12th century; it was woven primarily in Syria and Egypt. Damask fabric in a satin weave was also produced in China beginning in the 13th century [14, 15].

8.1 Fabric with a plant pattern [2, pp. 294, 347]

Find circumstances: Prague 1 – New Town, waste layer
Storage; inventory number: The City of Prague Museum; 1_V31_82; 1_V31_280; N_R3_58
Dating: 14th century
Provenance: China
Technical analysis (Figure 9a, b)

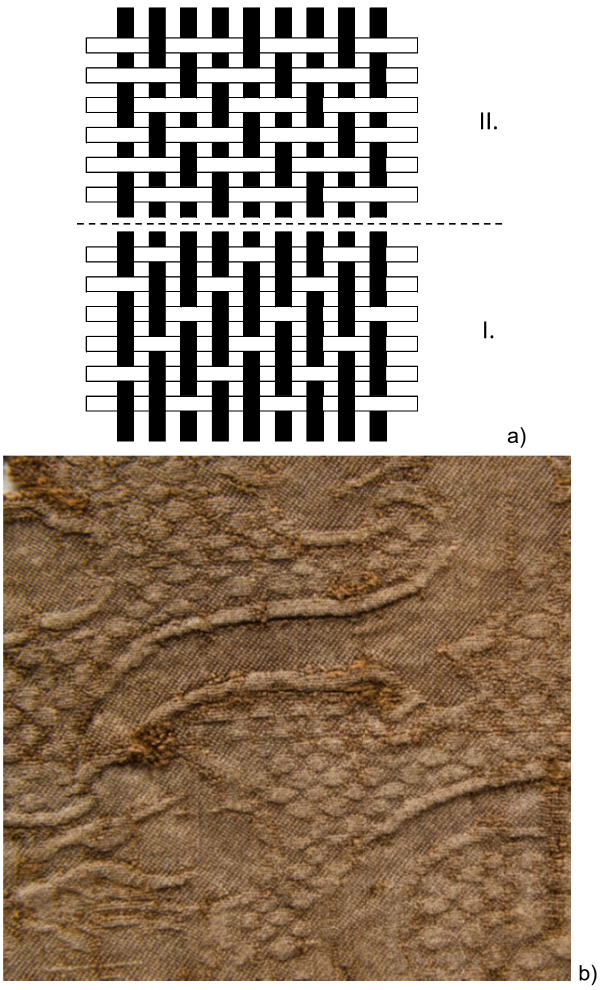

Figure 9 Fabric with plant pattern a) weave diagram: I. – ground; II. – pattern; b) fabric detail © Z. Kačerová

Textile type: damask
Warp silk, no visible twist, brown colour
découpure: 1 warp
count: 65 threads per cm
Weft silk, no visible twist, brown colour
découpure: 1 weft
count: c. 60 threads per cm
Characteristics of the weave: ground – warp-faced 2.1 twill Z; pattern – weft-faced 1.2 twill S
Pattern: rising in the warp direction are parallel and very wide wavy lines in the form of stylised tendrils with shoots and leaves reminiscent of lotus flowers; the space between the ornamentation is filled with a small geometric pattern
Pattern rapport: height 7 cm, width 4.5 cm
Original use: indeterminable

9 WEFT-FACED COMPOUND TWILL

Weft-faced compound twill is a weave employing a main warp, a binding warp, and a weft composed of two or more series of threads, usually of different colours. By the action of the main warp ends, only one weft thread appears on the face, while the other or others are kept to the reverse. The ends of the binding warp bind the weft in passes in twill, and the ground and the pattern are formed simultaneously. The entire surface is covered by weft floats that hide the main warp ends.

Weft-faced compound twill first appeared in Persia roughly in the period of 300-500. The oldest fabric woven in this manner has a ratio of one main warp thread to one binding warp thread. In the Near East and the Byzantine Empire, weft-faced compound twill was later made in a ratio of two main warp threads to one binding warp thread, a weave that spread towards Central and Eastern Asia, with Arabs to the west across the Mediterranean to southern Spain. The greatest expansion of weft-faced compound twill dates to around the year 1000; the fabric also occurred in the 12th century before fading from use in the 14th century [14, 16].

9.1 Fabric with lions [2, p. 294]

Find circumstances: Prague 1 – New Town, waste layer
Storage; inventory number: The City of Prague Museum; 1_V31_80
Dating: 13th century
Provenance: Spain
Technical analysis (Figure 10a, b)
Weave: 1.2 weft-faced compound twill
Warp proportion: 2 main warps to 1 binding warp
- main: silk, no visible twist, yellow colour
- binding: silk, no visible twist, yellow colour
count: 24 threads per cm (main warp), 12 threads per cm (binding warp)
découpure: 1 main warp
Weft proportion (pass): 3 wefts
- I. *latté*: silk, no visible twist, yellow colour
- II. *Interrompu*: silk, no visible twist, yellow colour
- III. *Interrompu*: probably a strip from silver- plated and gold-plated animal substrate wound around a flax core; preserved in minute remnants
count: c. 24 passes per cm
découpure: 1 pass

Characteristics of the weave: weft-faced compound twill with three weft series; binding warp interlaces in 1.2 twill S in passes
Pattern: only part of the pattern with a pair of sitting lions with their backs to one another have been preserved
Pattern rapport: indeterminable
Original use: indeterminable

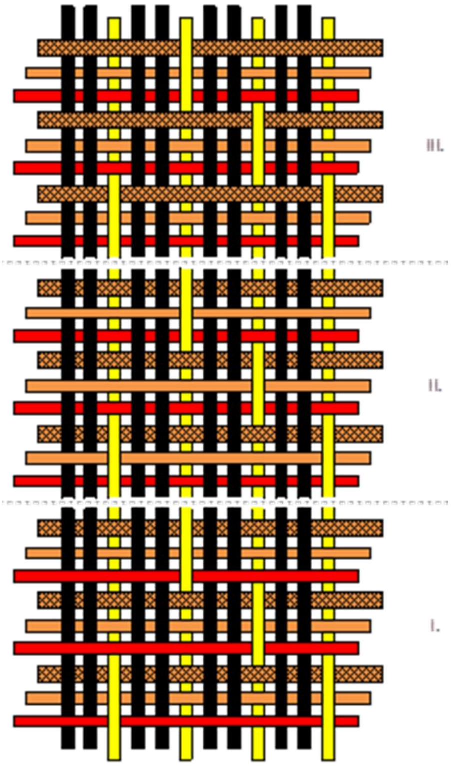

a)

b)

Figure 10 Fabric with lions: a) weave diagram: I. – effect of weft I.; II. – effect of weft II.; III. – effect of weft III.; b) fabric detail © Z. Kačerová

9.2 Fabric with birds in medallions [17]

Find circumstances: Prague Castle, St. Vitus Cathedral, Royal crypt, perhaps the Romanesque chest apparently used to transport the remains of Conrad II Oto, Duke of Bohemia (†1191)
Storage; inventory number: Prague Castle collection; PHA 95/01, HS 12038
Dating: second half of the 12th century
Provenance: Sicily
Technical analysis (Figure 11)

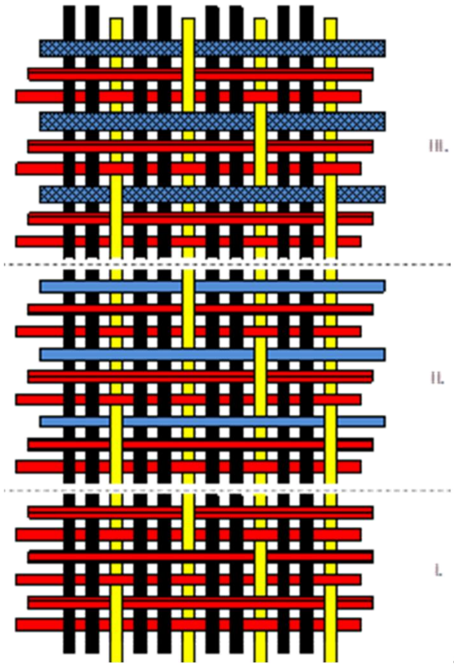

a)

b)

Figure 11 Fabric with birds in medallions: a) weave diagram: I. – effect of weft II.; II. – effect of weft III. or IV.; III. – effect of weft V.; fabric detail © Prague Castle collection, J. Gloc

Weave: 1.2 weft-faced compound twill
Warp proportion: 2 main warps to 1 binding warp
- main silk, z-twist, ochre colour
- binding silk, z-twist, ochre colour
découpure: 2 main warps
count: 40-48 threads per cm (main warp),
20-24 threads per cm (binding warp)

Weft proportion (pass): 5 wefts
- I. silk, no visible twist, ochre colour
- II. silk, no visible twist, ochre colour
- III. brocading: silk, no visible twist, brown-red colour
- IV. brocading: silk, no visible twist, red-pink colour
- V. brocading: gold-plated animal substrate wound around a silk core (Z twist, ochre colour), assembly Z, *couvert* (?)

count: 26-35 passes per cm
découpure: 1 pass

Characteristics of the weave: weft-faced compound twill with five weft series; binding warp interlaces in 1.2 twill S in passes; weft I. remains on reverse, weft II. on the obverse forms the background of the pattern; the pattern is composed of three brocading wefts

Pattern: the round medallions from two lines are filled with pearl roundel with the Tree of Life with cordate leaves; two birds with their bodies facing away from each other and the heads turned towards one another stand in front of the tree; there are four small stars in the space between individual medallions

Pattern rapport: indeterminable

Original use: possible wrap for the relics of Conrad II Oto, Duke of Bohemia

10 REFERENCES

1. Bravermanová M., Březinová H., Urbanová K.: Metodika výzkumu archeologických textilních nálezů (Methodology of Research of Archaeological Textile Finds), Zprávy památkové péče 71(2), 2011, pp. 97-104
2. Březinova H., Kohout D., Bravermanová M., Otavská V., Selmi Wallisová M.: Středověké textilní a barvířské technologie. Soubor textilních fragmentů z odpadních vrstev z Nového Města pražského (Medieval Textiles and Dyeing Technologies. An Assemblage of Textile Fragments from the Waste Layers of Prague's New Town), Institute of Archaeology of the CAS, Praha, 2016
3. Bravermanová M., Lutovský M.: Hroby a hrobky našich knížat, králů a prezidentů (The graves and tombs of our princes, kings, and presidents), Praha, 2007
4. Bravermanová M.: Pražský hrad jako pohřebiště lucemburské dynastie (Prague Castle as the burial site of the Luxembourg dynasty), In: Koruna království, Katedrála sv. Víta a Karel IV (The Crown of the Kingdom, Charles IV and the Cathedral of St. Vitus) Bravermanová M., Chotěbor P. (Eds.), Praha, 2016, pp. 78-114
5. Březinová H.: Finds of textile fragments and evidence of textile production at a major excavation site of the Great Moravia in Mikulčice (South Moravia, Czech Republic). In NESAT XI. The North European Symposium for Archaeological Textiles, Banck-Burges J., Nübold C. (Eds.), Verlag Marie Leidorf (Rahden/Westfalen), 2013, pp. 193-196
6. Broudy E.: The Book of Looms, Hanover – London, 1979
7. Peter M.: A Head Start through Technology: Early Oriental Velvets and the West, In: Oriental Silks in Medieval Europe, Fircks J., Schorta R. (Eds.), Riggisberger Berichte 21, Abegg-Stiftung, Bern, 2016, pp. 300-315
8. CIETA: Vocabulary of Technical Terms, Lyon, 1964
9. for example Grömer K.: The Art of Prehistoric Textile Making: The Development of craft traditions and clothing in Central Europe, Wien, 2016
10. Bravermanová M., Leppin B., Otavská V.: Fragment pohřebních šatů a závoj, tzv. kruseler, z rakve českých královen z královské hrobky v katedrále sv. Víta. Das Fragment eines Begräbniskleides und ein Schleir, ein sog. Kruseler, aus dem Sarg böhmischer Königinnen aus der Königsgruft im St. Veitsdom (Fragment of a Funeral Dress and a Kruseler Veil from the Casket of Czech Queens in the Royal Tomb, St. Vitus Cathedral), Archaeologia historica 36, 2011, pp. 593-625
11. Bravermanová M., Kloudová R.: Geometricky zdobená tkanina z královské hrobky v katedrále sv. Víta. Geometrisch verziertes Gewebe aus dem Königsgrab im Veitsdom (Fabric with Geometrical Patterns from the Royal Tomb in St Vitus Cathedral), Archaeologia historica 34, 2009, pp. 463-481
12. Bravermanová M., Kloudová R., Sliwka A.: Pohřební výbava pražského biskupa Mikuláše. Die Grabausstattung des Prager Bischofs Nikolaus (Funeral Equipment of the Prague Bishop Mikuláš), Archaeologia historica 32, 2007, pp. 477-489; about the fabric with stylised diamond mesh see pp. 483-486
13. yet unpublished finding
14. Wilckens L. von: Die Textilen Kunste. Von der Spätantike bis um 1500 (The textile arts. From late antiquity until 1500), München, 1991
15. Kuhn D. – Zhao Feng (Eds): Chinese Silks. The Culture and Civilization of China, Yale University, 128-130, 2012, pp. 344-346
16. Geijer A.: A History of Textile Art, London, 1979
17. Bravermanová M., Otavská V.: Románská tkanina z královské hrobky na Pražském hradě. Ein romanisches Gewebe aus der königlichen Gruft (Roman fabric from the royal tomb), Archaeologia historica 25, 2000, pp. 405-428

The Part 2 will be published in the next issue.

Footnotes:

[1] Definition of weaves and terms in textile technological studies are taken from professional terminology codified by CIETA [8]. Illustrations of weave diagrams are processed according to the following key:

[2] In all cases, the stated colours are current colours, most of which do not correspond to the original colour.

MODELLING THE CROSS-SECTIONAL PROPERTIES OF YARN ALONG THE FABRIC

R. Befru Büyükbayraktar

Dokuz Eylül University, Textile Engineering Department, Izmir, Turkey
befru.buyukbayraktar@deu.edu.tr

Abstract: *Three dimensional (3-D) fabric geometry defines the fabric's physical and mechanical properties. For this reason, it is important to obtain realistic fabric models. In this study, the yarn path of the woven fabric was modeled according to structural properties of fabric using Pierce geometry. On the other hand, the cross-sectional properties of the yarn along the weave unit were modeled depending on the movement of the yarn and the interactions between adjacent and perpendicular yarns. The yarn path was divided into regions and the cross-section of the yarn was defined according to region properties. By an experimental study, the variation of the yarn dimension at each region was measurement and the flattening ratio of yarn was determined. These data were used in the cross-section model. The simulations of yarn path and cross-sectional models were obtained by using SolidWorks. These simulations present the variation of yarn cross-section along the weave unit.*

Keywords: *Yarn cross-section, yarn path, yarn diameter, woven fabric.*

1 INTRODUCTION

Three dimensional (3-D) fabric geometry was formed according to structural parameters and manufacturing processes. Raw material, yarn properties such as yarn production type, yarn linear density, twist, packing ratio, etc., and construction properties of fabric such as settings and weave type are some of the important structural parameters defined fabric geometry. The fabric geometry affects the physical properties of the fabric, such as mechanical, sensory, permeability and conductivity properties of the fabric. Therefore, the structural parameters of the fabric must be chosen well to design a special product for a defined using area. However, the relationship between structural parameters and fabric geometry and also the performance properties of a fabric is complicated. Thus, modeling studies about the fabric geometry are needed to predict the performance behaviours of product. Besides, determination of fabric properties at the designing step is important for both designers and manufacturers in terms of time and cost.

Generally, fabrics were idealized into simple geometrical forms. The yarn path along the fabric was described by circular arcs, straight lines, sinus curves, elastic forms, and the yarn cross-section was modeled as circular, elliptical, lenticular, racetrack shapes [4-9]. However, yarn cross-section varies inside the fabric due to inter-yarn compression. In recent years, irregular cross-section shapes of yarns were also studied [1-3, 10-12]. The shape of a yarn cross-section shape and size are affected by many factors such as raw material, twist degree, yarn spinning technology, weave type, settings, etc. It is important to provide an efficient modeling technique for creating the yarn cross-sections properties.

In this study, fabric geometry was modeled into two steps. First, the yarn path was defined according to structural parameters and B-spline method was used to get a smooth yarn center line along the weave unit. It is important to define the variation at the cross-sectional shape and size of the yarn into the fabric in order to create more realistic 3-D fabric geometry. In the second step, the cross-sectional properties of yarn were modelled along the yarn path according to the interactions between adjacent and perpendicular yarns. An experimental study was carried out to get data about the variation of yarn size along the yarn path. Yarn dimensions of different cotton fabrics were measured from different regions of fabric images. The fabric geometry simulations were performed by using SolidWorks 2014.

2 EXPERIMENTAL

2.1 Materials

In this study, both theoretical and experimental studies were carried out. In the experimental part of the study, four different commercial cotton woven fabrics having different structural parameters were used. The structural properties of these fabrics given in Table 1 were analyzed by related standards.

Table 1 Structural properties of measured fabrics

Fabric code	Weave type	Unit weight [g/m^2]	Warp count [tex]	Weft count [tex]	Warp setting [cm^{-1}]	Weft setting [cm^{-1}]	Thickness [cm]
P1	Plain	106	11	11	60	35	0.0228
P2	Plain	114	11	11	56	30	0.0226
P3	2/2 Twill	126	10	9	62	56	0.0256
P4	4/1 Twill	215	12	19	90	50	0.0416

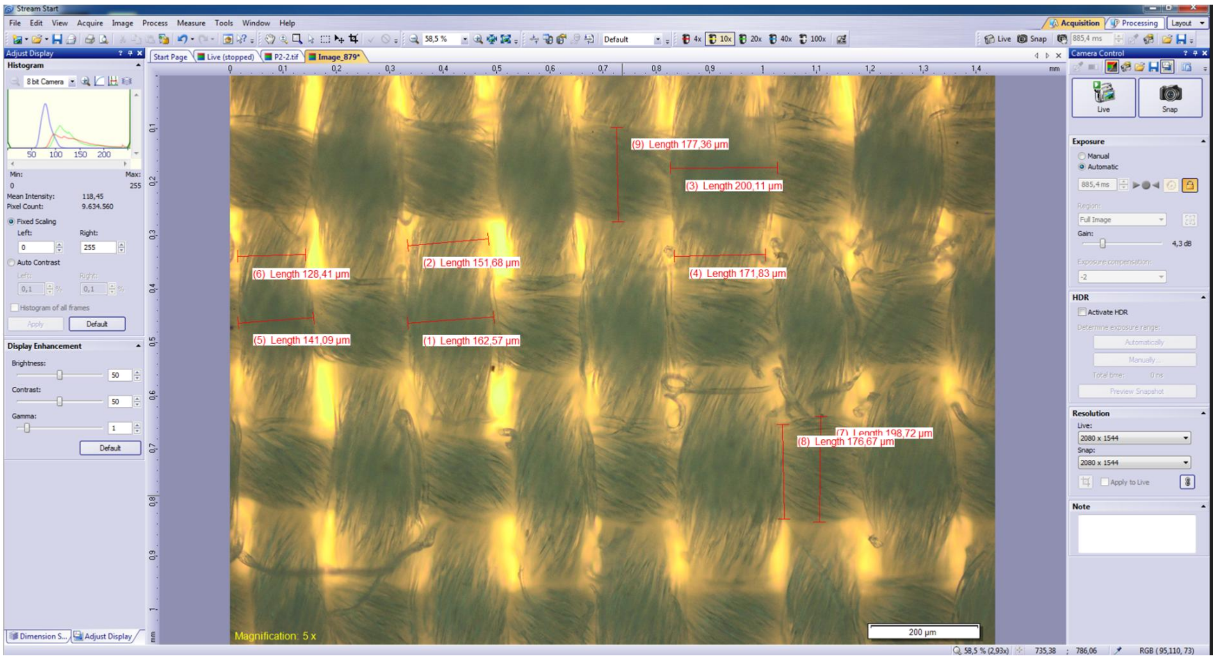

Figure 1 Measurement of yarn diameter at different regions of the yarn path

2.2 Methods

Sectioning is a more realistic method in order to obtain cross-sectional dimensions of yarn into the fabric. But this is a laborious and time-consuming method. For this reason, in this study measuring of yarn dimensions onto the 2D surface images of fabrics were preferred. The images of various cotton fabrics were observed by a camera system integrated to a microscope. The dimensions of warp and weft yarns were measured from captured images by using the application of the camera system as seen in Figure 1. Measurements were done from the different regions of the weave unit. Regions were defined as the peak point of the intersecting region and the middle point of the interchanging region, for plain weave. For twill weaves, the middle of the floating region was also measured. Ten measurements were done for each region of warp and weft yarns. The results were used to estimate the variation of the yarn dimension along the yarn path. Besides, the possible flattening ratio of different regions was predicted from the measurements.

3 THEORETICAL

In the theoretical part of the study, the yarn path and yarn cross-section were modeled in order to get realistic fabric simulations. The basic yarn path was defined depending on the structural properties of the fabric according to Pierce geometry [8]. In Peirce geometry, when weaving angle is assumed a small value then the amplitude of yarns (h) can be calculated as in Equation 1. Here, p is yarn spacing, c is crimp factor. Subtitles 1 and 2 were used for warp and weft yarns, respectively. This formula was defined according to plain fabric in Peirce geometry. Some modifications were done and the crimp factor of 2/2 twill and 4/1 twill weaves were calculated in order to use this equation for these weave types, too.

$$h1 = p2\frac{\sqrt{2c_1}}{1-c_1} \tag{1}$$

B-spline curve method was used in order to obtain yarn path as a smooth curve. The open non-uniform cubic B-spline curves with a continuity of the order 2 were used. First, a linear control polygon was defined, for each weave types. The B-spline curve generally follows the shape of control polygon. Seven control points were defined for each weave unit, as seen in Figure 2. The coordinates of these points were calculated by using the Peirce geometry. Appling B-spline method, 21 new points confirmed yarn path were calculated. Yarn paths were obtained individually for warp and weft yarns.

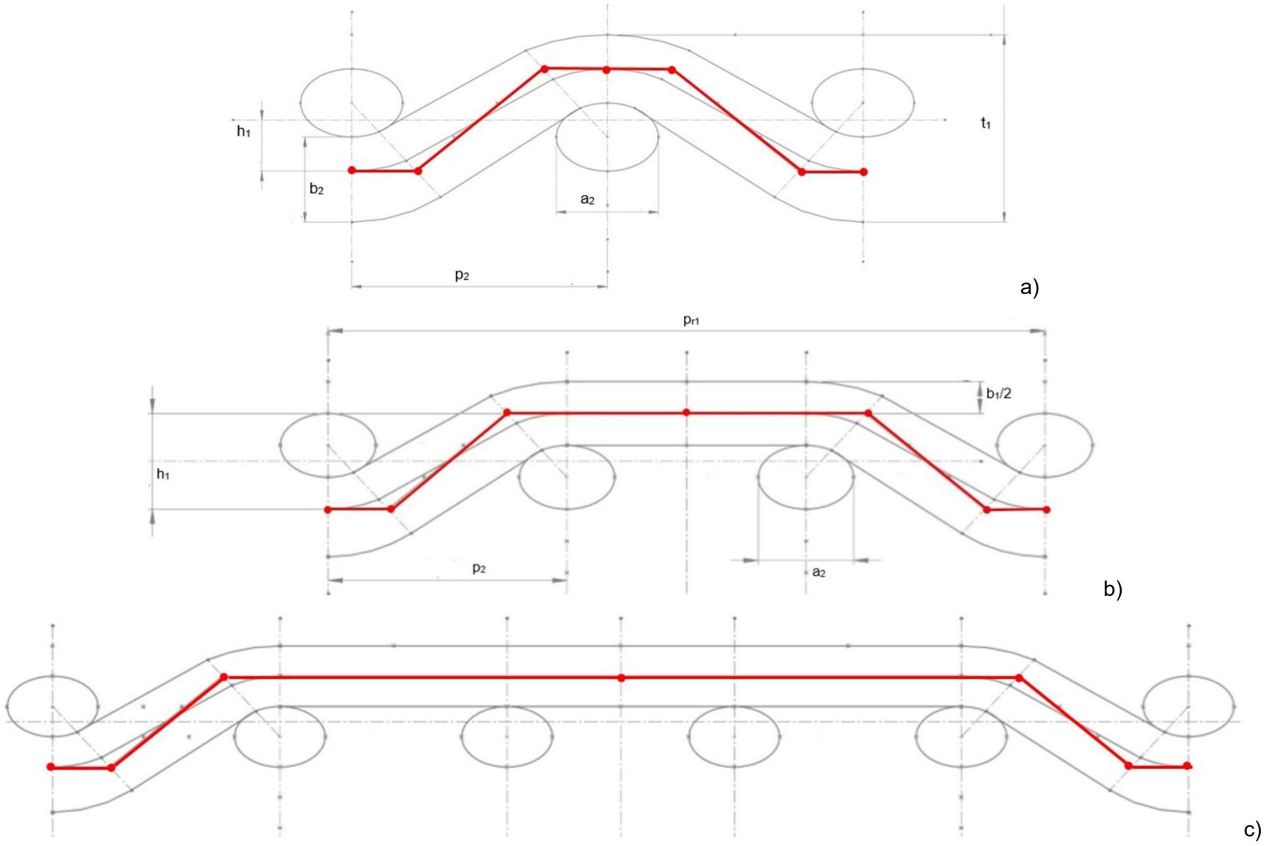

Figure 2 B-Spline control polygon and control points for a) Plain, b) 2/1 Twill, c) 4/1 Twill weave units

In many studies, the cross-sectional shape of yarn in the woven fabric was modeled as circular. However, it was known that the shape and dimension of yarn changed along the yarn path because of interactions between adjacent and perpendicular yarns. In this study, the dimensions of yarn cross-section were defined by using theoretical calculations and experimental measurements. Theoretical yarn diameter was accepted as the real circular diameter of the yarn before weaving. The theoretical circular yarn diameter depending on yarn count was calculated by Ashenhurst theory (13) given in Equation 2. But, from previous studies and literature, it was known that the cross-sectional shape of the yarn is changed during weaving and this shape is not constant along the yarn path. Therefore, in this study, it was accepted that this circular yarn shape became elliptical during the weaving. The dimensions of an ellipse having the same perimeter with a circle were calculated by Equation 3. Here, *a* is the major and *b* is the minor diameter. Besides, flattening ratio (*e*) is defined as being the ratio of the minor diameter to the major (*e=b/a*). In the theoretical study, the minor dimension of the ellipse could be calculated by using the relation between fabric thickness (*t*) and the amplitude of warp yarn (h_1) as given in Equation 4. So, the value of major diameter could be calculated theoretically.

In addition, in the experimental study, the dimension of major diameter was be measured by using surface pictures of fabrics. Thus, the minor diameter of the yarn was predicted by using the relationship between theoretical circular diameter and major diameter.

$$h1 = p2\frac{\sqrt{2c_1}}{1-c_1} \tag{1}$$

$$d = \frac{1}{K\sqrt{N}} \tag{2}$$

$$d = \frac{a+b}{2} \tag{3}$$

$$t = h1 + b1 \tag{4}$$

The variation of major diameter was measured along the yarn path, in the experimental study. Flattening ratio of yarn was calculated for different regions. Using these values, the yarn cross-sectional shape and size of yarn along the yarn path were defined for each region. Thus, a realistic yarn geometry which does not accept a constant cross-sectional shape and size was formed.

4 RESULTS AND DISCUSSION

In Table 2, theoretical circular yarn diameter and mean value of the measured major diameter of elliptical yarn cross sections were summarized. Measurement of yarn dimension was done in different regions of weave unit onto the fabric images. In Table 2, $a_{p\text{-}m}$ denotes major diameter at the peak point of intersecting region, $a_{i\text{-}m}$ is major diameter at the middle point of the interchanging region, $a_{c\text{-}m}$ is major diameter at the middle point of floating region (for twill weaves). It was found that differences of major diameter between different regions of yarn path are significant according to statistical analysis.

Table 2 Calculated circular yarn diameter and measured major diameters

Fabric Code		d_t [cm]	$a_{p\text{-}m}$ [cm]	$a_{i\text{-}m}$ [cm]	$a_{c\text{-}m}$ [cm]
Warp	P1	0.0129	0.0163	0.0148	x
	P2	0.0126	0.0161	0.0140	x
	P3	0.0118	0.0157	0.0126	0.0142
	P4	0.0131	0.0173	0.0133	0.0144
Weft	P1	0.0129	0.0171	0.0148	x
	P2	0.0129	0.0174	0.0154	x
	P3	0.0116	0.0139	0.0124	0.0128
	P4	0.0167	0.0198	0.0169	0.0211

$a_{p\text{-}m}$ - major diameter at the peak point, $a_{i\text{-}m}$ - major diameter at interchanging region, $a_{c\text{-}m}$ - major diameter at middle of floating (for twill weaves)

Minor diameter at the peak point of the intersecting region was calculated by using Equation 4, depending on fabric measured fabric thickness (t) and calculated amplitude of warp yarn (h_1). Here, the thickness was accepted forming by warp yarns. In addition, minor diameter at the different regions was calculated by using Equation 3, depending on the relation between theoretically calculated circular diameter and experimentally measured major diameter. In plain fabrics, the minor diameter values at the peak point of the intersecting region were found similar for both calculations. But in twill weaves, especially in 4/1 twill weave, real thickness (measured) was formed differently from the theoretical aspect because of long floating. So the minor dimension value calculated from fabric thickness was bigger. In order to eliminate this problem, a certain flattening ratio at the peak point of 4/1 twill was used to define yarn dimensions as being 0.6.

Flattening ratio of yarn for different regions was calculated. Maximum flattening was found at the peak of intersecting region in which warp and weft yarns contact each other. The flattening ratio was found nearly 0.5-0.6 at that region. At the interchanging region, the flattening ratio was increased because of the pore region. It was nearly between 0.7-0.85 for different weave types. At the midpoint of the floating region (twill weaves), e was calculated nearly 0.6-0.7.

Table 3 Theoretical calculated yarn dimensions and experimental calculated minor diameter

Fabric Code		$a_{p\text{-}t}$	$b_{p\text{-}t}$ [cm]	$b_{p\text{-}m}$ [cm]	$b_{i\text{-}m}$ [cm]	$b_{c\text{-}m}$ [cm]
Warp	P1	0.0164	0.0095	0.0095	0.0110	X
	P2	0.0149	0.0103	0.0092	0.0113	X
	P3	0-0143	0.0093	0.0079	0.0110	0.0094
	P4	0.0084	0.0117	0.0088	0.0128	0.0117

In the theoretical study, the yarn path was defined by using B-spline curve method. The control points of B-spline polygon were calculated depending on structural properties of fabric such as fabric thickness (t), settings, yarn count, crimp ratio. Then the B-spline method was applied by an algorithm written in Visual Basic 2010. Fabric unit weight area (w) and crimp ratios (k) of yarns were calculated as control factors as given in Table 4. This geometrical model is achieved for plain fabrics. But, because of interactions between long floating, the theoretical results of 4/1 twill weave was found different from experimental results.

Table 4 Structural fabric properties calculated by B-spline method

Fabric Code	W	k_1	k_2
P1	121	1.11	1.09
P2	104	1.07	1.11
P3	132	1.2	1.16
P4	246	1.19	1.26

The fabric geometry simulations were performed by using SolidWorks. In Figure 3, some steps of SolidWorks drawing were shown. First, the yarn path was defined as a spline curve using 21 points. Then the planes for cross-sections were defined along the yarn path depending on the region. Five different plains were defined for each weave units. Flattening ratio of different regions was found different and in this study, the cross-sectional dimensions were defined individually for all planes. Then, loft property of SolidWorks was used and different cross-sections at different planes were connected along the yarn path. By this simulation, the variation of the yarn cross-section was reflected, realistically. Both warp and weft yarns were modelled depending on the structural properties of fabrics. In the end, drawn solid yarn simulations were repeated and 3D fabric simulations were acquired as given in Figure 4. In addition, B-spline curve based on control points could be obtained in SolidWorks. Yarn path could be drawn automatically after determined the number and coordinates of control points. This is a faster way to obtain yarn path geometry in SolidWorks. But, the calculation of spline points was chosen in that study in order to define some structural properties of the fabric. Thus, the experimental and the theoretical properties of fabrics could be calculated.

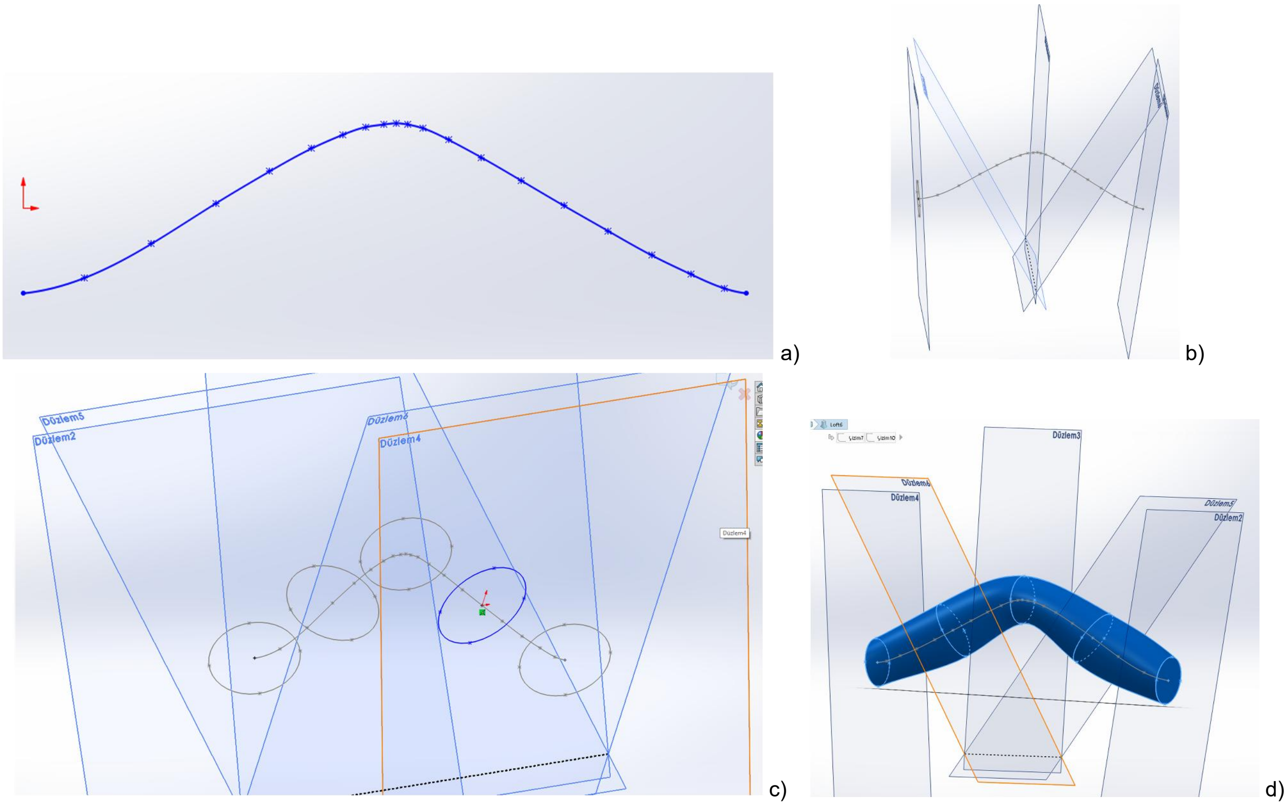

Figure 3 The B-spline curve of yarn path (a), definition of planes for different regions of yarn path (b), various cross-sections in different planes (c), simulation of solid yarn model having various cross-section along the yarn path (d)

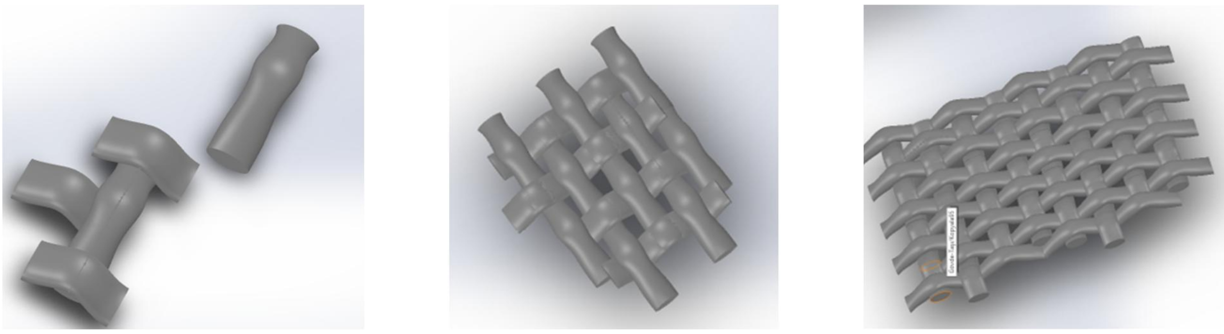

Figure 4 The simulation of fabric (for P1)

5 CONCLUSIONS

In this study, first, yarn path was modeled according to structural parameters of fabric such as weave type, settings, yarn counts, fabric thickness.

The B-spline method was used to get a smooth yarn curve. Then, the yarn cross-section was modelled depending on the yarn path.

The experimental results were used in order to get the flattening ratio of yarn cross-section at different regions of yarn path. After defining the cross-sectional properties of each region on the yarn path the yarn geometry of fabric weave unit was obtained. The performed fabric simulations were more realistic because of reflecting the variation of yarn cross section along the yarn path. This would help more realistic mechanical models with CAD system. The only disadvantage of using this program is the material selection. In further studies, it is aimed to generate 3-D fabric geometry with multifilament yarns and to use these fabric models in the prediction of performance properties of fabrics. Besides, an exhaustive experimental study contained different raw materials and structural parameters were planned.

6 REFERENCES

1. Alamdar-Yazdi A., Heppler G.R.: Cross-sectional shapes of the yarn in cotton gray woven fabric, Journal of Textile Institute 102(3), 2011, pp. 248-262, https://doi.org/10.1080/00405001003703864
2. Gong R.H, Ozgen B., Soleimani M.: Modeling of yarn cross-section in plain woven fabric, Textile Res J 79(11), 2009, pp. 1014-1020, https://doi.org/10.1177/0040517508101799
3. Jiang Y., Chen X.: Geometric and algebraic algorithms for modelling yarn in woven fabrics, J Textile Inst 96(4), 2005, pp. 237-245, https://doi.org/10.1533/joti.2005.0005
4. Hamilton J.B.: A general system of woven-fabric geometry, J Textile Inst. 55(1), 1964, pp. 66-82, https://doi.org/10.1080/19447026408660209
5. Hearle J.W.S., Shanahan W.J.: An energy method for calculations in fabric mechanics part I: Principles and methods, J Textile Inst. 69(4), 1978, pp. 81-91, https://doi.org/10.1080/00405007808631425
6. Keefe M., Edwards D., Yang J.: Solid modeling of yarn and fiber assemblies, J Textile Inst. 83(2), 1992, pp. 185-196, https://doi.org/10.1080/00405009208631189
7. Kemp A.: An extension of Pierce's cloth geometry to the treatment of non-circular threads, J Textile Inst. 49(1), 1958, pp. 44-48, https://doi.org/10.1080/19447025808660119
8. Peirce F.T.: The geometry of cloth structure, J Textile Inst. 28(3), 1937, pp. 45-96, https://doi.org/10.1080/19447023708658809
9. Olofsson B.: A general model of a fabric as a geometric mechanical structure, J Textile Inst. 55(11), 1964, pp. 541-557, https://doi.org/10.1080/19447026408662245
10. Ozgen B., Gong H.: Yarn geometry in woven fabrics, Textile Research Journal 81(7), 2010, pp. 738-745, https://doi.org/10.1177/0040517510388550
11. Smith A., Chen X.: CAD and constraint-based geometric modelling algorithms for 2D and 3D woven textile structures, Journal of Information and Computing Science 3(3), 2008, pp. 199-214
12. Turan R.B., Okur A.: The variation of the yarn cross-section in the fabric, Textile Research Journal 82(7), 2012, pp. 719-724, https://doi.org/10.1177/0040517511435009
13. Ashenhurst T.R.: A treatise on textile calculations and the structure of fabrics, 5th ed. London: J. Broadbent and Co., 1902

THE SET-UP OF A LABORATORY TYPE COATING/LAMINATING UNIT AND THE OPTIMISATION OF LAMINATION PROCESS OF DENIM FABRICS

Ayşe Genç[1], Mehmet Yüceeer[2], Nihan Karakaplan[2] and Cem Güneşoğlu[3]

[1]Çalık Denim R & D Centre, The 1st Organized Industrial Zone, Malatya, Turkey
[2]İnönü University, Chemical Engineering Department, Malatya, Turkey
[3]Gaziantep University, Textile Engineering Department, Gaziantep, Turkey
Ayse.KorkmazGenc@calikdenim.com

Abstract: *Lamination process is a finishing process applied to bring functionality, physical modification and change at appearance by combining two separate materials (fabric, polymer film layer or membrane). The process increased its popularity at denim industry especially in fabric-fabric lamination form in the last decade. Despite its market interest, lamination has setbacks in R&D studies for optimization to enhance the product performance due to large numbers of parameters and difficulties in producing samples. In this study, an adaptive laboratory type coating/laminating unit was developed as the first time in textile industry and the lamination of denim-denim fabric process has been optimized through statistical analysis and modelling studies by artificial neural network (ANN) and least-square support vector (LS-SVM) machine.*

Keywords: *Lamination, optimization, artificial neural network, least-square support vector machine.*

1 INTRODUCTION

Coating is a process in which a polymeric layer is applied directly to one or both surfaces of the fabric, on the other hand lamination is defined as finishing process applied to bring functionality, physical modification and change at appearance by combining two separate materials. Conventional laminated textiles normally consist of one or more textile substrates that are combined using a prepared polymer film or membrane by using adhesives or by using heat and pressure [1]. Lamination found increased interest in denim market, especially in fabric-fabric lamination form by adhesive usage. It is clear that adhesive amount (weight) in the process strongly affect laminated product various properties; also it is a matter of cost. In many cases, producers use adhesive amount as recommended by the supplier, however it is needed to examine to determine the optimum adhesive amount for high volume of production. However, experimental study on fabric lamination is limited since there is large number of parameters to examine and the lamination machinery works with whole fabric width which results large amount of sample and adhesive consumption. Best to our knowledge, there is no laboratory type lamination machine available. In this study, we developed an adaptive laboratory type coating/laminating machine with lower than 40 cm working width which has two separate fabric roll feeding, powder scattering head (for particle loadings), hot-melt adhesive tank and adhesive feeding units. The roller pins are adaptive to change the feeding positions, material type and adhesive feeding face also it is possible to control material and adhesive feeding speeds. The scheme and actual view of the laboratory machine is given in Figure 1.

In this study, denim-denim fabric lamination is conducted by the mentioned machine; various properties are measured and lamination process parameters are optimized through statistical analysis (ANOVA and Design Expert) to find the most suitable adhesive weight for industrial scale applications and modelling studies (ANN and LS-SVM) to assess the predictability of the results and to decide if this study can be applied for industrial scale works as proposed.

2 EXPERIMENTAL

2.1 Materials

100% cotton, denim fabric samples used at lamination were supplied by Çalık Denim, Malatya, Turkey. The constructional details of the samples are given in Table 1. The lamination adhesive was polyurethane based (HB Fuller, USA) reactive hot-melt adhesive with low curing temperature and adhesive weight was varied as 25, 50, 75 and 100 g/m^2 at the trials and 30 m/min fabric feeding speed.

Table 1 Sample details

Sample code	Weave type	Fabric sett [thread/cm]	Yarn count (Warp x Weft)	Weight [g/m^2]
D1	3/1 Z twill	47 x 25	Ne 24/1 x Ne 30/1	342
D2	3/1 Z twill	42 x 26	Ne 20/1 x Ne 18/1	355

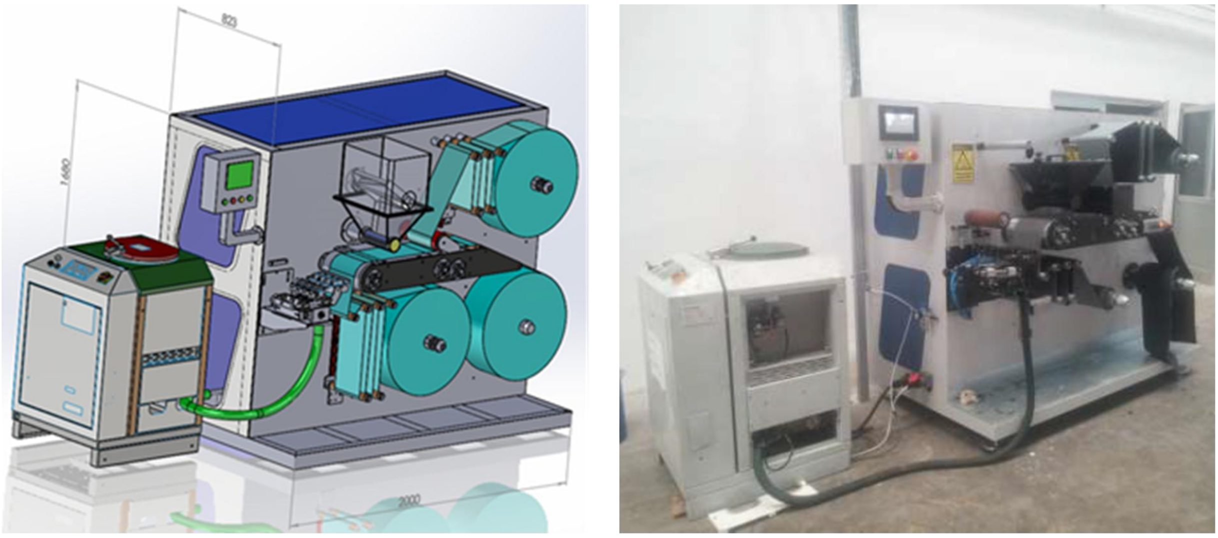

Figure 1 General view of developed coating / laminating machinery

2.2 Methods

After the laminations, the samples were rinsed, dried and tensile strength (ASTM D 5034), tearing strength (ASTM D1424), delamination strength (ASTM D 2724-07), air permeability (ISO 9237), water resistance (ISO 20811) and water vapor permeability (ISO 11092) measurements at the standard laboratory conditions were conducted. All the measurements were repeated for five times and results were recorded as data for optimization studies. All data were subjected to statistical analysis with ANOVA to find out the contribution importance and proposed model strength between adhesive weight and measured property and the optimization study was then applied first with Design Expert V.10. The study is also validated through ANN and LS-SVM modelling as mentioned before.

A typical ANN has feed forward architecture and consists of three or more layers of neurons: one input layer, one output layer and one or more hidden layers (Figure 2). Each of the layers has a set of connections, with a corresponding scalar weight, between itself and each neuron of preceding layer. When the weight of a particular neuron is updated, it is said that neuron is learning and ANN is training. In a feed forward back-propagation ANN, the input data (x_i) is passed to the neurons in input layer as signal. The data is weighted in hidden layers (y_i) by associated weights in each interconnection through non-linear transfer function. The sum of weighted inputs is converted to outputs (z_i) through activation function [2].

On the other hand, support vector model (SVM) is a machine learning technique which is based on the statistical learning theory and structural risk minimization principle. The SVM uses a based quadratic programming optimization to identify model parameters, while avoiding local minima and have an advantage over other regression methods.

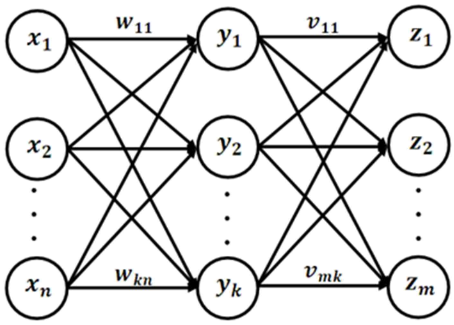

Figure 2 ANN architecture

A modified version of SVM, called the least square support vector model (LS-SVM) results in a set of linear equations instead of quadratic optimization problem [3]. A general LS-SVM architecture is as also given in Figure 3. Detailed information is given elsewhere [4-6].

In the modeling studies, adhesive weights and denim sample mechanical parameters (sett value, yarn count and weight) were selected as input and output was limited to delamination strength, air permeability and water vapour permeability parameters of laminated samples. The random 65% of the measured values were used for the training and the rest for the test. In the course of training of ANN, which was based on Levenberg–Marquardt method [7], the number of neurons in the layers, training accuracy and number of iterations were determined by using trial and error method; thus the optimum number of neurons obtained in the layers were determined as 9. For the development of the models, Neural Network Toolbox, LS-SVM Lab v1.7 and MATLAB 7.0 were used.

$$Input\ layer \begin{cases} x_i \\ x_{i+1} \\ x_{i+2} \end{cases} \rightarrow\rightarrow\rightarrow \boxed{\begin{matrix} Training\ LS\text{-}SVM\ \ with \\ optimized\ \gamma\ and\ \delta^2 \end{matrix}} \rightarrow\ y$$

Figure 3 LS-SVM architecture

Table 2 Measurement results of the samples

Property	Sample Code					
	D1	***D2***	***D1-D2 (25)****	***D1-D2 (50)****	***D1-D2 (75)****	***D1-D2 (100)****
Tensile strength [kgf]	64 (warp) 24 (weft)	67 (warp) 26 (weft)	110 (warp) 59 (weft)	102 (warp) 64 (weft)	110 (warp) 64 (weft)	112 (warp) 69 (weft)
Tearing strength [kgf]	3197 (warp) 1892 (weft)	4567 (warp) 2610 (weft)	6263 (warp) 3262 (weft)	4893 (warp) 3131 (weft)	4175 (warp) 2871 (weft)	3653 (warp) 2022 (weft)
Delamination strength [kgf]	-	-	5.56	11.67	> 20	> 20
Air permeability [mm/s]	139.08	455.65	88.85	49.83	15.20	3.95
Water resistance [mbar]	13.13	6.77	17.10	19.60	19.76	23.20
Water vapour permeability [g/m^2/day]	1061.18	956.74	929.66	776.45	570.82	193.35

*The number in brackets is the adhesive weight used to laminate D1 and D2.

The model performances were then assessed by evaluating the scatter between the experimental and predicted results via statistical parameters, that is correlation coefficient (*R*), mean absolute percentage error (*MAPE* %), and root mean square error (*RMSE*). The statistical values were determined as follows:

$$\mathrm{R} = \frac{\sum_{i=1}^{N}(\mathbf{x_i} - \bar{\mathbf{x}})(\mathbf{y_i} - \bar{\mathbf{y}})}{\sqrt{\sum_{i=1}^{N}(\mathbf{x_i} - \bar{\mathbf{x}})^2}\sqrt{\sum_{i=1}^{N}(\mathbf{y_i} - \bar{\mathbf{y}})^2}} \quad (1)$$

$$\mathrm{RMSE} = \sqrt{\frac{\sum_{i=1}^{N}(y_i - x_i)^2}{N}} \quad (2)$$

$$\mathrm{MAPE}\ (\%) = \frac{1}{N}\sum_{i=1}^{N}\left(\left|\frac{y_i - x_i}{x_i}\right|\right) \cdot 100 \quad (3)$$

where, x_i is an observed value, y_i is a simulated value, N is the number of data points, $\bar{x}$ is the mean value of observations, and $\bar{y}$ is the mean value of simulations. A higher value of the *R* and smaller values of *MAPE* and *RMSE* would indicate a better performance of the model.

3 RESULTS AND DISCUSSION

The averages of the measurements are given in Table 2. CV values [%] of the measurements were lower than 10% in all cases. Table 2 showed that increase in adhesive weight resulted trends in the properties.

The ANOVA tables are given in Table 3-10. The proposed models are given at the bottom of ANOVA tables.

Table 3 ANOVA table for tensile strength in warp direction

Source	Sum of Squares	F value	Probability > F
Model	2420.53	15.10	0.0076
A	1922.00	23.97	0.0045
A^2	498.53	6.22	0.0549
Residue	400.84		

Tensile strength (warp direction): 68.971 + 1.21 A - 7.075x10^{-3} A^2 (A: adhesive weight), Adjusted R^2: 0.8011,
Standard deviation: 8.95

Table 4 ANOVA table for tensile strength in weft direction

Source	Sum of Squares	F value	Probability > F
Model	2447.03	848.97	< 0.0001
A	0.12	0.13	0.7375
A^2	498.53	518.88	< 0.0001
A^3	128.44	133.69	
Residue	3.84		

Tensile strength (weft direction): 25.137 + 2.054 A - 0.0343A^2 + 1.813x10^{-4} A^3 (A: adhesive weight), Adjusted R^2: 0.9973,
Standard deviation: 0.98

Table 5 ANOVA table for tearing strength in weft direction

Source	Sum of Squares	F value	Probability > F
Model	5.196xE6	14.97	0.0122
A	2.104xE6	18.18	0.0130
A^2	2.964xE6	25.61	0.0072
A^3	1.731xE6	14.96	
Residue	4.629xE5		

Tearing strength (warp direction): 3929.637 + 157.51A - 3.703 A^2 + 0.02105 A^3 (A: adhesive weight), Adjusted R^2: 0.8568,
Standard deviation: 340.20

Table 6 ANOVA table for tearing strength in warp direction

Source	Sum of Squares	F value	Probability > F
Model	1.908xE6	62.35	0.0003
A	94902.72	6.20	0.0551
A^2	1.813xE5	118.49	0.0001
Residue	76522.48		

Tearing strength (weft direction): 2296.163 + 39.764 A - 0.427 A^2 (A: adhesive weight), Adjusted R^2: 0.9460,
Standard deviation: 123.71

Table 7 ANOVA table for delamination strength

Source	Sum of Squares	F value	Probability > F
Model	503.72	107.81	< 0.0001
A	495.50	212.09	< 0.0001
A^2	8.22	3.52	0.1195
Residue	11.68		

Delamination strength: -0.37371 - 0.30071 A - 9.08455 A^2
(A: adhesive weight), Adjusted R^2: 0.9683,
Standard deviation: 1.53

Table 8 ANOVA table for air permeability

Source	Sum of Squares	F value	Probability > F
Model	1.056xE5	86.21	0.0001
A	86393.09	141.00	< 0.0001
A^2	19251.07	31.42	0.0025
Residue	3063.49		

Air permeability: 287.39987 - 7.16737 A + 0.043962 A^2
(A: adhesive weight), Adjusted R^2: 0.9605,
Standard deviation: 24.75

Table 9 ANOVA table for water resistance

Source	Sum of Squares	F value	Probability > F
Model	185.23	64.54	0.0003
A	172.15	119.97	0.0001
A^2	13.07	9.11	0.0295
Residue	7.18		

Water resistance: 10.35763 + 0.23827 A - 1.14562 A^2
(A: adhesive weight), Adjusted R^2: 0.9478,
Standard deviation: 1.20

Table 10 ANOVA table for water vapour permeability

Source	Sum of Squares	F value	Probability > F
Model	7.955xE5	288.84	< 0.0001
A	7.395xE5	536.99	< 0.0001
A^2	56037.73	40.69	0.0014
Residue	6885.43		

Water vapour permeability: 1008.9712 - 0.60702 A - 0.075005 A^2
(A: adhesive weight), Adjusted R^2: 0.9880,
Standard deviation: 37.11

“The probability > F” value as recorded as input for optimization with Design Expert when it is smaller than 0.005.

Design Expert model was run to consider the highest possible property value with lowest adhesive weight as mentioned before and the result is as given in Table 11. According to Table 11, we concluded that the lowest hot melt adhesive weight in the selected denim fabrics lamination must be 37 g/m^2 to receive the highest possible property values.

The screening performances of the models are given in Table 12. The results showed that the ANN model produced *MAPE* values lower than that of the LS-SVM and *R* values were higher than 0.9 in all of the outputs. The ANN model exhibited better performance in predicting laminated fabric properties but overall evaluation demonstrated that the study performed at the laboratory scale coating/laminating machine could be predicted through the ANN or the LS-SVM modellings; thus it is concluded that the machinery meets industrial requirements of controlling and predicting concerns.

4 CONCLUSIONS

In this study, a laboratory type coating/laminating machine was developed as the first time in textile industry and the lamination of denim-denim fabric process has been optimized through statistical analysis and modelling studies by artificial neural network (ANN) and least-square support vector (LS-SVM) machine. We obtained the minimum adhesive weight to be used in the process when considering highest property values of laminated fabrics and the ANN and LS-SVM modelling study revealed that the findings were predictable and reliable. Thus we concluded that findings obtained by using the mentioned machine are applicable for industrial studies.

Acknowledgement: *This study is supported by TUBITAK under 1505 program with the contract No. 5140065.*

Table 11 Design Expert optimization

Run #	Tensile strength (weft)	Tensile strength (warp)	Tearing strength (weft)	Tearing strength (warp)	Delamination strength	Air permeability	Water vapour permeability	Adhesive weight [g/m^2]
1	100.933	63.4802	5745.19	3185.71	8.29737	60.0566	881.98	37.30
2	101.23	63.5188	5740.43	3186.91	8.34617	59.6796	881.028	37.45
3	100.838	63.4394	5750.07	3184.43	8.24663	60.4527	882.966	37.14

Table 12 Statistical parameters of the models

Output	Training set				Test set		
	Model	RMSE	MAPE [%]	R	RMSE	MAPE [%]	R
Air permeability	ANN	3.053×10^{-6}	7.96×10^{-6}	1.0000	3.7384	4.3420	0.9939
	LS–SVM	24.4744	29.07271	0.9585	29.4573	34.3360	0.9872
Water vapour permeability	ANN	1.50×10^{-9}	2.68×10^{-10}	1.0000	66.5430	3.1370	0.9804
	LS–SVM	28.0534	4.8537	0.9951	33.5706	6.0109	0.9954
Delamination strength	ANN	8.147×10^{-6}	1.33×10^{-7}	1.0000	361.316	2.989	0.9821
	LS–SVM	38.5502	0.8133	0.9998	784.960	14.512	0.8990

5 REFERENCES

1. Singha K.: A Review on coating & lamination in textile: Processes and applications, American Journal of Polymer Science 2(3), 2012, pp. 39-49, doi: 10.5923/j.ajps.20120203.04
2. Atasoy I., Yuceer M., Ulker E.O., Berber R.: Neural network based control of the acrylonitrile polymerization process, Chemical Engineering & Technology 30(11), 2007, pp. 1525-1531, DOI: 10.1002/ceat.200700225
3. Vishesh S., Manu S., Vivek A., Sumit K.S., Ashwani K.S., Vyshnav L.: Data mining and analytics: A proactive model, International Journal of Advanced Research in Computer and Communication Engineering 6(2), 2017, pp. 524-526, DOI 10.17148/IJARCCE.2017.62117
4. Vapnik V.: Statistical learning theory, John Wiley, NY, USA, 1998, ISBN-13: 978-0471030034
5. Suykens J.A.K., Vandewalle J.: Least squares support vector machines classifiers, Neural Network Letter 9(3), 1999, pp. 293-300, DOI https://doi.org/10.1023/A:1018628609742
6. Li C., Zhu X., Cao G., Suı Sh., Hu M.: Identification of the Hammerstein model of a PEMFC stack based on least squares support vector machines, Journal of Power Sources 175(1), 2008, pp. 303-316, https://doi.org/10.1016/j.jpowsour.2007.09.049
7. Iqbal J., Iqbal A., Arif M.: Levenberg–Marquardt method for solving systems of absolute value equations, Journal of Computational and Applied Mathematics 282, 2015, pp. 134-138, https://doi.org/10.1016/j.cam.2014.11.062

MECHANICAL FIXATION OF TUFTED PILE LOOPS INTO THE PRIMARY BACKING BY USING THE PARAMETERS OF FABRIC WEAVE DESIGN

Application of Newly Developed Yarn Tension Compensation Device for Tufting of Technical Yarns

Alexandra Glogowsky[1], Thomas Brunke[2], Karin Ratovo[1], Alexander Büsgen[1] and Bayram Aslan[2]

[1]Research Institute for Textile and Clothing (FTB), Niederrhein University of Applied Sciences, Mönchengladbach, Germany
[2]TFI - Institut für Bodenbeläge an der RWTH-Aachen e.V., Aachen, Germany
alexandra.glogowsky@hs-niederrhein.de, t.brunke@tfi-aachen.de

Abstract: *Tufting technology is commonly used exclusively for the production of textile floor coverings. With the e-Jerker, the TFI - Institut für Bodenbeläge an der RWTH-Aachen e.V. has developed a yarn storage element that can be parametrised and retrofitted to existing tufting machines, which allows the processing of low-stretch and high-strength pile yarns. In the future, this will enable tufting producers to offer completely new products for innovative applications in the field of technical textiles. A tufted textile is particularly suitable for applications where insulating, shielding or absorbing properties are required due to its three-dimensional pile structure. However, since the latex coatings traditionally used for securing the tufted backing are out of the question for technical applications in which high temperatures have to be considered, heat-resistant alternatives are required. In the current research project "High-Performance Tufting Structures", two alternatives were evaluated with regard to their suitability. On one hand, woven primary backing materials were developed which, in combination with the needled pile yarns, achieve the highest possible pile binding forces. This should allow the omission of coatings entirely, if necessary. On the other hand, temperature-resistant formulations for back coatings based on PU and silicone were also developed. The investigations focused on the use of glass yarns for both the primary backings and the pile yarns. In general, it can be said that both the feasibility of production and the acoustic and thermal properties of a tufted technical textile open up new application possibilities.*

Keywords: *Tufting, primary backing, technical textiles, weave design, heat-resistant coating, glass yarn.*

1 INTRODUCTION

Tufting technology is a process for the production of textile surfaces characterised by high productivity. It has been conventionally used for decades to produce textile floor coverings. A tufted product is created by needling pile yarns into a textile base material (non-woven or woven), thus creating a 3-dimensional textile with a pile-surface. In order to produce a stable and usable product, it is necessary to secure the pile to the backing using a back coating. This prevents the pile yarns from coming loose during use. Depending on the machine type and fineness, the tufted 3D structure can be very variable in terms of pile height and ranges from a few millimetres to several centimetres. Correspondingly, the overall density can also be adjusted. 85% of the yarns used to produce tufted floor coverings are synthetic bulked continuous filament yarns (possessing inherent elasticity) made from polyamide, polyester or polypropylene [1]. As only elastic pile yarns can be processed, tufting is limited to the product group of floor coverings.

Expanding the range of usable materials for tufted textiles, with their broad range of possible constructions, unlocks potential applications for technical tuftings. Due to its open pile surface, a tufted surface structure is particularly suitable for applications where insulating, shielding or absorbing properties are required. This, in combination with the use of heat-resistant materials for pile yarns and backings, allows manufacturing of tufted structures that have both high acoustic absorption and thermally shielding effects at the same time. However, since the synthetic latex coatings usually used to strengthen tufted floor coverings are thermally unstable, the only option is not to use a coating at all or, alternatively, to use temperature-resistant formulations.

Both options were investigated in the pre-competitive research project "High-Performance Tufting Structures". The absence of a backside coating to firmly bind the needled pile yarns to the primary backing means that the yarns need to be mechanically anchored in the primary backing with sufficient stability to ensure safe product use. In this project, fabrics for the primary backing were structurally optimized to exhibit the best possible pile clamping forces. For possible applications in which the pile clamping forces achievable in this way are not sufficient or a backside coating is desired, corresponding coating tests with temperature-resistant formulations were carried out.

2 WOVEN PRIMARY BACKINGS

As explained earlier, a core issue within this project is the production of a heat-resistant “primary backing”, i.e. a base fabric suitable for the tufting process. Glass fibres are the best option for a high-temperature-resistant base material for this purpose, as well as being a very economical option.

Pre-trials on different weave constructions using polyester-yarn showed that a tight construction (maximum weft density at high warp densities) as well as the use of texturized weft yarns have a major influence on the retention of tufted yarn in the finished product. Furthermore, warp backed weaves and multi-layer construction showed positive effects regarding the resulting tuft withdrawal forces [2].

The main challenge for the transfer of these results is the production of a stable and relatively tight fabric in warp-backed and double- or multi-layer construction in order to replicate the positive results of the pre-trials.

2.1 Materials and machinery

All trials were executed on a rapier loom (Dornier HTV8/S20). This machine has two warp beams (for increased flexibility regarding warp densities) and 16 shafts (+2 shafts for selvedge production).

Table 1 Materials used in pre-trials vs. experiments with glass yarn

	Code	PES-trials [2]	Glass-trials
Warp / Weft1	Y1	PES 1100dtex 200f Z60	Vetrotex EC11 204 Z28 T63C H8
Weft 2	Y2	PES 1400dtex bulked	Vetrotex ECO11 T220 T10C (voluminized)
Weft 3	Y3	PES 1400dtex air-texturized	Vetrotex ECT9 T370 T10C (air-jet texturized)
Pile Yarn	YP	HKO Thermo-E-Glass Yarn texturized ET6-300 tex x2 z100 TS	

All yarns were selected for their similarities regarding diameter and structure - however, this proved impossible (Y1, Y2, Table 1) due to the availability of certain glass yarn grades. All glass-trials were executed at a warp density of 22 ends/cm and utilized only 8 shafts.

2.2 Test Methods

On tufted samples the force needed to draw out one tuft is measured according to ISO 4919.

2.3 Experimental

Through intensive experimentation in the pre-trials [2] single layer and warp-backed weave constructions could already be eliminated from the main trials with glass yarn. Furthermore, it was found that one weave construction (weave 1, Figure 1) could not be woven with glass yarns, even if the results with PES were hopeful. This is due to the uneven distribution of interlacing points between warp yarns leading to slippage between threads and a high occurrence of warp breaks.

All weaves (Figure 1) are based on plain fabrics, with weaves 1 and 2 representing weft-backed constructions, weave 3 as a double layer fabric made up of plain weaves and weave 4 as a combination of both (one layer is a regular plain weave and one layer is weft-backed weave 2). All weaves were woven in various combinations of the threads listed in 2.1. Table 2 shows the full list of finished fabrics.

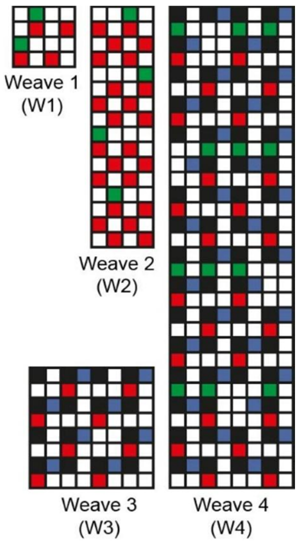

Figure 1 Weaves used in glass-trials

Table 2 List of weave / yarn combinations tested

Code	Max. weft density	
	Glass trials	PES-trials
W2_Y12	8	20
W2_Y13	7	-
W2_Y2	8	16
W2_Y3	6	-
W2_Y23	6	-
W3_Y12	11	14
W3_Y13	10	-
W3_Y2	11	14
W3_Y3	10	14
W3_Y23	10	-
W4_Y12	10	20
W4_Y2	10	20
W4_Y3	9	18

2.4 Results

Compared to the pre-trials on PES, where weft densities of up to 20 picks/cm were achieved for the same weaves, it can be seen that glass fabrics needed a lower density to be weavable, even if theoretical maximum densities should have been closer (Table 2). Nevertheless, these glass fabrics have good slippage resistance and were tufted. The respective tuft withdrawal forces are shown in Figure 2, with the grey line representing the tuft withdrawal force achieved by conventional tufting of bulked continuous filaments in non-woven primary backings.

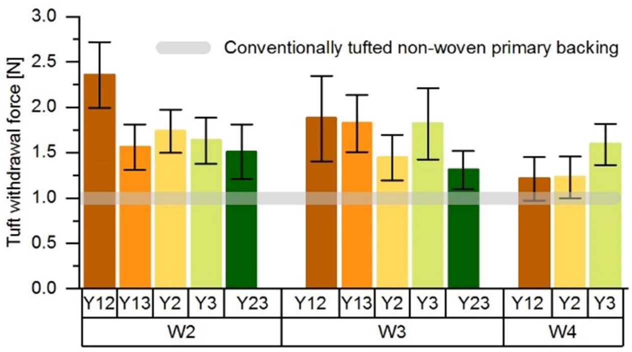

Figure 2 Tuft withdrawal forces of glass trials

2.5 Discussion

While the pre-trials gave some indication that choice of yarn and weave have a major influence on tuft retention, the glass trials do not follow these trends, as is shown in Figure 2. Furthermore, the tuft withdrawal forces do not show any relation to conventional fabric parameters such as thickness, areal weight or air permeability. Weave 4 shows remarkably low tuft withdrawal forces. However, weave W12_Y12 achieved a high tuft withdrawal force of 2.35 N, further confirming the conclusion from the pre-trials that weft-backed weaves result in high tuft withdrawal forces. This fabric will be used in further experiments. All primary backings surpass the tuft withdrawal force of conventional (raw, uncoated) tufted non-woven primary backings, thereby making it clear, that these textiles are stable enough to be manufactured into finished products.

3 TUFTING PROCESS

During tufting, many needles simultaneously stab through the primary backing at tufting cycles of up to 2000 stitches/min. The primary backing is transported by a set distance (stitch length) between each complete needle stroke. Below the primary backing, the pile yarns pierced by the tufting needles are transferred to hooks and formed into yarn loops. In the production of cut pile fabrics, the yarn loops held on the hooks are additionally cut open by knives arranged on the side of the hooks (Figure 3) [3].

A tuft cycle corresponds to a complete, vertical stroke of the needles from the top to the bottom dead center and back to the starting position. When the needle passes through the primary backing and the pile yarn is deposited on the hook, temporary deflections of the yarn feeding mechanism cause yarn consumption to vary over time. However, the vertical displacement of a standard jerker bar (horizontal perforated strip for yarn guidance), which is mechanically coupled to the lifting movement of the needles, does not permit any adjustable yarn storage. Instead, the elasticity of the yarns compensates for the difference between yarn demand and yarn supply.

3.1 Use of e-Jerker

In a previous project by the TFI-Institut für Bodensysteme an der RWTH Aachen e.V., a new yarn storage element was developed which, contrary to the method of operation described above, guarantees a programmable lateral yarn displacement and thus an optimised feeding of the pile yarns to the needles at any time during the tuft cycle [4]. The individual displacement of the pile yarns is effected by a servomotor drive of the e-Jerker. This was used in the project described in this paper in order to enable the use of glass fibres, which are non-elastic.

The programming of the e-Jerker is carried out for each new pile yarn individually to customize processing. For this purpose the variation in yarn feed tension during a single tuft is measured over several tufting cycles using a laser sensor that makes it possible to correlate yarn demand at a given point in the tuft cycle with the corresponding position of the needle.

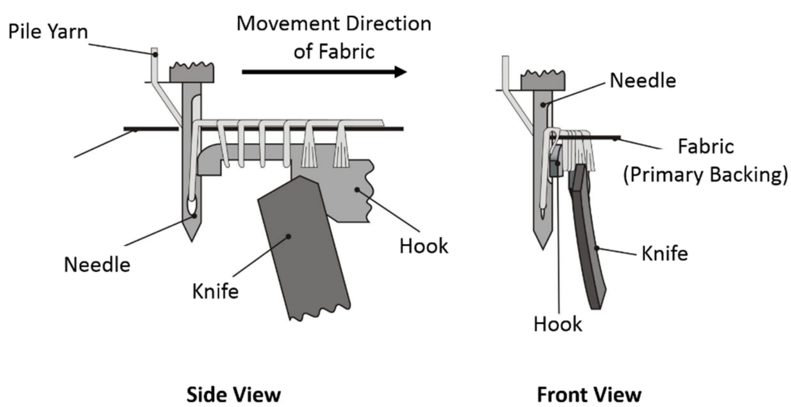

Figure 3 Tufting mechanism for pile fabrics

The motion profile is logged continuously, producing a typical curve which reflects the yarn requirement of this pile yarn for a tuft cycle (Figure 4). The angular positions shown in Figure 4 correspond to the following needle positions during a tuft cycle:

- 0° or 360° Needle at top dead center
- 90° Needle eye at the level of the primary backing
- 90° - 180° Needle to bottom dead center
- 180° - 270° Transfer of the loop to hook

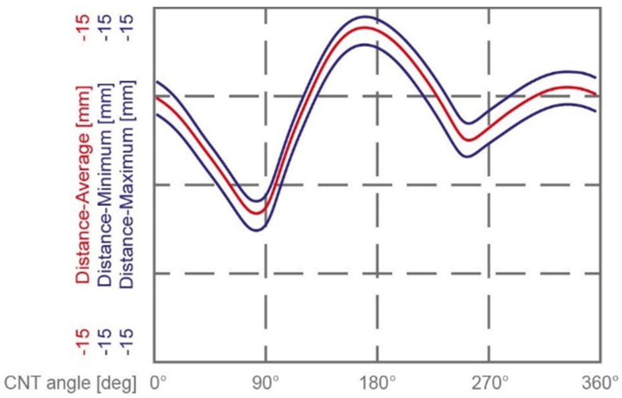

Figure 4 Typical yarn displacement during tufting cycle

The simultaneous video-assisted observation of the tufting tools then allows a precise analysis of any errors or inadequacies during yarn transfer or take-up between needles and hooks. This way it can be decided whether more or less yarn should be delivered from the needles to the hooks at any given time to ensure optimum pile loop formation at all points in the tuft cycle. The adjustment is made by changing splines in the recorded movement curve at those points where errors or inadequacies have been observed in relation to the position of the tufting tools. A motion curve manipulated in this way can then be read into the servomotor control of the e-Jerker as a yarn-specific reference curve.

3.2 Materials and machinery

In the manner described above, mainly glass yarns were measured and their processability in combination with the developed glass fabrics tested. In addition, further tests have shown that low-stretch pile yarns made of aramide, basalt or steel fibres can also be tufted by programming the yarn storage behaviour using the e-Jerker. In addition to the pile yarns mentioned above and the glass fabrics that were investigated in detail, the feasibility of using high-strength aramid fabrics as primary backings for tuftings could also be confirmed. In order to achieve different material finenesses and surface characteristics, test goods were produced on tufting machines of different designs. Cutting and looping machines with machine gauges of 1/10 inch and 1/8 inch were used.

4 HEAT-RESISTANT COATINGS

As the goal of a tuft withdrawal force higher than 7N cannot be reached by weave construction alone, a coating with comparable heat resistance is necessary for sufficient tuft retention. The main demands are avoidance of halogenated flame-retardants, improved mechanical stability of the glass fibre fabric after direct contact to flames, limited smoke emission and good coating behavior.

4.1 Materials

In order to achieve different draping behaviors, two different matrix-systems were considered: Polyurethane dispersions for a stiffer fabric and 2K-silicone for a softer drape. The flame retardants tested are shown in Table 3.

4.2 Test method

In order to test the coating resistance against direct contact to flames, testing according to ISO 15025 was considered, but no differences regarding coating performance were observed. Therefore a non-standardized method utilizing a Bunsen-burner and an infrared camera was developed (Figure 5).

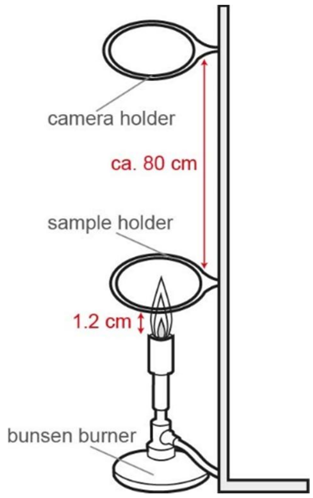

Figure 5 Test set-up for burn tests

The main criteria are burning behavior, smoke generation and fibre damage after burning. The infra-red videos can be used supplementally to gain more information on heat dissipation, especially in tufted fabrics. The camera used is a FLIR ONE thermal imaging camera. Figure 4 shows a sketch of the test set-up. The textile is placed coated side down on the sample holder and exposed to the flame for 12 seconds. The time and distance to the flame was set so that an uncoated fabric shows distinct signs of melting and a high degree of fibre damage, making it possible to observe the influence of the coatin

4.3 Experimental

The following recipes were tested and evaluated for the criteria listed below:

Table 3 Coating formulations (% of dry weight) using different matrix materials, coating and burning behavior

Sample no.	2a	2b	2c	3a	3b	4a	4b	5a	5b	5c	6a	6b	6c
PU1	x			x		x		x	x	x			
PU2		x			x								
2K-silicone			x				x				x	x	x
Ammonium polyphosphate (APP)	15	15	15	15	15	15	15	15	15	15	15	7.5	7.5
Aluminium-pigment	5	5	5	5	5	2.5	2.5	5	5	2	2.5	2.5	2.5
Dipentaerithriol	5	5	5	5	5	5	5	5	5	5	5	2.5	2.5
Melamine						5	5	5	5	5	5	2.5	2.5
Aluminiumtrihydrate (ATH)								7.5	7.5	7.5	7.5	7.5	7.5
Vermiculite (dispersion)				7	7								
Bentonite									1	1			1
Coating	+/-	+	-	+/-	+/-	+/-	-	--	-	+/-	--	+/-	+/-
Burning	+	+/-	+/-	-	+	+/-	+/-	--	+/-	--	No test	+/-	+/-
Smoke	-	-	-	+/-	+	+/-	-	--	-	--		+/-	+/-
Fabric damage	--	+	++	+	+	+/-	++	+/-	+/-	-		+	++

4.4 Results

It can be seen that in general coating behavior proved a bigger problem for the silicone-based recipes (Table 3), as for this product it is not possible to influence viscosity. Regarding smoke generation, silicone formulations in general produced smokier outcomes with little influence of the flame retardant combination used. However, while all PU-based samples are stiff, silicone-coatings retain their drapeability.

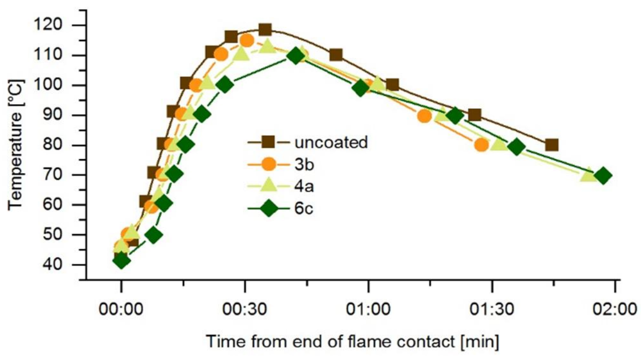

Figure 6 Effect of coating on surface temperature

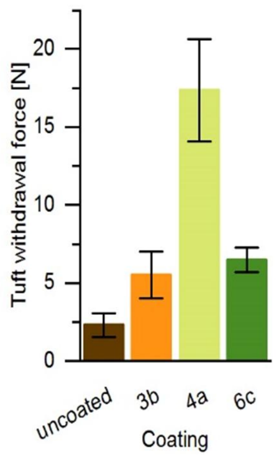

Figure 7 Tuft withdrawal force after coating

Formulations 3b, 4a and 6c were further evaluated for their coating behavior on tufted sample W2_Y12. The results of the infra-red camera reading are shown in Figure 6. Figure 7 shows the improvement of tuft withdrawal force that can be achieved with each formulation.

4.5 Discussion

Regarding coating performance it was found that certain coating formulas can achieve a good stability against open flames in regard to burning behavior as well as fibre damage. This subjective rating is corroborated by the measurements using an infra-red camera (Figure 6). It can be seen, that the surface of coated textiles does not get as hot as an uncoated sample, presumably due to the cooling and insulating effect achieved by flame retardants as well as heat reflection from the aluminium-pigment. However, on tufted samples there are big differences between the coatings tested regarding tuft withdrawal force after coating, so that a compromise needs to be made between good drapability and high tuft retention. The goal of a tuft withdrawal force >7N could only be achieved using a PU-based coating.

5 ACOUSTIC PROPERTIES

In order to check the acoustic properties, samples were tested using an impedance tube in accordance with EN ISO 10534-2. The sound absorption coefficient serves as a measure for the improvement of acoustics in a room. Samples tufted with the reference pile yarn (YP) on three different glass fabrics were compared. The coatings, regardless of matrix material, compared to the corresponding uncoated fabrics. All measurements show sound absorption levels similar to or slightly better than those of tufted floor coverings. Since the selected test products are constructions similar to those of tufted floor coverings, it can be concluded that the materials used for primary backings and pile yarns have no significant influence on the sound absorption coefficient. A comparison of the coated variants with the uncoated references does not show a uniform picture or a significant difference. Further tests with constructive modifications (pile height, pile density) for further improvement of acoustic properties are planned.

6 CONCLUSION AND OUTLOOK

It could be shown during this project that it is possible to produce primary backings for tufted textiles from glass yarns. The tuft withdrawal forces achieved using weft-backed weave constructions are higher than those of conventional (uncoated) tufted fabrics, allowing for further processing. Further, it was proven that tufting with glass yarn in the pile is feasible. The benefit of the retrofittable e-Jerker for the production of tuftings from technical yarns is evident in practical use. Furthermore, coatings developed for direct contact with flames improve heat-stability as well as mechanical properties of the tufted fabrics, allowing for a broad spectrum of applications. Lastly, the sound absorbing qualities of a tufted glass fabric were investigated and it could be shown that neither yarn material nor coating change the good acoustic properties known from conventional floor coverings.

In conclusion, both the feasibility of production as well as the acoustic and thermal properties of a tufted technical textile open possibilities for new applications. The fields currently considered for potential industrialization are lightweight building materials for passive fire safety as well as acoustic insulation for industrial machinery.

Acknowledgement: *The IGF project AiF-Nr. 19050N of the research association Forschungskuratorium Textil e. V. was financed by AiF as part of the Industrial Collective Research Programme by the Federal Ministry for Economic Affairs and Energy, based on a decision of the German Bundestag. The final report can be accessed publicly.*

Gefördert durch:

iGF Industrielle Gemeinschaftsforschung

Bundesministerium für Wirtschaft und Technologie

aufgrund eines Beschlusses des Deutschen Bundestages

7 REFERENCES

1. Kwoczek K.: Die Verarbeitung technischer Garne in der Tuftingtechnik, Tuftingtechnik [Processing of Technical Yarns in Tufting Technology], Diploma Thesis, University of Applied Sciences Niederrhein, Mönchengladbach, 2011
2. Glogowsky A., Gsell E., Brunke T., Büsgen A.: Glasfasertuftings als eine neue Art technischer Textilien [Glass-Fiber-Tuftings as a New Type of Technical Textile], In: Technologievorsprung durch Textiltechnik, Förderverein Cetex Chemnitzer Textilmaschinen e.V., Chemnitz, 2018, pp. 46-54
3. Brunke T., Lempa E., Rabe M., Winkler J.-C.: Dessinierung multistruktureller Tufting-konstruktionen mittels eines optimierten Spritzdruckverfahrens (AiF 15954) [Patterning of Multi-Structural Tufting Constructions via Optimized Spray-Printing Method (AiF 15954)], Schriftenreihe des TFI – Deutsches Forschungsinstitut für Bodensysteme e.V., No. 2011/96, 2011
4. Goetz C., Hanuschik D., Schröder E.: Erweiterung des Anwendungsgebietes der Tuftingtechnik durch den Einsatz einer elektronisch gesteuerten Jerkerbarre (AiF 16678) [Expansion of the Field of Application for Tufting Technology by Utilization of an Electronically Controlled Jerker-Bar (AiF16678)], TFI-Schriftenreihe, No. 2013/98, 2013

APPLYING THE ARTIFICAL NEURAL NETWORK TO PREDICT THE THERMAL PROPERTIES OF KNITTED FABRICS

Sinem Güneşoğlu[1] and Binnaz Kaplangiray[2]

[1]*Gaziantep University, Textile Engineering Department, Gaziantep, Turkey*
[2]*Uludag University, Textile Engineering Department, Gaziantep, Turkey*
sgunesoglu@uludag.edu.tr

Abstract: *Fabric thermal properties have been of great interest and importance for textile researchers, since they are among the major characteristics that determine wearing comfort. In this study, thermal conductivity and thermal contact properties of a large number of knitted fabrics were measured instrumentally and a learning group was proposed to train the artificial neural network (ANN) algorithm and then prediction was achieved with a strong regression coefficient. Therefore it is concluded that it was possible to predict thermal properties of knitted fabrics by using basic fabric properties as input.*

Keywords: *Thermal conductivity, warm-cool feeling, ANN.*

1 INTRODUCTION

Traditionally, most measurements of fabric thermal properties were conducted in a state of equilibrium (steady-state), analyzing such easily measured properties as thermal conductivity. Thermal conductivity is a familiar term applied to materials that conduct heat and it is defined as the heat flux divided by the temperature gradient where heat is transferred by conduction. However, the steady-state measurements cannot solely explain the heat-related subjective sensations that determine human comfort, because this approach does not reflect the real wearing situation, since the human body interacts dynamically with clothing. Sudden mechanical contact of textile fabric with human skin causes feeling of warmth or coolness due to the heat flow from human body to the fabric that is at a lower temperature than the skin surface. This dynamic- or transient-state thermal contact property, which is so called thermal absorptivity, is included in the overall assessment of the comfort of textile fabrics. Since both steady and dynamic- state measurements strongly affect the choice of people when buying the clothes or garments, there is an interest in predicting thermal properties of textile fabrics before they are submitted to customers and determining the relations between thermal properties and fabric structural properties [1, 2]. The artificial neural network (ANN) may be an efficient tool for predicting the thermal properties of knitted fabrics.

An ANN is an information processing system that roughly replicates the behavior of a human brain by emulating the operations and connectivity of biological neurons [3]. It performs a human-like reasoning, learns the attitude and stores the relationship of the processes on the basis of a representative data set that already exists. In general, the neural networks do not need much of a detailed description or formulation of the underlying process and thus appeal to practicing engineers who tend to mostly rely on their own data [4-7]. Recently, neural networks have been successfully applied to process modelling and control of textile surfaces [8-11].

A typical ANN has feed forward architecture and consists of three or more layers of neurons: one input layer, one output layer and one or more hidden layers (Figure 1). Each of the layers has a set of connections, with a corresponding scalar weight, between itself and each neuron of preceding layer. When the weight of a particular neuron is updated, it is said that neuron is learning and ANN is training. In a feed forward back-propagation ANN, the input data (x_i) is passed to the neurons in input layer as signal. The data is weighted in hidden layers (y_i) by associated weights in each interconnection through non-linear transfer function. In addition, a bias can also be used, which is another parameter that is summed with the neurons weighted inputs. The sum of weighted inputs is converted to outputs (z_i) through activation function (Net_j). The outputs can be defined as:

$$\mathrm{z} = f\left(Net_j\right) \tag{1}$$

where:

$$\mathrm{Net_j} = \sum w_i\, x_i + b \tag{2}$$

and where x_i and w_i are the input data and weightings of neuron, b is the bias and $f(\ldots)$ is the activation function.

The most common used activation functions in ANN architectures are linear (*purelin*) and sigmoid (*logsig*) transfer functions. A transfer function determines the relationship between inputs and outputs of a neuron and a network. Selection of transfer function for layers is an important parameter. The best structure of transfer functions is evaluated on the basis of mean square error (MSE) of the training data set. *logsig* function produces outputs in the range of 0 to 1 and it can be defined as:

$$f(Net_j) = \frac{1}{1+e^{-Net_j}} \tag{3}$$

where *purelin* function produces outputs in the range of -∞ and +∞ and can be defined as:

$$(Net_j) = Net_j \tag{4}$$

In this study, the optimum configuration is achieved by using *logsig* transfer function in output and hidden layers.

This study aims to use the ANN with a feed-forward back-propagation learning algorithm for the prediction of thermal conductivity (steady-state) and thermal absorptivity (dynamic-state) properties of knitted fabrics. The results were found to be compatible for prediction of thermal properties of the knitted fabrics by using basic fabric properties as input.

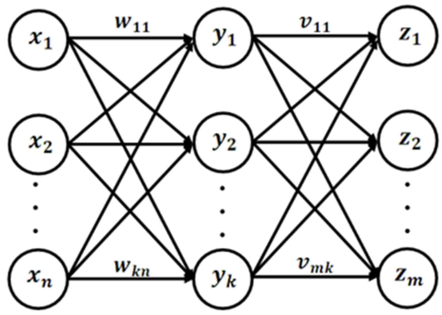

Figure 1 ANN architecture

2 EXPERIMENTAL

2.1 Materials

Knitted fabric samples with various constructions in ready to apparel conditions were supplied by various suppliers. The constructional details of the samples are given in Table 1.

Table 1 Some details of the samples

Sample	Weave type	Yarn type and count	Weight [gr/m^2]	Thickness [mm]
RL1	RL supreme	95% Polyamide (78/23 dtex), 5% elastane (33 dtex)	198.4	0.53
RL2	RL supreme	95% Polyamide (78/23 dtex), 5% elastane (33 dtex)	205.5	0.54
RL3	RL supreme	95% Polyamide (78/68 dtex), 5% elastane (33 dtex)	210.2	0.47
RL4	RL supreme	95% Polyamide (78/68 dtex), 5% elastane (33 dtex)	226.6	0.47
RL5	RL supreme	95% Polyester (100/36 Denier) , 5% elastane (40 Denier)	101.2	0.6
RL6	RL supreme	100% Polyamide (150/136 Denier)	169	0.43
RL7	RL supreme	95% Polyester (100/136 Denier), 5% elastane (40 Denier)	189.6	0.83
RL8	RL supreme	100% Polyamide (70/68/2 Denier)	212	0.45
RL9	RL supreme	30% Polyamide (70/46 Denier) 70% Cotton (Ne 40/1)	185	0.69
RL10	RL supreme	100% Polyester (70/46/1 Denier)	99	0.56
RL11	RL supreme	86% Polyamide (110 dtex), 14% elastane (44 dtex)	240	0.72
RL12	RL supreme	93% Polyamide (156 dtex) 7% elastane (22 dtex)	220	0.48
RL13	RL supreme	84% Polyamide (78 dtex), 16% elastane (44 dtex)	160	0.47
RL14	RL supreme	100% Cotton (Ne 30/1)	200	0.66
RL15	RL supreme	95% Cotton (Ne 30/1), 5% elastane (20 Denier)	193.5	0.77
RL16	RL supreme	95% Viscone (Ne 20/1), 5% elastane (20 Denier)	263.7	0.69
RR1	RR ribana	95% Poylamide (150/140 Denier), 5% elastane (20 Denier)	269.7	0.76
RR2	RR ribana	100% Polyester (90/36 Denier)	95.6	0.57
RR3	RR ribana	95% Cotton (Ne 30/1) 5% elastane (20 Denier)	228.6	1.14
RR4	RR ribana	100% Cotton (Ne 24/1)	284	0.97
RR5	RR ribana	100% Vsicone (Ne 28/1)	220	0.88
RR6	RR interlock	100% Polyamide (78/23 dtex)	175.6	0.99
RR7	RR interlock	100% PA (78/23 dtex)	186.7	1.01
RR8	RR interlock	%50% Polyamide (78/23 dtex), 50% Cotton (Ne 30/1)	186.3	1.14
.RR9	RR interlock	100% Polyamide (78/23 dtex)	173.9	0.87
RR10	RR interlock	100% Polyester (75/34 Denier)	124.2	0.41
RR11	RR interlock	96% Polyester (70/46 Denier), 4% elastane (22 dtex)	150	0.81
RR12	RR interlock	55% Polyamide (70/46 Denier), 45% Cotton (Ne 30/1)	200	1.03
RR13	RR interlock	100% Cotton (Ne 30/1)	235.9	1.08
RR14	RR interlock	53% Viscone (120 denier) 47% Polyester (100 Denier)	253	0.71
RR15	RR interlock	100% Polyester (180 Denier)	324.9	1.0
RR16	RR interlock	50% Polyester (190 Denier), 50% Viscone (Ne28/1)	217.5	0.98
AS1	RL 2-yarn fleece	100% Cotton (Ne 20/1) (out), 100% Cotton (Ne 10/1) (in)	302.7	1.25
AS2	RL 2-yarn fleece	100% Polyester (Ne 20/1) (out), 100% Polyester (Ne 10/1) (in)	313	1.15
AS1R	RL 2-yarn fleece	100% Cotton (Ne 20/1) (out), 100% Cotton (Ne 10/1) (in – raised)	273.8	1.76
AS2R	RL 2-yarn fleece	100% Polyester (Ne 20/1) (out), 100% Polyester (Ne 10/1) (in - raised)	295.5	1.37

2.2 Methods

Thermal conductivity and thermal absorptivity of the samples were measured by the ALAMBETA instrument as described before [1]. All the measurements were completed in an uncontrolled laboratory environment of about 24°C and 55% R.H. and repeated for three times. The mean of three measurements was taken as data. The measuring head temperature of the ALAMBETA was approximately 32°C, and the contact pressure was 200 Pa in all cases to simulate the pressure of a finger on a fabric [1].

A three-layered (one input, one hidden and one output layer) feed-forward and back-propagation algorithm was chosen for the ANN model. For the development of the ANN model, CORTEX 3.0 was used. The output data for the ANN were thermal conductivity and thermal absorptivity and the input data were selected as fabric weight, fabric thickness, fabric density (determined as fabric mass divided by fabric thickness), fiber density and fiber conductivity as given in [12] and package factor (determined as fabric density divided by fiber density). For the samples which have more than one fiber type, fiber density and fiber conductivity values were calculated by using Equation (5):

$$Property_{A/B} = (Volume\ ratio_{A})x(Property_{A}) + (Volume\ ratio_{B})x(Property_{B}) \quad (5)$$

The output data were divided into training and test sets randomly (accomplished by the modelling software) The 16 data was used for training and the rest was used for the test set. In the course of training, which was based on Levenberg - Marquardt method [13], the number of neurons in the layers, training accuracy and number of iterations were determined by using trial and error method; thus the optimum number of neurons obtained in the layers were determined as 6. Mean square error (MSE) value was calculated around 0.01 for 210000 epochs. All data were normalized to be between 0 - 1 using Equation (3) in order to increase accuracy of both models and prevent any parameter from dominating the output. The output data were later de-normalized after the actual application in the models. Finally, the ANN model was applied to all sample inputs.

3 RESULTS AND DISCUSSION

The data obtained from both the ALAMBETA and the ANN were given in Figure 2. It is seen that the ANN model gave reliable results in predicting the thermal properties of knitted fabrics. The regression coefficient between ALAMBETA and ANN data were 0.916 and 0.937 for thermal conductivity and thermal absorptivity, respectively.

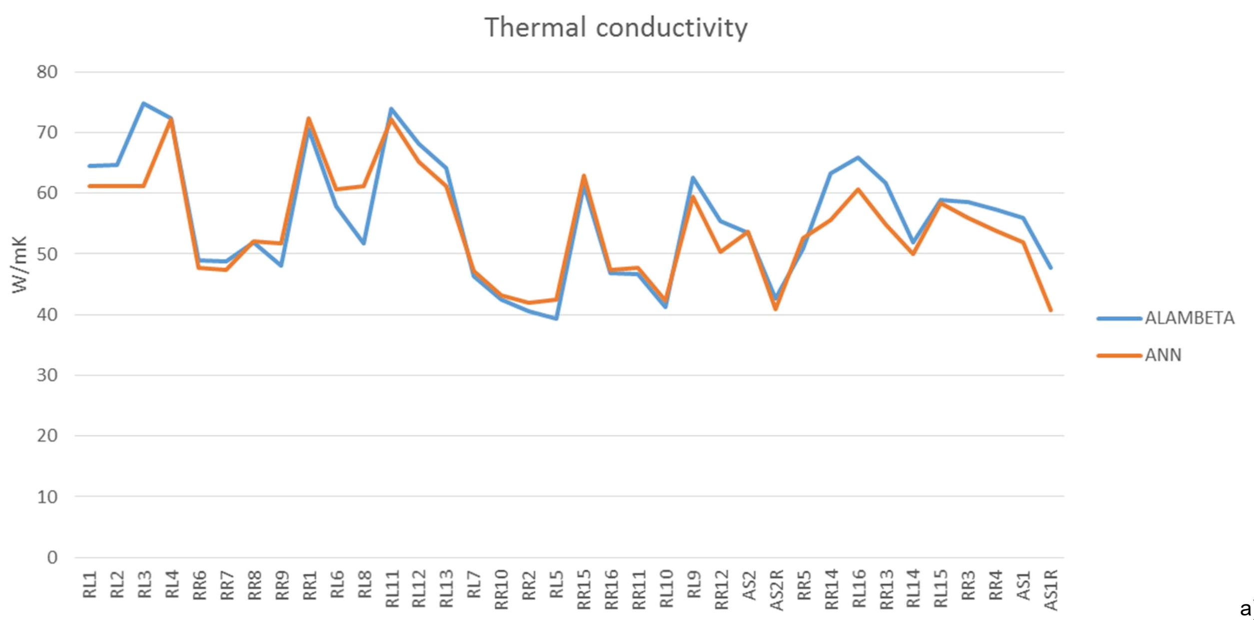

a)

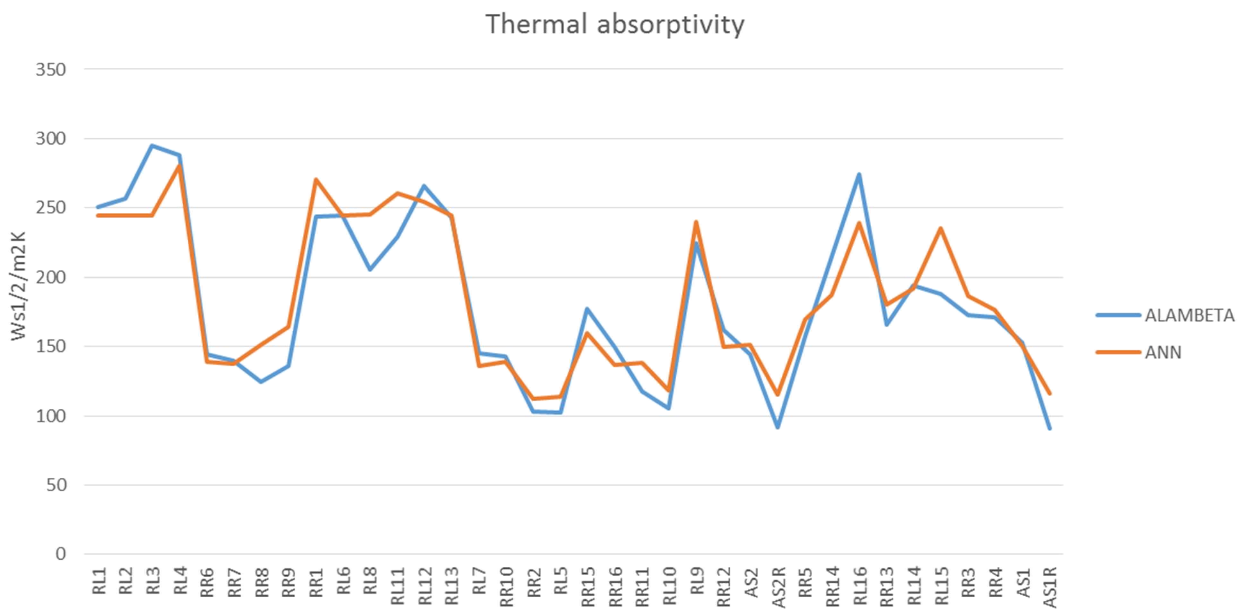

b)

Figure 2 The ALAMBETA and the ANN data for a) thermal conductivity and b) thermal absorptivity of the samples

4 CONCLUSION

In this paper, thermal conductivity and thermal absorptivity of various knitted fabrics were first measured instrumentally by the ALAMBETA and via using the results as output data; an ANN model was applied to predict the thermal parameters of those fabrics. In this case, basic properties which are easily measured and/or found in the literature were used as input. The study showed that the ANN model would be used to predict thermal properties of knitted fabrics by using basic fabric properties without an instrumental measurement.

5 REFERENCES

1. Gunesoglu S., Meric B., Gunesoglu C.: Thermal contact properties of 2-yarn fleece knitted fabrics, Fibers & Textiles in Eastern Europe 13(2), 2005, pp. 46-50
2. Güneşoğlu S.: An investigation of comfort properties of sportwear clothings, PhD Thesis, Uludag University, 2005
3. Golden R.M.: Mathematical methods for neural network analysis and design, MIT Press, USA, 1996, ISBN:0262071746
4. Hand J.W.: Modelling the interaction of electromagnetic fields (10 MHz–10 GHz) with the human body: methods and applications, Physics in Medicine and Biology 53(16), 2008, pp. 243-286, https://doi.org/10.1088/0031-9155/53/16/R01
5. Mujtaba I.M., Aziz N., Hussain M.: A. neural network based modelling and control in batch reactor, Chemical Engineering Research and Design 84(8), 2006, pp. 635-644, https://doi.org/10.1205/cherd.05096
6. Khataee A.R., Dehghan G., Zarei M., Ebadi E., Pourhassan M.: Neural network modeling of bio treatment of triphenylmethane dye solution by a green macroalgae, Chemical Engineering Research and Design. 89(2), 2011, pp. 172-178, https://doi.org/10.1016/j.cherd.2010.05.009
7. Atasoy I., Yuceer M., Ulker E.O., Berber R.: Neural network based control of the acrylonitrile polymerization process, Chemical Engineering & Technology 30(11), 2007, pp. 1525-1531, https://doi.org/10.1002/ceat.200700225
8. Jeong S.H., Kim J.H., Hong C.J.: Selecting optimal interlinings with a neural network, Textile Research Journal 70(11), 2001, pp. 1005-1010, https://doi.org/10.1177/004051750007001111
9. Parki K.C., Kang T.J.: Objective rating of seam pucker using neural networks, Textile Research Journal 67(7), 1997, pp. 494-502, https://doi.org/10.1177/004051759706700704
10. Abd Jelil R., Zeng X., Koehl L., Perwuelz A.: Modeling plasma surface modification of textile fabrics using artificial neural networks, Engineering Applications of Artificial Intelligence 26(8), 2013, pp. 1854-1864, https://doi.org/10.1016/j.engappai.2013.03.015
11. Matusiak M.: Application of artificial neural networks to predict the air permeability of woven fabrics, Fibers & Textiles in Eastern Europe 23(1), 2015, pp. 41-48
12. Warner S.B.: Fiber Science, Prentice Hall, NJ, USA, 1995, ISBN 0024245410 9780024245410
13. Iqbal J., Iqbal A., Arif M.: Levenberg–Marquardt method for solving systems of absolute value equations, Journal of Computational and Applied Mathematics 282, 2015, pp. 134-138, https://doi.org/10.1016/j.cam.2014.11.062

EXPERIMENTAL TESTING AND FINITE ELEMENT SIMULATION OF TH-7 BENDING TEST OF SPORTS BRA TEXTILES

Michaela Hassmann[1] and Wolfgang Krach[2]

[1]*University of Vienna, Institute of Sport Science, Vienna, Austria*
[2]*CAE Simulation & Solutions GmbH, Vienna, Austria*
michaela.hassmann@univie.ac.at

Abstract: *The measurement of mechanical properties of textiles is essential for Finite Element (FE) simulation and virtual garment try-on software. For the determination of bending, the TH-7 device, developed by Technical University of Liberec, Faculty of Textile Engineering, was used. It offers testing of specimens in different shapes. Circular shaped specimens with a diameter Φ = 5 cm were cut from three fabrics used in the Anita momentum sports bra. These specimens were subjected to the bending test in directions from 0° to 360° turned by every 22.5° both up and down. The shape of the specimen during testing was recorded using video. From the measured bending force F_m [mN] the bending rigidity B [Nm^2/m] was calculated as described in literature. The value of bending rigidity was verified in FE simulation of TH-7 bending test by comparing resulting specimen shape and bending force. None of the bending tests proposed in literature seems to provide correct values for Young's modulus E, whereas the simulation of non-linear behaviour requires a more complex approach of piecewise linear modelling.*

Keywords: *bending force, bending rigidity, material properties, knitted fabrics, anisotropy.*

1 INTRODUCTION

Bending rigidity is an important mechanical property of textile fabrics. Therefore, several different procedures and devices for measuring bending behaviour have been proposed in literature. ASTM D1388 proposes the Cantilever test (Option A) and Heart Loop test (Option B) [1] which both subject the specimens to their own weight. They provide limited information about the mechanical behaviour due to the fixed amount of bending and, moreover, they don't include force measurement. The KES-FB (Kawabata Evaluation System) pure bending tester suggests that the fabric is subjected to bending only, which is not thoroughly correct in case of horizontal clamping of fabric. In addition, this device is rather expensive [2]. Yet, the advantage over Cantilever and Loop tests is the ability to detect the non-linear bending behaviour by measuring the relationship between bending momentum and curvature [2]. In the Czech standard ČSN 80 0858 "Testing of stiffness and resiliency of textile fabrics" a similar bending tester is used [3]. The TH-7 bending tester is a much cheaper and more practical device, as it allows the measurement of small specimens in both bending directions (up and down) in one cycle, directly providing bending hysteresis. In addition, good correspondence to the KES-FB was proven [4].

In sports bras, mainly knitted fabrics are used for the construction of cups and wings. The loop structure of knitted fabrics leads to an anisotropic, usually orthotropic, mechanical behaviour, which has to be taken into account when choosing the direction in which the fabrics are sewn. Due to the assumption of orthotropic behaviour, material properties of knitted fabrics have to be tested in several directions. The idea of using circular shaped specimens was first mentioned by Peirce [5]. Circular shape has the advantage of reducing curl and moreover the benefit that the stiffness can be measured in any direction using only one specimen. This significantly reduces the amount of required specimens compared to using rectangular ones [4].

2 EXPERIMENTAL

2.1 Specimens

Fabric samples of the required size of the Anita momentum sports bra were available for the wing (5), cup (6) and cup liner (7) fabric (see Figure 1).

Loop structure was analysed under the microscope to determine the type of knitting for each sample. Wing fabric (5) is a single layered warp knit mesh with fillet, three guide bar structure (one elastan thread) (see Figure 2a). Cup fabric (6) is double layered, the outer layer is a 2 layer rip structure (weft knit with tuck) and the inner layer is standard plush to make the cup more comfortable (see Figure 2b). Cup liner fabric (7) is double layered, with locknit (charmeuse) outer layer and tricot inner layer to provide high strength in machine direction (see Figures 2c and 2d).

Figure 1 Unstitched Anita momentum sports bra, machine direction of samples indicated by arrow

From these three samples, three circular shaped specimens each with a diameter Φ = 5 cm were cut. The specimens were marked with lines at every 22.5° with the machine direction as 0°.

Thickness was measured according to EN ISO 5084 [6] and density was calculated as weight per unit area divided by thickness (see Table 1).

2.2 Experimental TH-7 bending test

The circular shaped specimens were clamped in the TH-7 bending tester (see Figure 3). Measuring range was set to 40 mN. For each direction, 10 cycles of 90° up and down bending were performed and filmed to analyse the deformed shape during the bending test.

The measured bending force F_m [mN] was output as mean value for the 10 cycles and averaged for three specimens per sample, for each direction as well as up and down separately. This bending force can be converted into the bending rigidity B [Nm^2/m] (1), where sample width s = 50 mm and the constant κ = 0.0334 [m²] as described in [4]. Instead of bending rigidity of unit width B [Nm^2/m], bending rigidity for sample width B_s [Nm²] (2) was used for further calculations:

$$B = \kappa \cdot \frac{F_m}{s} \tag{1}$$

$$B_s = \kappa \cdot F_m \tag{2}$$

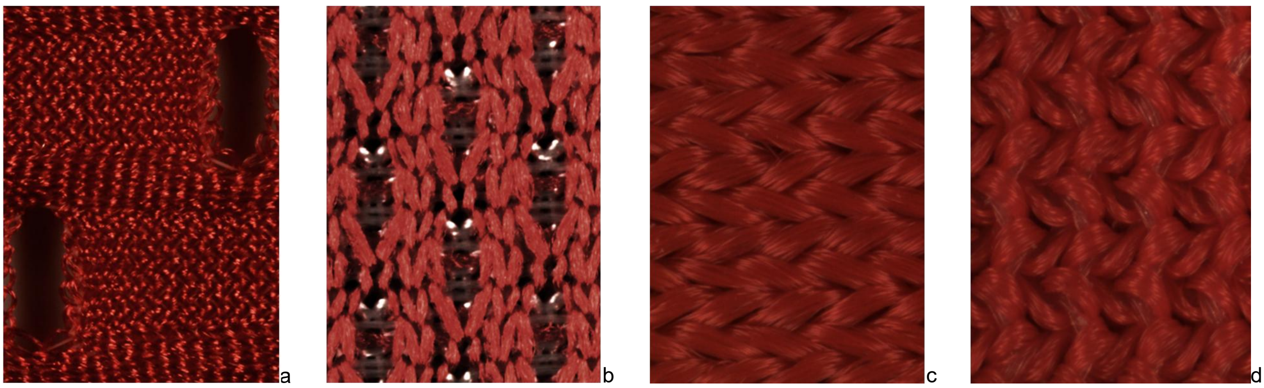

Figure 2 a) Sample 5 (back) b) Sample 6 (face) c) Sample 7 (inner layer, face) d) Sample 7 (outer layer, face); machine direction up

Table 1 Specifications of sports bra samples

sample	description	weight per unit area M [g/m²]	thickness T [mm]	density ρ [t/mm³]
5	wing	245.8	0.85	$2.892 \cdot 10^{-10}$
6	cup	266.3	1.25	$2.131 \cdot 10^{-10}$
7	cup liner	367.4	1.00	$3.674 \cdot 10^{-10}$

Figure 3 Specimen clamped in the TH-7 bending tester, front and side view

2.3 FE-modelling of TH-7 bending test

FE models were pre-processed in MSC Patran 2016. The fabric was modelled as a semi-circle corresponding to the free bending length of the sample in the test using standard PSHELL shell formulation with linear CQUAD4 and CTRIA3 elements. The sensor jaws were modelled as half cylinders fixed to one node by RBE2 constraints (see Figure 4).

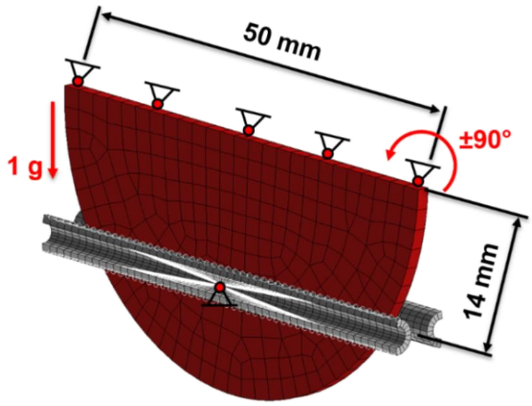

Figure 4 FE model of TH-7 bending test (shell thickness display) with boundary conditions and load case

Linear elastic material MAT1 for course fitting and stress-dependent MATS1 for piecewise linear fitting were assigned to the fabric. Considering the bending rigidity of a thin structure being the product of Young's modulus *E* and area moment of inertia *I* [mm^4] (3, 4), Young's modulus *E* [MPa = N/mm²] can be derived from the bending rigidity for sample width B_s [Nm²] calculated from the experimental TH-7 bending and from the measured thickness *T* [mm] of the sample (5).

$$B_s = E \cdot I \tag{3}$$

$$I = \frac{s \cdot T^3}{12} \tag{4}$$

$$E = \frac{12 \cdot \kappa \cdot F_m}{s \cdot T^3} \tag{5}$$

Poisson ratio *v* was used from previously performed tensile test. For the Teflon sensor jaw properties were assigned, including a friction coefficient μ = 0.05 in the fabric-jaw contact. The clamped top row of nodes of fabric was rotated by ±90° in steps of 2° in accordance with the TH-7 measurement procedure. Inertial load was included to account for the influence of gravity. The solver MSC Nastran Implicit Nonlinear analysis (SOL 400) was used for achieving the numerical results.

3 RESULTS AND DISCUSSION

3.1 Experimental TH-7 bending test

Textiles usually exhibit hysteresis behaviour under bending loading, which can be measured when bending the specimen consequently in both directions. Figure 5 shows exemplarily the hysteresis loop for sample 6 obtained by TH-7 bending test at 0° orientation as the arithmetic mean of 10 cycles averaged for three specimens.

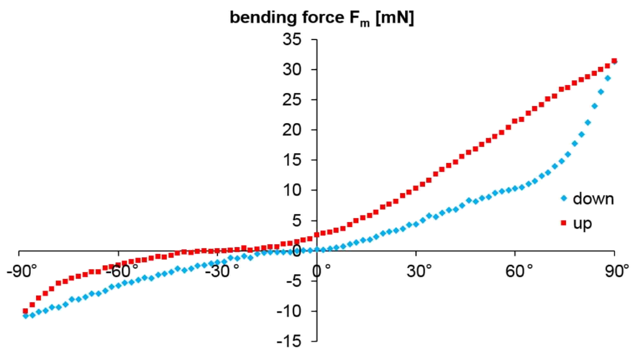

Figure 5 Hysteresis loop obtained by TH-7 bending test (sample 6, degree 0° = machine direction)

The anisotropic mechanical behaviour obtained by subjecting the same specimen to bending in several directions can be evaluated and depicted in a polar diagram.

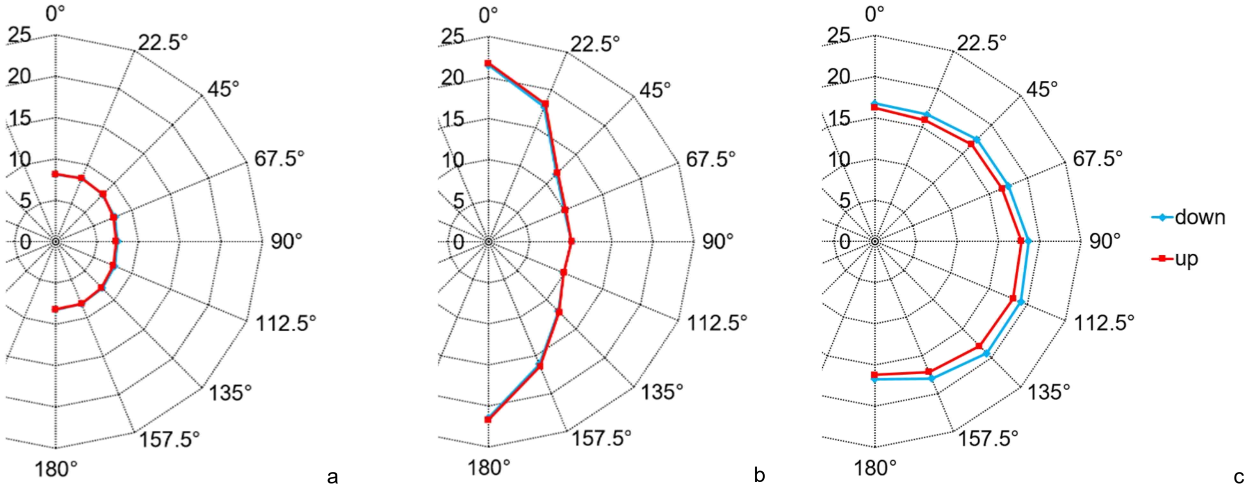

Figure 6 Polar diagram of bending rigidity *B* [Nm²/m] at +90° bending a) Sample 5 b) Sample 6 c) Sample 7

The highest value of bending rigidity *B* [Nm²/m] for +90° bending was chosen for comparison of the three samples. Due to symmetry, specimens were measured only for directions from 0° to 157.5°. The data could be copied to the other half of the polar diagram as mentioned in [4] or simply omitted (see Figure 6).

Sample 6 shows far more anisotropy than samples 5 and 7, while sample 7 shows the greatest deviation between up and down bending direction. For all three samples, the measurement for directions from 0° to 90° would be sufficient as the first and second quadrant are very similar.

3.2 FE-modelling of TH-7 bending test

Table 2 shows the mechanical properties used for the FE simulation of the TH-7 bending test for the three sports bra samples. Young's modulus E calculated from TH-7 bending test for bending direction 0°, and previously performed tensile test in machine direction are compared. It can be concluded that TH-7 bending test overestimates Young's modulus by a factor of 1000. Therefore, FE simulation had to be performed with values obtained by tensile test to gain comparable bent shape. Based on the resulting values for horizontal bending force F_m, Young's modulus was fitted for 0° to +90° bending, which can be approximated by linear material behaviour.

The resulting bent shape from experimental TH-7 bending test and FE simulation are compared in Figure 7 exemplarily for sample 6 in machine direction (0°). The shell elements representing the sensor jaws were modelled with offset in order to show the outer surface contacting with the specimen.

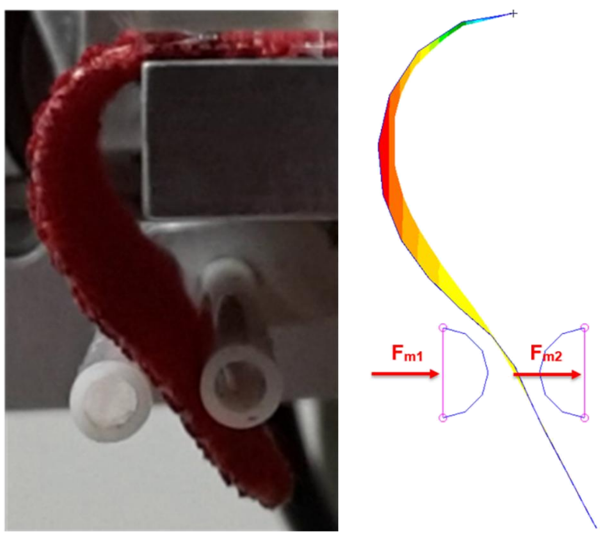

Figure 7 Comparison of bent shape at bending angle +90° of sample 6, a) TH-7 test b) FE simulation

Table 2 Mechanical properties of sports bra samples for FE simulation

sample	thickness T [mm]	density ρ [t/mm³]	Young's modulus E [MPa] TH-7 test	Young's modulus E [MPa] tensile test	Poisson ratio ν [-]
5	0.85	$2.892\cdot10^{-10}$	158.791	0.165	2.416
6	1.25	$2.131\cdot10^{-10}$	421.603	0.409	2.022
7	1.00	$3.674\cdot10^{-10}$	321.480	0.332	0.409

The nearly linear material behaviour for bending direction up could be coarsely approximated by Young's modulus E = 0.147 MPa. The non-linear material behaviour for bending direction down was taken into account by piecewise linear modelling defining stress-dependent MATS1 material. The stress values were calculated from resulting maximum strain for the respective bending angle and adjusted to resulting bending force F_m at the sensor jaw. The sum of horizontal bending forces F_m at both sensor jaws for FE simulation was compared with the measured values for +90° bending (see Figure 8); the procedure for -90° bending was identical. Fluctuations in FE result occur due to stick-slip at the contact of specimen and sensor jaw.

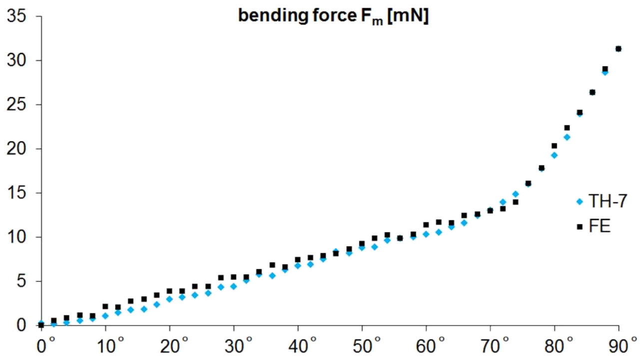

Figure 8 Comparison of horizontal bending force F_m of sample 6 in TH-7 bending test and FE simulation

4 CONCLUSIONS

The TH-7 bending test provides a fast and cheap option to measure the mechanical properties of fabrics. The proposed finite element calculation allows an evaluation of the required Young's modulus for each measured direction. Using this procedure the orthotropic properties of the fabric required for a mechanical analysis of can be derived. Therefore, a numerical procedure has been performed for the verification of Cantilever bending test [7]. None of the bending tests proposed in literature seems to provide correct values for Young's modulus E. The proposed bending rigidity [4] seems to calculate unreasonably high values. The constant κ = 0.0334 m² was calculated by a simple discrete model of continuous bending curve [4] to match TH-7 results with KES-FB results. We suppose that this constant considers using bending force F_m in [mN] rather than in [N] as mentioned in [4]. The assumption of using bending rigidity as a value for FE simulation should be rejected, only tensile tests are able to provide the necessary material properties for simulation when assuming linear behaviour.

The measured bending force F_m is a function of the bending angle. There is no advice given in [4] on which value at which bending angle to use for the calculation of bending rigidity. Considering the non-linear behaviour of knitted textiles requires piecewise linear fitting defining nonlinear (stress-dependent) material properties adjusted to the resulting bending force F_m at the sensor jaw for the respective bending angle. This procedure is time-consuming, but it allows for realistic bending simulation of sports bra fabrics in one direction. In addition, hysteresis behaviour cannot be taken into account in MSC Nastran solvers.

ACKNOWLEDGEMENTS: *The authors would like to thank Prof. Ludmila Fridrichová and Prof. Irena Lenfeldová (Technical University of Liberec, Faculty of Textile Engineering) for their help with the TH-7 device and determination of knitted structures.*

5 REFERENCES

1. ASTM D1388-14 Standard Test Method for Stiffness of Fabrics, 2014
2. Naujokaityte L., Strazdiene E., Fridrichova L.: Comparative analysis of fabrics' bending behavior testing methods, Tekstil 56(6), 2007, pp. 343-349
3. ČSN 80 0858 Zkoušení tuhosti a pružnosti plošných textilií (Testing of stiffness and resiliency of textile fabrics), 1974
4. Fridrichová L.: A new method of measuring the bending rigidity of fabrics and its application to the determination of the their anisotropy, Textile Research Journal 83(9), 2013, pp. 883-892, https://doi.org/10.1177/0040517512467133
5. Peirce F.T.: 26 – The "handle" of cloth as a measurable quantity, Journal of the Textile Institute Transactions 21(9), 1930, pp. T377–T416, https://doi.org/10.1080/19447023008661529
6. EN ISO 5084 Textiles - Determination of thickness of textiles and textile products, 1996
7. Hassmann M., Stöger S., Mentel N., Krach W.: Bending behaviour of sports bra fabrics: Experimental and finite element simulation of ASTM D1388 Cantilever test, Vlákna a Textil (Fibres and Textiles) 24(1), 2017, pp. 73-77

DEVELOPMENT AND CHARACTERISATION OF NONWOVEN FABRICS FOR APPAREL APPLICATIONS

M. S. Cheema[1], T. H. Shah[2] and S. C. Anand[1]

[1]*Institute of Materials Research and Innovation (IMRI), University of Bolton, Deane Road, Bolton BL3 5AB, UK*
[2] *National Textile University, Pakistan*
chscheema@gmail.com

Abstract: *The cost of making apparel fabrics for garment manufacturing is very high because of their conventional manufacturing processes and new methods/processes are being constantly developed for making fabrics by unconventional methods. With the advancements in technology and the availability of the innovative fibres, durable nonwoven fabrics by using the hydroentanglement process that can compete with the woven fabrics in terms of their aesthetic and tensile properties are being developed. In the work reported here, the hydroentangled nonwoven fabrics were developed through a hybrid nonwoven manufacturing processes by using fibrillated Tencel® and bi-component (sheath/core) polyethylene/polyester (PE/PET) fibres, in which the initial nonwoven fabrics were prepared by the needle-punching method followed by hydroentanglement process carried out at optimal pressures of 50 to 250 bars. The prepared fabrics were characterised according to the British Standards (BS 3356:1990, BS 9237:1995, BS 13934-1:1999) and the attained results were compared with those for a standard plain-weave cotton, polyester woven fabric and commercially available nonwoven fabric (Evolon®). The developed hydroentangled fabrics showed better drape properties owing to their flexural rigidity of 252 mg.cm in the MD, while the corresponding commercial hydroentangled fabric displayed a value of 1340 mg.cm in the MD. Tensile strength of the developed hydroentangled fabrics showed an approximately 200% increase than the commercial hydroentangled fabrics. Similarly, the developed hydroentangled fabrics showed higher properties in term of air permeability, such as the developed hydroentangled fabric exhibited 448 mm/sec and Evolon fabric exhibited 69 mm/sec at 100 Pa pressure. Thus for apparel fabrics, the work combining the existing methods of nonwoven production, provides additional benefits in terms of cost, time and also helps in reducing the carbon footprint for the apparel fabric manufacture.*

Keywords: *hydroentanglement; nonwoven apparel; durable nonwovens; Tencel®; Evolon®.*

1 INTRODUCTION

Traditionally, it is being assumed that garments are made through woven and knitted fabrics. Because of their acceptable aesthetical and mechanical properties, these conventional methods of making fabrics for garments captured a big market. From the literature review, it was found that there was very limited penetration of nonwoven fabrics in outerwear owing to their inherent limitations in term of strength, appearance and workability. In 1960, for the first time nonwoven fabric was developed as an outer wear, but could not succeed came as outer fabric but could not success because of its limitations. Nonwoven fabrics are thus being used as supporting materials in garment manufacturing industry, such as garment lining, insulation, and fusing etc. Recently, there has been a great deal of interest in the area of research and innovation activities in nonwoven fabrics for apparel applications, such as Evolon [1] and Miratech. Traditionally, it was assumed that nonwoven fabrics can only perform in wipes, scaffolds, geo textiles, filters and disposable articles [2] and only 1 percent of nonwoven fabrics are utilised in apparel sector [3]. Now, because of the new advancements in the nonwoven technologies, especially in the hydro-entanglement process, the applications of hydro-entangled nonwoven fabrics have diversified into many fields and apparel fabrics application is one of them. The key area of research is to develop the nonwoven fabrics that can withstand the external forces in the use and provide comfort to the wearer in terms of softness, moisture management, appearance and also exhibit enough strength that can withstand the laundry process [4] etc.

Nonwoven fabrics are made directly from the fibres without making any yarn and without the use of weaving or knitting processes. A nonwoven fabric is defined by INDA as follows: “Sheet or web structure bonded together by entangling fibres or filament, by various mechanical, thermal and/or chemical processes. These are made directly from the separate fibres or from molten plastic or plastic film”. The unique advantage of the nonwoven fabric manufacture is that it is a continuously linked process, in which at the first stage raw materials (fibres) are converted into webs via the carding process and at the second stage these fibrous webs are bonded into finished products. The first nonwoven apparel fabric was the disposable paper clothing that was launched in early 1966 by an American company Scott Paper, however, the fabric could not capture any significant part of the apparel market because of its ill fit and uncomfortable nature. In the same era, Mars Manufacturing Company invented different types of nonwoven dresses that were used as evening wear and wedding gowns. However, these all-paper-clothing were short-lived and became obsolete in 1968 [5]. The breakthrough in the nonwoven apparel fabrics came in 1970, when DuPont invented the hydroentanglement technique for the nonwoven fabrics, known as spunlace technology [5]. This new technique gave a competitive edge to nonwovens, as the nonwoven fabrics produced by the hydroentanglement process possessed much superior aesthetical properties than the conventional nonwovens. The company also developed the foam bonded spunlaced fabric (polyester spunlaced fabric), wherein 30% soft acrylic latex was used to strengthen the spunlaced fabric that withstood five laundering cycles [6].

In this study, functional hydroentangled fabrics have been developed through a hybrid process of needling and hydroentanglement, by utilising innovative Tencel and bi-component sheath/core (PE/PET) staple fibres. The resultant fabrics, when compared against the industry standard commercially available Evolon® and woven plain-weave cotton/polyester fabric exhibited acceptable test values related to the aesthetical and mechanical properties of the garments such as flexural rigidity, air permeability and tensile strength, etc. The resultant fabrics can be used in different applications such as in the hospital for patients' uniforms. Owing to its comfortability, it can be used in the processing industry as uniforms such as in the meat industry, printing industry and in the chemical industry. Further research work is being carried out in order to enhance the quality of the fabrics especially in relation to laundering and washing.

2 EXPERIMENTAL

2.1 Materials

The fabrics were produced in collaboration with the Nonwovens Research Institute, University of Leeds by utilising two different types of fibres: Tencel® and bi-component sheath/core (PE/PET) staple fibres. Tencel® fibres were 1.4 dtex, 38 mm in length with a smooth surface, while the PE/PET bi-component fibres were 2.2 dtex and 40 mm in length with a crimped surface. The required amount of each fibre was separately weighed and initially hand blended in preparation of the next process. These hand-mixed fibres were manually opened into small tufts and further mixed in order to obtain a smooth web. After manually opening the fibres, the fibres were then carded through the pilot carding machine and a parallel-laid web produced was used in the next process. Before going into the hydroentanglement process, the carded web was lightly needled by using 8 mm penetration and 100 strokes per min, after which the needled substrate was rolled and packed for the next process of hydroentanglement.

2.2 Hydroentanglement process

The needled fibrous webs were uniformly hydroentangled by using pilot hydroentanglement system, as illustrated in Figure 1.

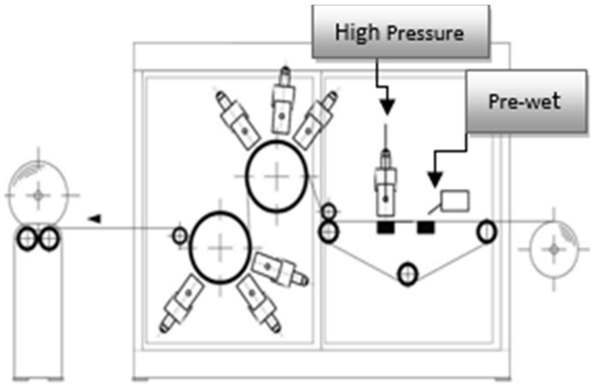

Figure 1 Action view of hydroentanglement process

Before going under the high pressure area of the hydroentanglement process, the fibrous web was pre–wetted to minimise the dispersion ratio of the fibres in high pressure zone. After pre-wetting, the material is passed through the high water pressure jet head for bonding of the fibres as shown in Figure 1. The fabrics were prepared at varying hydroentanglement pressures of 100 and 125 bars with two passes, at the line speed of 3 m/min. The orifice of jet strip was 150 μm and the density of the jet orifice was 5.56/cm. All the fabrics were manufactured from the same web with 120±5 $g.m^{-2}$ nominal weight. It was observed that for these specific blends, at lower pressures (50-75 bars), the fibres were not consolidated to the required level, which negatively affected the mechanical properties by reducing the tensile strength of the obtained fabric. On the other hand, at higher pressures (150-250 bars), the fibres were easily dispersed and consequently very limited number of fibres per unit area of the fabric was observed, which reduced the GSM as well as the tensile properties to below the acceptable values. The two hydroentangled nonwoven fabrics denoted as fabric 1 and fabric 2, were prepared at 100 and 125 bars, respectively, at the same constituent levels of 70% Tencel and 30% PE/PET bi-component fibres. The properties of developed fabrics are shown in Table 1.

Table 1 Details & characteristics of the hydroentangled nonwoven fabrics prepared in this study

Fabric number	Hydroentanglement pressure [bar]	Content	Area density [g.m^{-2}]	Thickness [mm]	Bulk density [g.cm^{-3}]
Fabric 1	100	Tencel (70%) and sheath core PE/PET (30%)	150 ± 2.5	0.99 ± 0.05	0.15 ± 0.01
Fabric 2	125	Tencel (70%) and sheath core PE/PET (30%)	145 ± 2.5	0.88 ± 0.05	0.17 ± 0.01

2.3 Mechanical and aesthetical testing

The prepared fabrics were tested according to the British Standards (BS 3356: 1990, BS 9073-6: 2003, BS 13934-1: 1999) in order to determine their mechanical and aesthetical properties. For flexural rigidity, Shirley flexometer apparatus was used, where a 25±1 mm x 100±1 mm strips were cut and the flexural rigidity values were determined according to the standard procedures. The tensile tests were performed by the Instron apparatus according to the appropriate standard methods. The cross-head speed was 200±1 mm/min and the fabric size was 200±1 x 50±1 mm. Three specimens of each fabric were tested. The wicking test was performed by strip test method and absorption test was carried out by dipping (10x10 cm) fabric specimens into water for 20 min at 20°C and 65±25% relative humidity.

The results obtained were then compared with the commercially available nonwoven fabric “Evolon” and with the reference fabric of a plain weave of woven fabric to ascertain the suitability of our developed fabrics for use as apparel fabrics.

3 RESULTS AND DISCUSSION

3.1 Dimensional properties

The results presented in Figure 2 show that fabrics 1 and 2, produced at 100 and 125 bars hydro pressure had thickness values of 0.99±0.05 mm and 0.88±0.05 mm, respectively. This indicates that when the hydroentanglement pressure was increased, a small reduction in the fabric thickness was observed due to a higher compaction and alignment of the fibres, which is expected to influence the tensile properties and bending rigidity of the produced fabric. In a study by Zheng et al [6], it was shown that by increasing the specific energy (hydro pressure), the fabric area density decreased due to the fabric stretching caused by the impact of the water jets.

Moreover, it was observed that both the fabrics exhibited almost very similar bulk density values, which is an indication that the number of fibres per unit area in these fabrics were similar to each other. When compared to the values for the commercial nonwoven fabric and a typical woven fabric, these comparative results clearly show that the dimensional properties such as thicknesses of the hydroentangled nonwoven fabrics (1 and 2) were higher, because fabric 1 exhibited 0.99±0.05 mm and fabric 2 exhibited 0.88±0.05 mm thickness and Evolon and woven fabrics showed 0.43 and 0.50 mm thickness values respectively. The bulk densities of both fabrics were lower than Evolon® and woven fabrics. Woven and Evolon fabrics’ higher bulk density values were because of their compact structures as shown in Table 2.

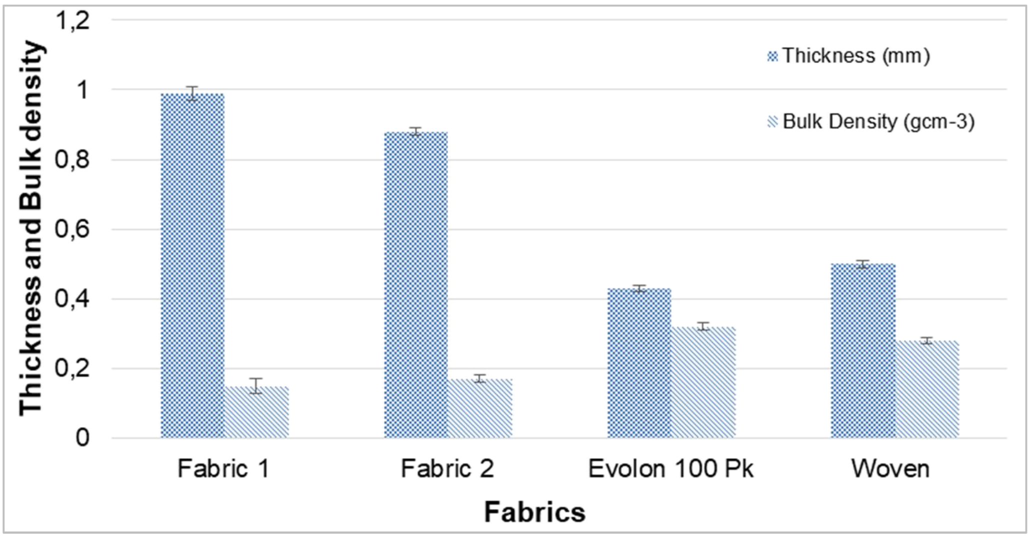

Figure 2 Thickness and bulk density of developed fabrics 1 (100 bars) and 2 (125 bars)

Table 2 Details of reference fabrics

Fabrics	Processes	Contents	Area Density [g.m^{-2}]	Thickness [mm]	Bulk Density [g.cm^{-3}]
Evolon®	Hydroentanglement	PET and PA	140	0.43	0.32
Woven	Plain weave	Cotton and PET	144	0.50	0.29

3.2 Flexural rigidity

The flexural rigidity of the fabrics is a pivotal property for apparel applications. The fabric stiffness is related to its inherent properties, such as fibre material and the structure itself of the fabric [7]. The flexural rigidity results in the machine (MD) and cross (CD) directions for the fabrics produced during this research are presented in Figure 3.

It was observed that the flexural rigidity values for the nonwoven fabrics prepared in this study were much lower than the commercial nonwoven fabrics (Evolon®) in both the MD and CD. Furthermore, these values were very similar to those observed for the woven fabric (Figure 3). These results clearly show that the flexural behaviour of fabrics 1 and 2 was very similar to that of the woven fabric and it can be further enhanced through the finishing processes.

The bending rigidity of the fabrics depends on the movement of the fibres within the fabric structure. It seems that the Evolon fabrics exhibit higher bending rigidity as the fibres are highly intertwined with its neighbouring fibres due to the nature of the spun-laid process and the inherent fine filaments of the bi-component PA6/PET "island in the sea" filament structure. Additionally, due to the high hydroentanglement pressure, the fine filaments form a tight structure with little or no space for fibre movement to occur within the fabric. On the other hand, the prepared fabrics showed lower flexural rigidity as compared to the commercial nonwoven fabric due to the more open structure of these experimental nonwoven fabrics. In their study, Smith et al [8] have reported that if the fibres are able to act independently in the fabric structure, a reduction in the flexural rigidity of the fabric is observed. Hence, it is evident that bending rigidity does not depend on the thickness of the fabric and rather is directly proportional to the movement of the fibres within the structure of the fabric. Evolon® exhibited higher flexural rigidity in both the machine and cross directions, even though it had a lower thickness value. On the other hand, the developed hydroentangled nonwoven fabrics exhibited lower flexural rigidity in the machine and cross directions, as compared with the Evolon, while showing higher thickness values than the Evolon® fabric. Woven fabric had similar thickness as compared with the Evolon® but exhibited much lower values' of flexural rigidity in the machine and cross direction. Ancutiene et al [9], found in their studies that the fabric structure has a more significant effect on the flexural rigidity of the fabric. Yuksekkaya et al. [7] too have endorsed this principle that the fabric parameters affect the stiffness of the fabric. Figure 4 represents the microscopic images of the three different types of fabrics studied during the course of the work.

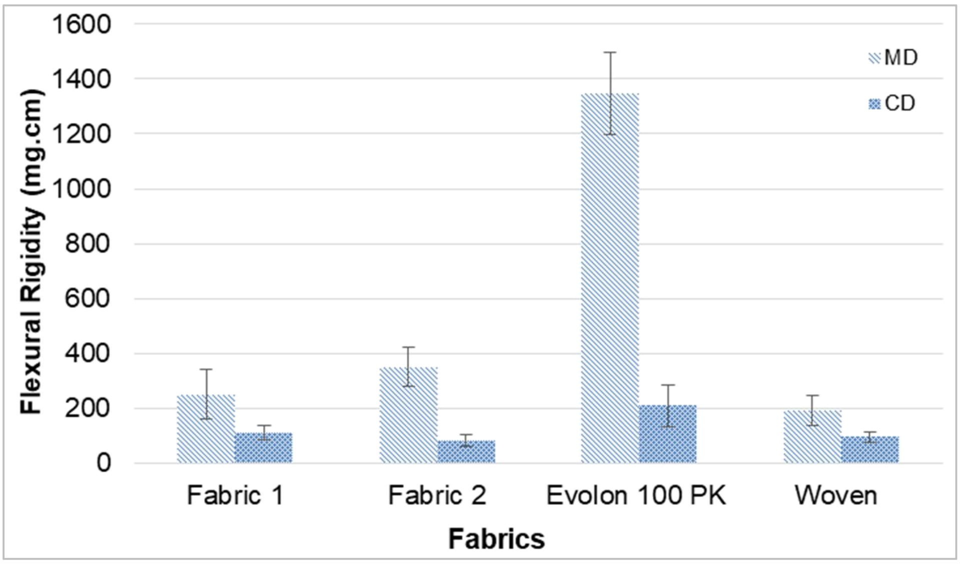

Figure 3 Flexural rigidity comparison of developed fabrics 1 and 2 with Evolon 100PK and woven fabric

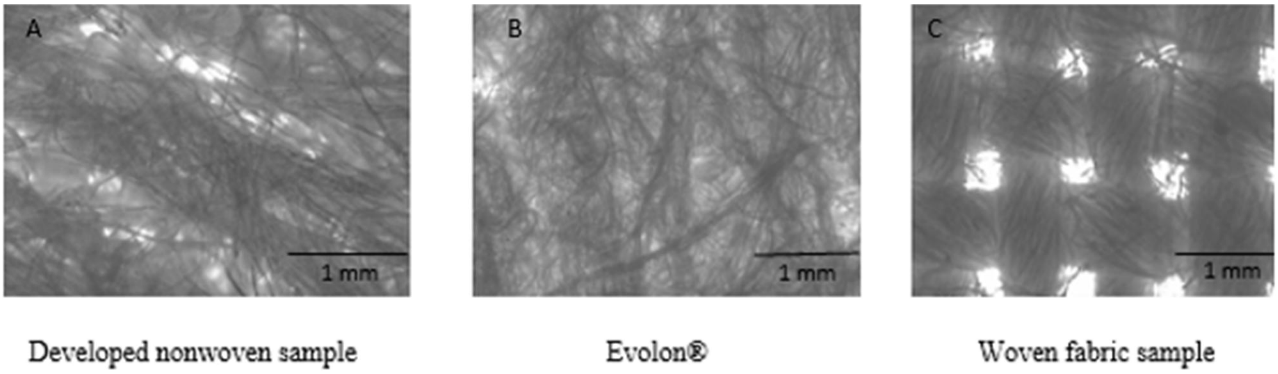

Figure 4 Microscopic views of (a) developed hydroentangled, (b) Evolon® and (c) woven fabric

These images show that the nonwoven fabrics developed in this study and the woven fabric have similar open structures and the fibres appear to be better aligned than the commercially available Evolon, wherein the fibres appear to be randomly placed. Komori [10] found that the arrangement of the fibres in the fabric structure has a major influence on the mechanical properties of the fabric. Thus, the experimental nonwoven and woven fabrics exhibit similar flexural behaviour and have significantly lower flexural rigidity values as compared to the commercial nonwoven fabric. In the developed hydroentangled fabrics, the fibres are largely aligned in a single direction and the open spaces between the fibres can lead to the lowering of the flexural rigidity. Similar results have been obtained by Bahari [11] and Smith [8], wherein it was observed that the fibre's independent movement within the fabric structure led to a lower fabric flexural rigidity.

3.3 Absorption and wicking tests

The moisture transportation in a fabric determines its cooling effect and thus provides comfort to the wearer. The wear comfort of clothing is continually gaining importance owing to the consumer demand and therefore considerable efforts have been made to study the wicking characteristics of apparel fabrics [12]. During exercise or working conditions, the human body produces sweat and if it does not evaporate from the skin to the atmosphere, because of the clothing, then the wearer feels uncomfortable and this may give rise to a loss in working efficiency of the wearer. Therefore moisture management by the fabric is very important in order to optimise the wearer's comfort. The fibre types (natural or synthetic), blending ratio of fibres, the fabric structure and fabric characteristics (densities of yarns, thickness) etc. are the parameters that affect the moisture management and the thermal properties of the fabrics [13]. The prepared nonwoven and woven fabrics were characterised for their absorption and wicking properties and the results are presented in Table 3 and illustrated in Figure 5.

Table 3 Absorption and wicking properties of nonwoven fabrics

Fabrics	Area Density [g.m^{-2}]	Absorption [g.g^{-1}]	Wicking [g.cm]	
			MD	CD
Fabric 1	150	6.78	9.61	9.26
Fabric 2	145	4.96	12.44	8.21
Evolon®	140	0.7	1.4	0.6
Woven	144	1.5	1.4	0.6

The results show that the experimental fabrics 1 and 2 exhibit better absorption and wicking behaviour than Evolon 100PK and the woven fabric. The absorption value of fabric 1 was ~78% higher than the woven fabric and about 90% higher than Evolon® 100PK. Similarly, fabric 2 exhibited 70% and 86% higher absorption values than woven and Evolon® fabrics, respectively. This enhanced absorption is mainly due to the fact that the experimental nonwoven fabrics have a more porous structure and the fibres are well oriented within the fabric structure. Moreover, owing to the Tencel fibres' hygroscopic nature, it absorbs the water molecules readily, thus providing higher absorption values. Furthermore, the Tencel® fibres used have a higher wet and dry strength than the other cellulosic fibres, viscose fibres show 22-26 cN/tex tenacity in dry state and 10-15 cN/tex in wet state and on the other hand Tencel fibres show 34-38 cN/tex and 38-42 cN/tex in dry and wet states respectively and have higher moisture regain properties than the polyamide and polyester fibres used in the commercial nonwoven fabric (Evolon). Additionally, the fibril structure of Tencel fibres provides superior capillary action within the fabric structure [14]. Woven fabric displayed restricted absorption properties owing to its fabric structure, wherein, due to the high number of crimps per unit area, along with the highly twisted yarns, did not allow the fibres to act as capillaries, unlike the exhibited properties of the nonwoven fabrics.

The results presented in Table 3 also show that the wicking values obtained for fabrics 1 and 2 were considerably higher than the woven fabric and Evolon 100PK nonwoven fabrics, both in the MD and CD. The wicking properties mainly depend on the fibre fineness and the fabric structure. Fabric 1 and 2 showed 9.61 and 12.44 g.cm wicking values in MD where as Evolon and woven exhibited wicking values of 1.4 g.cm in MD. The higher wicking values of the developed fabrics were because of the Tencel fibres consist of countless hydrophilic and crystalline nano fibrils which act as tubes and absorb the water through the capillary action between the fibrils [14]. On the other hand, Evolon, composed of polyester and polyamide fibres, show lower absorption, as the synthetic fibres like polyester are hydrophobic in nature. The fibre orientation also contributes in the absorption values of the fabric. Miller [15] has studied the pore size effects on the capillary behaviour of the material. For the developed hydroentangled fabrics, the smaller pore size along with the higher capillary action from Tencel fibres led to the enhanced wicking properties, as compared to the other fabrics.

3.4 Tensile properties

The tensile properties of fabrics 1 and 2 in MD and CD are shown in Figure 6 (a, b), respectively.

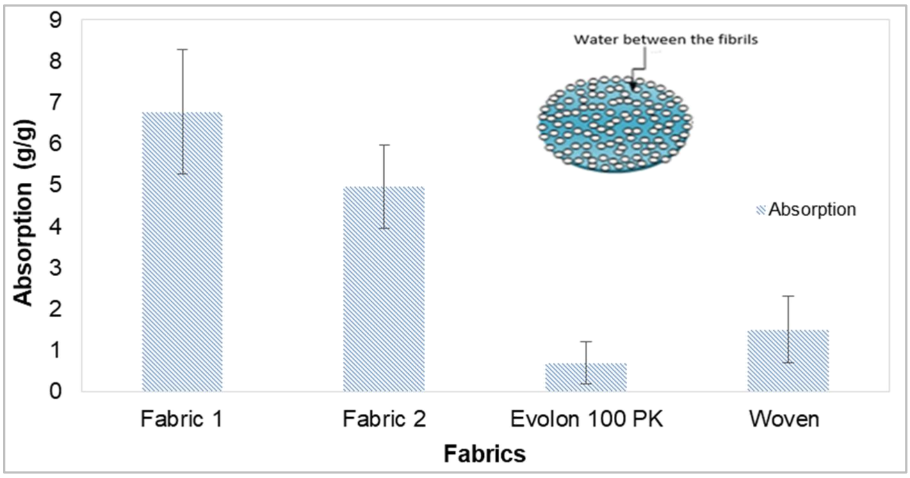

Figure 5 Absorption properties of nonwoven fabrics

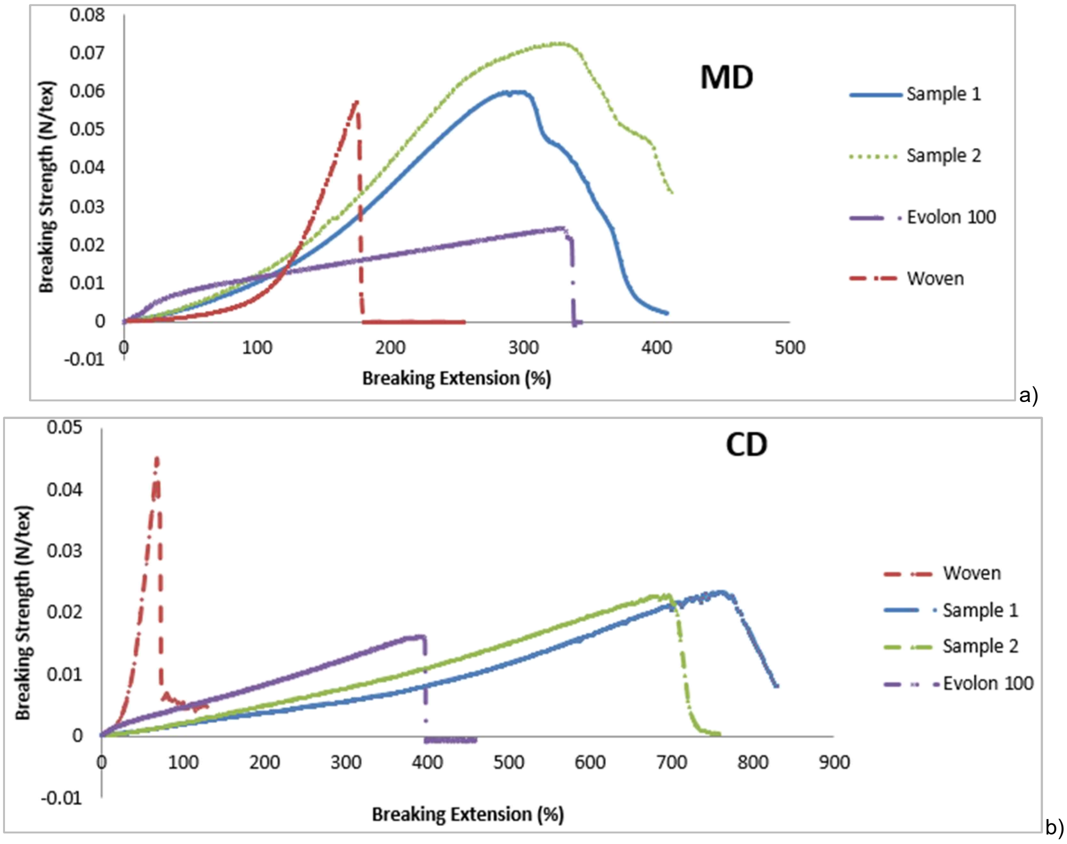

Figure 6 Tensile tests of nonwoven fabrics in MD and CD

The results show that the tensile strength of fabrics 1 and 2 are higher than the Evolon 100 PK and woven fabric in MD (Figure 6a). It also appears that the tensile behaviour of the fabrics 1 and 2 is significantly different from both the woven and the commercial nonwoven fabrics. As mentioned earlier, the developed fabrics were prepared at 100 and 125 bars, respectively. In their study, Connoly [16], have observed that an increase in the hydroentanglement pressure results in an increase in the tensile strength due to the higher degree of entanglement of the fibres. The tensile strength also depends on other factors, such as the fibre and web properties. As discussed previously by Ghassemieh [17], to prepare a hydroentangled fabric, a sufficient amount of energy is essential to get an optimal product with suitable dispersion and sufficient tensile strength, which itself depends on the web making parameters and fibre properties such as modulus, stiffness, length and friction between the fibres. Mao [18] found in his research that less stiff fibres consumed less energy for attaining the maximum fibre entanglement within the fabric structure. Moreover, because of the staple fibres in the developed fabrics, during hydro-entanglement process, more fibres were twisted around with surrounding fibres, because of the rebound of the water after hitting the plate underneath the web, resulted in intensive entangling behaviour of the fibres that caused the higher tensile strength of the developed fabrics as compared with other fabrics. The experimental nonwoven fabrics have breaking extension values that are similar to the Evolon fabrics, however their failure mechanism is quite different as these fabrics tend to yield before they fail. Due to its rigid structure, the woven fabric exhibited higher modulus and lower breaking extension values as compared to the nonwoven fabrics.

The tensile properties of the various fabrics in CD are illustrated in Figure 6b. The results show that the ultimate strength values of these experimental nonwovens are slightly lower than the woven fabric but higher than Evolon 100PK. The breaking extension values of all the nonwovens are in excess of 80% and these are considerably higher than the woven fabric. The Evolon fabric is composed of continuous filaments of bi-component Island in the sea that can impart higher strength to the fabric, whereas the woven fabric is composed of twisted yarns with a compact weave that give additional strength to the fabric. On the other hand, fabrics 1 and 2 are composed of fine staple fibres and the fibres were aligned in machine direction so because of less number of fibres in the cross direction region, the developed fabric exhibited lower tensile strength in CD. Evolon fabric is also based on synthetic fibres and is produced by using split able bi-component fibres which are finer in diameter than those used for preparation of the experimental fabrics and are therefore able to entangle more intensely in the fabric structure and also the filaments were in different directions that caused higher tensile strength in CD than the developed fabrics as shown in Figure 7.

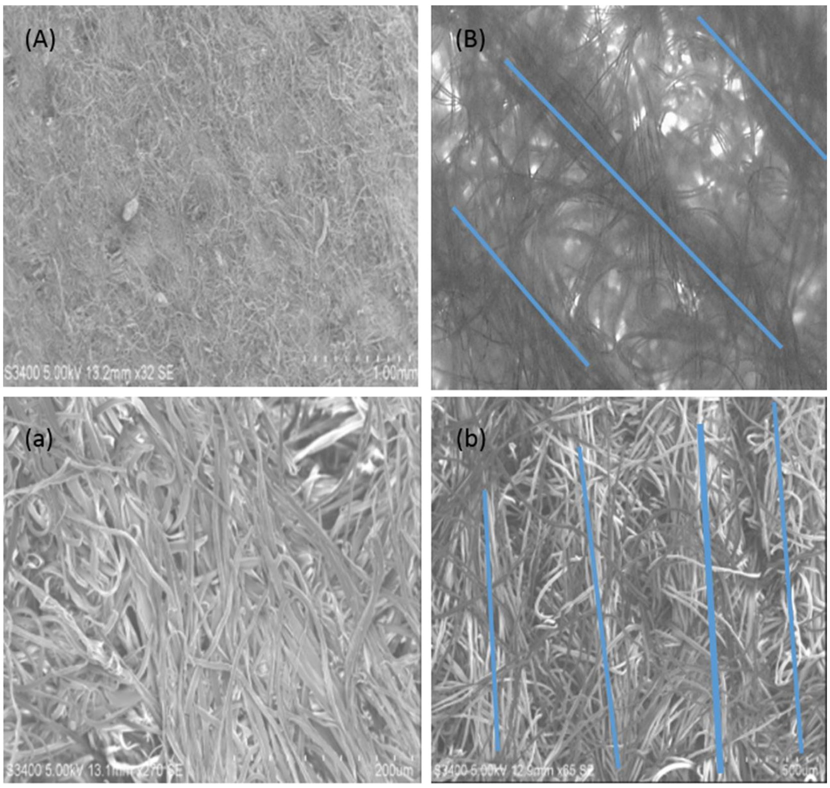

Figure 7 Optical and SEM views of Evolon 100 PK (A, a) and developed hydroentangled (B, b) fabric

4 CONCLUSIONS

In this study, an attempt has been made to develop nonwoven fabrics that are suitable for apparel applications. A hybrid nonwoven approach has been adopted where the fibres are first converted into a parallel-laid web followed by needlepunching of the web. The needlepunched fabric is then subjected to the hydroentanglement process at optimal values of 100 and 125 bars. The results demonstrate that the nonwoven fabrics produced in our study have superior moisture management properties such as developed fabric gave 6.78 g/g values of absorption and Evolon and woven gave 0.7 and 1.5 g/g, respectively. The bending flexural rigidity characteristics of the developed fabrics were also lower than the Evolon fabrics, wherein the developed fabrics exhibited 252 mg.cm in MD while the Evolon fabrics showed a value of 1347 mg.cm in MD. The tensile properties of the experimental nonwoven fabrics are higher than the commercially available nonwoven fabrics, especially the breaking extension values. The developed fabric exhibited a value of 0.07 N/tex in MD and Evolon exhibited value of 0.02 N/tex in MD. The tensile strength of the woven fabric is somewhat higher in CD than the nonwoven fabrics, but the bending rigidity values are very similar to the experimental nonwovens. The absorption and wicking properties of the developed fabrics were higher than the Evolon and woven fabric in both the machine and cross directions because of the hygroscopic and fibril structure of the Tencel fibres. The developed fabric exhibited an absorption value of 6.78 g/g and Evolon fabric exhibited 0.7 g/g absorption value. This proves that the developed fabrics quickly absorb the sweat from the body and because of their strong wicking action; the sweat disperses in the fabric structure that assists in the evaporation into the environment. The wicking values of developed fabric fabrics were 9.61 and 12.44 g.cm and the wicking values of Evolon and woven fabrics were 1.4 g.cm. It is strongly believed that with further optimisation of the hybrid process parameters and the fabric finishing techniques, nonwoven textile structures can be developed that are suitable for many apparel applications, including patients' uniforms, uniforms for processing industries, outer wear etc.

Acknowledgements: *The authors wish to thank Dr S. Rathore at NRI, University of Leeds, for his help with the processing of experimental fabrics.*

5 REFERENCES

1. www.Evolon.com
2. Lukic S., Jovanic P.: Structural analysis of abrasive composite material with nonwoven textile matrix, Material Letters 58(3-4), 2004, pp. 439-443, https://doi.org/10.1016/S0167-577X(03)00521-4
3. Lee H.J., Cassill N.: Analysis of world nonwoven market, Journal of Textile and Apparel, Technology and Management 5(2), 2006, pp. 1-19
4. Dhange V.K., Webster L., Govekar A.: Nonwoven in fashion apparel applications, International Journal of Fibre and Textile Research 2(2), 2012, pp. 12-20,
5. Andrew D.H.: Colouration of hydroentangled nonwoven fabrics, PhD. Thesis, University of Leeds, 2008
6. Zheng H., Seyam A.M., Stiffler D.: The impact of input energy on the performance of hydroentangled nonwoven fabrics, International Nonwovens Journal 12(2), 2003, pp. 34-44
7. Yuksekkaya M.E., Howard T., Adanur S.: Influence of the fabric properties on fabric stiffness for the industrial fabrics, Tekstil ve Konfeksiyon 18(4), 2008, pp. 263-267
8. Smith K., Ogale A.A., Maugans R., Walash L.K., Patel R.M.: Effect of bond roll pattern and temperature on the microstructure and properties of polyethylene nonwovens, Textile Research Journal 73(10), 2003, pp. 845-853, https://doi.org/10.1177/004051750307301001
9. Ancutiene K., Strazdiene E., Nesterova A.: The Relationship between Fabrics Bending Rigidity Parameters Defined by KES-F and FAST Equipment, Materials Science 16(4), 2010, pp. 346-352
10. Komori T., Itoh M.: Analyzing the compressibility of a random fiber mass based on the modified theory of fibre contact, Textile Research Journal 67(3), 1997, pp. 204-210, https://doi.org/10.1177/004051759706700308
11. Bahari N., Hasani H., Zarrebini M., Hassanzadeh S.: Investigating the effects of material and process variables on the mechanical properties of low-density thermally bonded nonwovens produced from Estabragh (milkweed) natural fibers, Journal of Industrial Textiles 46(3), 2015, pp. 719-736, https://doi.org/10.1177/1528083715591593
12. Birrfelder P., Dorrestijn M., Roth C., Rossi R.M.: Effect of fibre count and knit structure on intra- and inter-yarn transport of liquid water, Textile research Journal 83(14), 2013, pp. 1477-1488, https://doi.org/10.1177/0040517512460296
13. Hassan M., Qashqary K., Hassan H.A., Shady E., Alansary M.: Influence of sportswear fabric properties on the health and performance of athletes, Fibres & Textile in Eastern Europe 20(4), 2012, pp. 82-88
14. Firgoa H., Schustera K.C., Suchomela F., Männera J., Burrowa T., Abu-Rousb M.: The functional properties of TENCEL® - a current update, Lenzinger Berichte, 85, 2006, pp. 22-30
15. Miller B.: Critical evaluation of upward wicking tests, International Nonwoven Journal 9(1), 2000, pp. 1-9
16. Connolly T.J., Parent L.R.: Influence of specific energy on the properties of hydroentangled nonwoven fabrics, Tappi Journal 76, 1993, pp. 135-141
17. Ghassemieh E., Acar M., Versteeg H.K.: Improvement of the efficiency of energy transfer in the hydro-entanglement process, Composites Science and Technology 62(12), 2001, pp. 1681-1694, https://doi.org/10.1016/S0266-3538(01)00074-4
18. Mao N.: Effect of fabric structure on the liquid transport characteristics of nonwoven wound dressing, PhD thesis, University of Leeds, UK, 2000, http://etheses.whiterose.ac.uk/id/eprint/3171

COMPOSITE BASED ON GEOPOLYMER MORTAR REINFORCED CHOPPED BASALT FIBER AND CARBON TEXTILE

Hiep Le Chi, Petr Louda, Totka Bakalova and Vladimir Kovacic

Department of Material Science, Faculty of Mechanical Engineering, Technical University of Liberec, Studenstká 2, 461 17 Liberec, Czech Republic
hiepletul09@outlook.com

Abstract: *This paper deals with the evaluation of the four-point bending strength of geopolymer composite thin plates, which made of carbon grid embedded in geopolymer mortar containing various contents of chopped basalt fiber. Sodium-based geopolymer binder along with silica sand and chopped basalt fiber (0%, 3%, 5%, 7.5% by weight of geopolymer resin) are mixed together to make fresh geopolymer mortar. Then thin-plate specimens with the dimension 400x100x15 mm^3 (length, wide, thickness) are produced by using one-layer of carbon grid embedded in fresh geopolymer mortar. The specimens were tested at a time period of approximately 28 days after casting. The tested results show that the increase in the chopped fiber percentage improves flexural strength (both at first-crack and peak load) of geopolymer composite thin plates.*

Keywords: *Geopolymer, four-point flexural strength, geopolymer mortar, carbon textile, chopped basalt fiber.*

1 INTRODUCTION

Geopolymers are inorganic polymer materials with a chemical composition similar to natural zeolite but containing an amorphous microstructure and possessing ceramic-like in their structures and properties. Geopolymers are formed by reacting an alumino-silicate rich source (metakaolin, fly ash or nature pozzolanic, etc.) with an alkaline solution of the balancing cation of choice. Their amorphous structure composed of cross-linked alumina (AlO_4^-) and silica (SiO_4) tetrahedra to form polysialates, with an alkali metal ion to balance with the negative charge [1-4]. Geopolymers have recently emerged as novel engineering binder materials with environmentally sustainable properties. The reduced energy consumption and CO_2 emission during manufacture make them attractive alternative over Portland cement [5, 6].

Textile-reinforced concrete (TRC) is a new composite material composed of a fine-grained matrix with textile materials such as alkali-glass, carbon, basalt or polymer alternative to usual steel reinforced bars [7]. The major advantages of TRC are its high tensile strength and pseudo-ductile due to its tolerance of multiple cracking. Furthermore, such textile-reinforcement has the ability to withstand corrosion, aggressive environments and therefore does not require a strong covering layer in contrast to steel reinforced concrete, where requires sufficient thickness of the concrete layer to protect the corrosion of steel-reinforcement during the lifetime of the structure [8]. Therefore, it is resulting in thinning and reduction of the mass of the whole structure. Thanks to their excellent material properties, the TRC composite is used in a wide range of application such as thin-walled elements, repairing and/or strengthening in structural elements, façade elements, bridges and also freeform and lightweight structures [9-13]. The textile in composite materials plays an important role in carrying the capacity and stiffness of composite. As compared to other textiles, carbon textile better supported capacities, high tensile strength, high Young's modulus, low weight, high chemical resistance, etc. It is the main reason for the manufacture of Carbon textile as a commercial product for application in TRC composite. This study is extended to the production of carbon textile reinforced geopolymer composite based on the fine-grain geopolymer mortar matrix containing various contents of chopped basalt fibers. The workflow is carried out by evaluating the four-point flexural strength of geopolymer thin plates at a time period of 28 days after casting.

2 EXPERIMENTAL

2.1 Materials

Baucis LNa alumino-silicate geopolymer binder based on metakaolin was purchased from Ceske Lupkove Zavody, a.s. Czech Republic (in weight percent: SiO_2 - 47.4; Al_2O_3 - 29.7; CaO - 14.5; MgO - 2.6; TiO_2 - 1.8; Fe_2O_3 - 0.5; K_2O - 0.3; Na_2O - 1) along sodium silicate activator of modul 1.73 (in weight percent: SiO_2 - 20.72; Na_2O - 12.33; H_2O – 66.68). The metakaolin geopolymer was synthesized from calcined kaolin and shale clay residues with Si/Al ratio of 2.0. The kaolin was mainly composed of kaolinite with small amounts of quartz, whereas shale clay was composed of kaolinite with low amount of quartz and anatase. Two different types of silica sand were used as the fine aggregates for geopolymer mortar matrix (grain size: 0-0.063 mm and 0.6-1.25 mm). The chopped Basalt fibers were provided by Kamenny Vek, and the tows were 6.4 mm long with the individual fiber diameters of 13 μm, the density of 2.67 g/cm^3. Basalt has a softening and melting point of 1060°C, 1250°C, respectively. It is non-combustible, making it useful for high-temperature applications. The silane coating or sizing helps to protect the brittle fibers from premature fracture and prevents them from binding to each other. In this work, 3%, 5%, and 7.5% of chopped Basalt fiber additions (all by weight of geopolymer resin) were considered.

Carbon meshes of open size 12x16 mm were provided by Frisiverto s.r.o Company, Czechia. The carbon mesh was made up of 48000 individual filaments for the yarns in the longitudinal direction and 12000 individual filaments for yarns in the transverse direction, and density of 1.8 g/cm^3 (details see in Table 1). In the four-point bending test of geopolymer composite specimens, carbon grids were placed such that the load applied on the specimen was in the longitudinal direction of yarn.

Table 1 Properties of Carbon textile

Form	Carbon fiber grid
Fiber type **Binder yarn**	Carbon fiber HTC 10/15-40 PP 11 0dtex
Fiber construction **Tex**	Fiber orientation 0/90° (bi-directional) 800 g/km
Fiber density	1.8 g/cm^3
Number of threads/m	78 (lengthways) and 55 (crossways)
weight	350 g/m^2
Coating	Styro Butadien
Stitch spacing	10 mm x 15 mm (center to center distance)
Tensile strength **Elongation lengthways** **Elongation crossways**	2551 N/mm^2 (lengthways) and 2847 N/mm^2 (crossways) 1.17% 1.24%

2.2 Specimen preparation and testing method

Geopolymer mortar matrix was prepared as the following steps. Pure geopolymer resin is the two-component mixture including aluminosilicate source (metakaolin) and alkaline liquid (sodium silicate liquid). This mixture is prepared in a ratio of solid to alkaline liquid (1:0.8) and mixed by mechanically stirring for approximately 5 min to ensure fresh mixture homogenously. After that micro-silica sand added into the prepared mixture and stirring for around 3 min more.

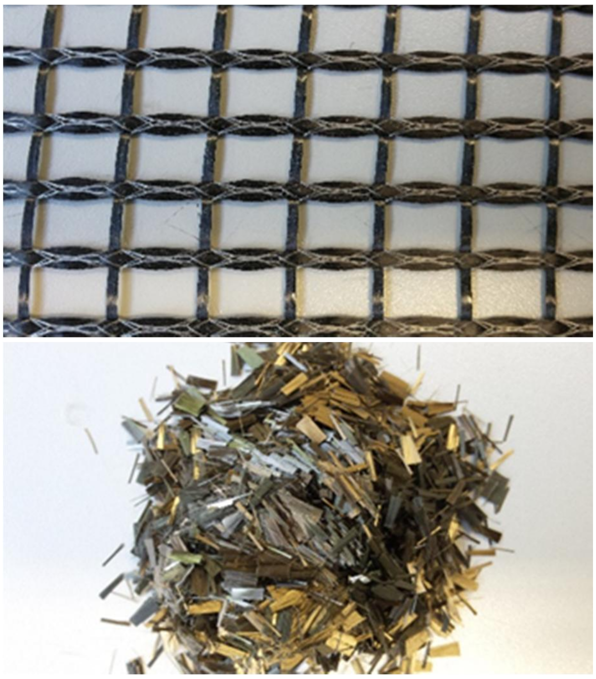

a) b)

Figure 1 Textile reinforcement: (a) Carbon grid, (b) chopped Basalt fiber

Finally, chopped Basalt fiber (with the various percentage contents for each mixture) together with rough sand was added into the prepared mixture followed by stirring for another several minutes to ensure a homogenous mixture. The fresh mortar was cast into 30x30x150 mm^3 prismatic molds for the flexural and compressive test to evaluate the mechanical strength of geopolymer matrix. Three samples for each mixture were used for flexural test and then the compressive strength was measured on the far edge of both residual pieces obtained from flexural strength according to EN 196-1 standard [14]. The thin-plate molds with a dimension of 400x100x15 mm^3 for four-point bending were prepared. First the fresh mortar was poured in to the molds with a thickness 6 mm. Then one layer of textile is carefully laid over geopolymer mortar followed by filling the rest of the molds. Three thin plate specimens for each mixture were casted. All samples were cured at room temperature until test at a time period of 28 days after casting.

Figure 2 shows four-point bending test with constant bending moment zone (support span 100 mm) was used to determine the bending strength of geopolymer thin plate specimens. The INSTRON testing machine located at Technical University of Liberec Laboratory with the applied load under displacement control at loading rate of 2 mm/min. Three samples from each of the examined were tested.

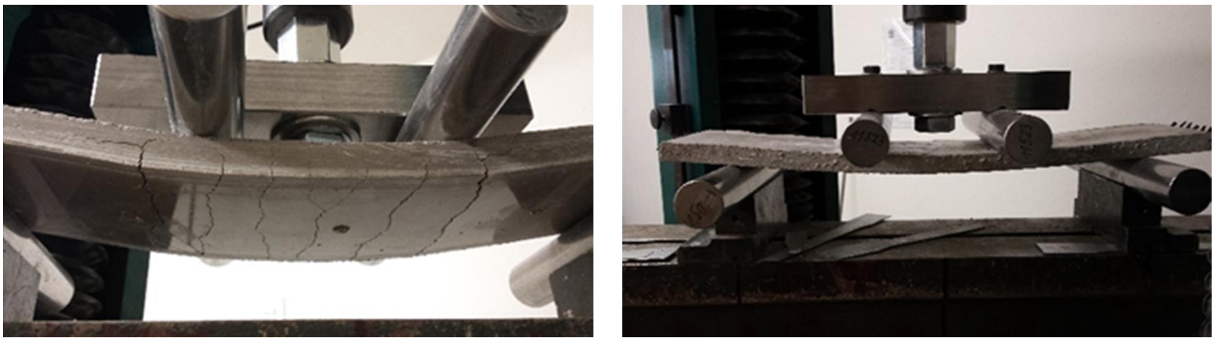

Figure 2 Four-point bending test of geopolymer composite thin plate

The calculation of the measured data and the evaluation of the test results were made using the following equation (1):

$$\sigma = F.l/(b.h^2) \quad [MPa] \qquad (1)$$

where σ is the four-point flexural strength in MPa; F is load at a given point on the load-deflection curve in N; b is the width of the tested sample in mm; h is the thickness of tested sample in mm; l is the support span (300 mm).

3 RESULTS AND DISCUSSION

Table 2 shows the compressive and flexural strength results of geopolymer mortar matrix at a maturation period of 28 days. In general, it can be seen that the addition of chopped Basalt fibers and their increasing percentage improved both of the compressive and flexural strength of geopolymer mortars. The strength of reference mortar is 11.04 MPa (flexural strength), and 64.36 MPa (compressive strength). After that addition of fiber increases the mechanical strength in gradually small value, it reaches a maximum value of 12.52 MPa (flexural strength), and 78.5 MPa (compressive strength) for fiber content of 7.5%.

Figure 3 shows the average flexural load-deflection curves of all the geopolymer thin plates containing various contents of chopped basalt fiber. In general, the flexural load-deflection curves of all the tested specimens exposed the similar behavior. It consists of the three parts corresponding to the stages in the flexural test. The three behavior areas are clearly visible. The first stage represents the linear uncrack state where the geopolymer matrix takes the load. Then, as the load increases, the stress transfers from the geopolymer matrix to the textile, which is represented by the multi-crack processing of the matrix. At the point or stage where the first crack takes the place is called transition point.

Then, the specimens continue to undergo a multi-cracking process, in which all of the stresses are transferred from matrix to the textile. At this stage, the textile is only carrying the load until it fails by rupturing or slipping. This behavior is similar to textile reinforced cementitious matrix [8].

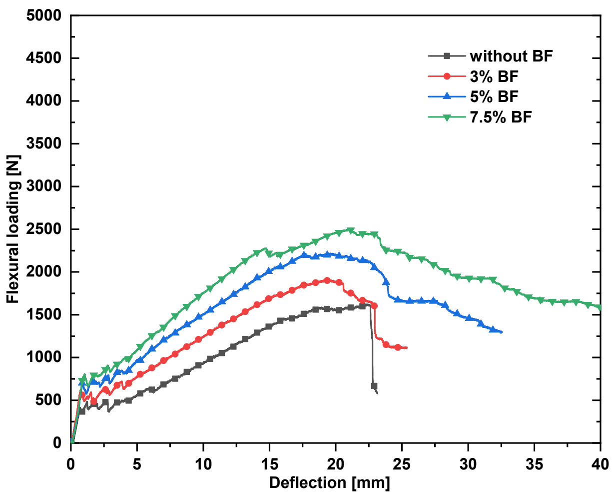

Figure 3 Flexural loading and deflection curves of one textile layer reinforced geopolymer composite thin plates with respect to various contents of BF

Figure 4 is presented average values of the first-crack stress, ultimate stresses and flexural toughness of thin plate specimens. It can be seen that the addition of BF reinforced geopolymer mortar is helpful to improve both the first-crack load and the ultimate load of textile reinforced geopolymer specimens. It can be observed by fact that BF contributes to improve the early age performance of the geopolymer mortar, leading to fewer micro-cracks in geopolymer mortar.

Table 2 Results of mechanical strength of geopolymer mortar matrix at time period of 28 days after casting

Mode	Various contents of chopped basalt fiber [wt.%]			
	0	3	5	7.5
Flexural strength [MPa]	11.23(0.39)	11.95(0.41)	12.77(0.19)	13.05(0.43)
Compressive strength [MPa]	64.36(3.17)	70.05(4.42)	78.52(1.67)	80.50(1.10)

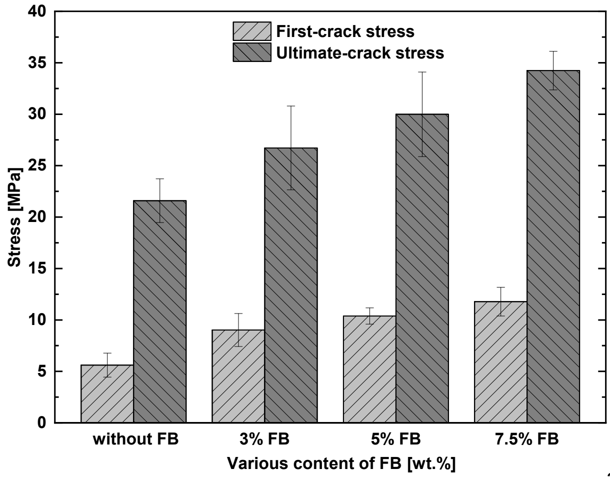

a)

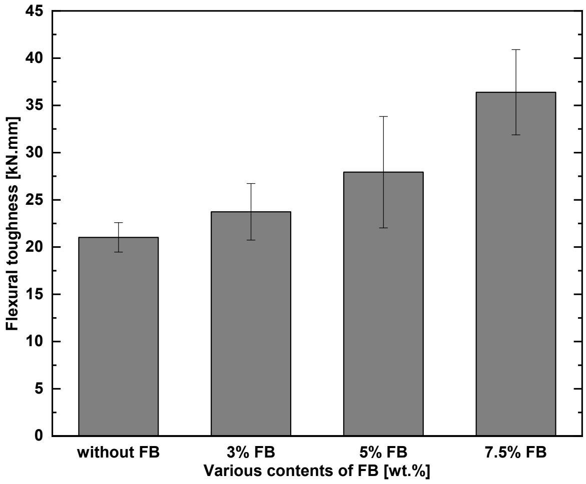

b)

Figure 4 Summary of tested results of one textile layer reinforced geopolymer containing the various content of chopped basalt fiber: a) flexural strength; b) flexural toughness

Moreover, thanks to the bridge effect of basalt fiber at the cracks, the interface bond between yarns of textile and geopolymer matrix is improved, and thus it contributes to improving the efficiency of textile in reinforcing as well. BF reinforced geopolymer composites showed beneficial improvement in terms of flexural strength and the growing fiber content yielded the higher flexural strength when compared to geopolymer composites without addition BF.

The bearing capacity of textile reinforced specimens improved gradually with increasing content of BF. The average ultimate strength of specimens without addition BF is 21.59 MPa. The average ultimate strength of specimens with 3%, 5%, and 7.5% of addition BF increased by approximately 23.76%, 38.90%, and 58.59%, respectively, compared to specimens without addition BF (see in Figure 4a). Moreover, the flexural toughness of the specimens increases with increasing content of BF (see in Figure 4b). The average flexural toughness of specimens without BF addition is 21.03 kN.mm. The average flexural toughness of specimens with 3%, 5%, and 7.5% of addition BF increased by 12.89%, 32.81%, and 73.04%, respectively, compared to specimens without addition BF. Toughness is the ability of a material, which indicates how much energy it can absorb before rupturing. Toughness (energy absorption) is calculated as the area under the respective load-deflection curves up to peak load of each specimen.

Figure 5 displayed the failure modes of several thin plate specimens, which represented for the common failure modes of all the thin plate specimens after finishing bending test. Figure 5a showed the failure mode of specimens reinforced with one textile layer and without addition of BF. When these specimens failed, the bottom of specimens was broken and debonding along the matrix-textile interface did occur. As the applied load continue to increase, the interfacial debonding increased followed by collapse of geopolymer matrix. On the contrary, specimens with addition of 7.5% BF, matrix-textile interfacial debonding did not occur, as seen clearly in Figure 5b. Failure mode of these specimens resulted in flexural failure by slipping of textile yarn in geopolymer matrix.

a)

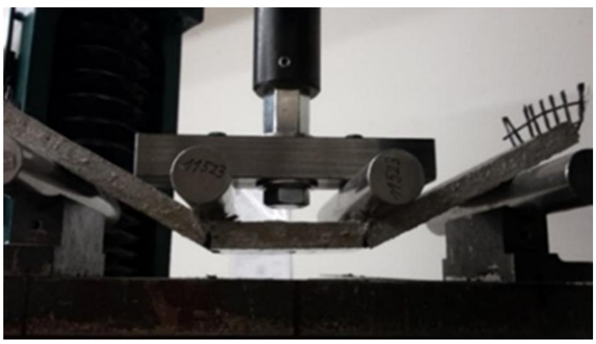

b)

Figure 5 Failure modes of geopolymer composite: a) geopolymer thin plates with one-layer of textile and without addition of BF; b) geopolymer thin plates with addition of 7.5% BF and one-layer of textile

4 CONCLUSIONS

The flexural behavior of one-layer textile reinforced geopolymer thin plates containing various contents of BF was investigated and tested. The attained results from experiment show that the addition of BF reinforced geopolymer mortar is helpful to improve both the first-crack load, the ultimate load, and flexural toughness of textile reinforced geopolymer specimens. By visual observation of the specimens during the bending test, they indicated the different failure behaviors. The specimens without BF or with low content of BF exhibited the similar failure by debonding along the matrix-textile interface, whereas the specimens with high content of BF resulted in bending failure by slipping of textile yarn in matrix.

Acknowledgements: *This publication was written at the Technical University of Liberec, Faculty of Mechanical Engineering with the support of the Institutional Endowment for the Long Term Conceptual Development of Research Institutes, as provided by the Ministry of Education, Youth and Sports of the Czech Republic in the year 2018 and by the project „Application of geopolymer composites as fire, AGK", registration number VI20172019055, were obtained through the financial support of the Ministry of interior in the program "The Safety Research of the Czech Republic" 2015-2020 (BV III/1-VS).*

5 REFERENCES

1. Subaer, Van Riessen A.: Thermo-mechanical and microstructural characterisation of sodium-poly(sialate-siloxo) (Na-PSS) geopolymers, J Mater Sci. 42(9), 2007, pp. 3117-3123, doi:10.1007/s10853-006-0522-9
2. Al Bakri A.M.M., Kamarudin H., Abdulkareem O.A.K.A., Ruzaidi C.M., Rafiza A.R., Norazian M.N.: Optimization of alkaline activator/fly ASH ratio on the compressive strength of manufacturing fly ASH-BASED geopolymer. Applied Mechanics and Materials 110-116, 2011, pp. 734-739, doi:10.4028/www.scientific.net/AMM.110-116.734
3. Saidi N., Samet B., Baklouti S.: Effect of composition on structure and mechanical properties of metakaolin based PSS-geopolymer, Int J Mater Sci. 3(4), 2013, pp. 145-151, doi:10.14355/ijmsci.2013.0304.03
4. Rickard W.D.A., Temuujin J., Van Riessen A.: Thermal analysis of geopolymer pastes synthesised from five fly ashes of variable composition, J Non Cryst Solids. 358(15), 2012, pp. 1830-1839, doi:10.1016/j.jnoncrysol.2012.05.032
5. Alomayri T., Shaikh F.U.A., Low I.M.: Mechanical and thermal properties of ambient cured cotton fabric-reinforced fly ash-based geopolymer composites, Ceram Int. 40(9 PART A), 2014, pp. 14019-14028, doi:10.1016/j.ceramint.2014.05.128
6. Rickard W.D.A., Vickers L., van Riessen A.: Performance of fibre reinforced, low density metakaolin geopolymers under simulated fire conditions, Appl Clay Sci. 73(1), 2013, pp. 71-77, doi:10.1016/j.clay.2012.10.006
7. Mechtcherine V.: Novel cement-based composites for the strengthening and repair of concrete structures, Constr Build Mater. 41, 2013, pp. 365-373, doi:10.1016/j.conbuildmat.2012.11.117
8. Jabr A., El-Ragaby A., Ghrib F.: Effect of the fiber type and axial stiffness of FRCM on the flexural strengthening of RC beams, Fibers 5(1), 2017, 22 p., doi:10.3390/fib5010002
9. Amran Y.H.M., Rashid R.S.M., Hejazi F., Safiee N.A., Ali A.A.A.: Response of precast foamed concrete sandwich panels to flexural loading, J Build Eng. 7, 2016, pp. 143-158, doi:10.1016/j.jobe.2016.06.006
10. Atahan H.N., Pekmezci B.Y., Tuncel Y.: Behavior of PVA fiber reinforced cementitious composites under static and impact flexural effects, J Mater Civ Eng. 25(10), 2013, https://doi.org/10.1061/(ASCE)MT.1943-5533.0000691
11. Williams Portal N., Flansbjer M., Zandi K., Wlasak L., Malaga K.: Bending behaviour of novel Textile Reinforced Concrete-foamed concrete (TRC-FC) sandwich elements, Compos Struct. 177, 2017, pp. 104-118, doi:10.1016/j.compstruct.2017.06.051
12. Dey V., Zani G., Colombo M., Di Prisco M., Mobasher B.: Flexural impact response of textile-reinforced aerated concrete sandwich panels, Mater Des. 86, 2015, pp. 187-197, doi:10.1016/j.matdes.2015.07.004
13. Colombo I.G., Colombo M., Di Prisco M.: Bending behaviour of Textile Reinforced Concrete sandwich beams, Constr Build Mater. 95, 2015, pp. 675-685, doi:10.1016/j.conbuildmat.2015.07.169
14. BS EN 196-1:2005. Methods of testing cement – part 1: Determination of strength

AUTOMATIC ANALYSIS THE BRAIDING ANGLE OF THE BRAIDED FABRICS USING IMAGE PROCESSING

Yisheng Liu[1] and Yordan Kyosev[2]

[1]Zhejiang Sci-Tech University, Hangzhou, The Second Street 298, Xiasha, 310018, China
[2]Hochschule Niederrhein University of Applied Sciences, Webschulstrasse 31, D - 41065 Mönchengladbach, Germany
Lysleo@zstu.edu.cn

Abstract: *The braiding angle is one of the most important parameters of the braided structures, because it influences their mechanical properties. For this reason, any way of automatic inspection of the braiding angle can simplify the quality control of such products. Image analysis is one of the feasible non-contact measurement methods to obtain braiding angle. In this paper is presented a new program for image processing and analysis of the braiding angle. Nine different braided structures are analyzed manually and with the help of the program. The comparison of the results demonstrates that in the most cases the created algorithm produces accurate results but in few situations it analyses different geometrical properties in the image than those, analyzed by humans.*

Keywords: *Braiding angle, automatic detection, Image analysis, Image processing, Python, Hough line detection*

1 INTRODUCTION

Braided products are not so popular like the woven and knitted but are used in large number of applications. In each car are integrated more than 1500 meter of braided products [1]. Large part of the ropes for industrial and marine application are braided and the climbing ropes are as well braided products [2]. In one braided structure there are direct relations between the elasticity, strength, bending stiffness and other parameters and the braiding angle [3, 4]. For this reason its automatical control is important step in the ensuring the quality of the braided products. This paper presents the development of algorithm for automated analysis of the braiding angle based on the Python libraries.

2 APPLICATION OF THE IMAGE PROCESSING

Python is a high-level language with an open source, high-quality, peer-reviewed code, written by an active community of volunteers [5]. Now Python become one of the most popular program languages in the world. For the image analysis and angle identification, several modules such as Numpy, Scipy, Scikit-image and matplotlib were used and all of these can be found on the web.

Scikit-image [6], Image processing in Python, is a collection of algorithms for image processing. For braiding angle identification, it provides a set of functions for image loading, visualization, manipulation, and analysis. The flow chart of the executive program is shown in Figure 1 and it includes several steps from loading image to calculation of the braiding angle. The interface of the executive program is shown in Figure.2.

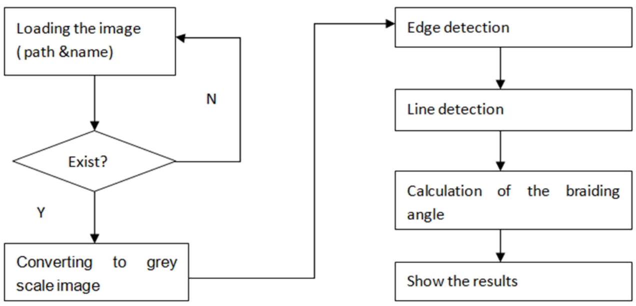

Figure 1 The flow chart of the executive program

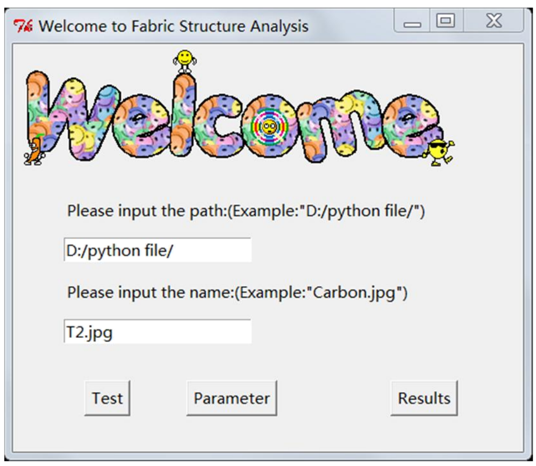

Figure 2 Interface of the executive program

2.1 Loading image

The first step for the analysis is loading image into the executive program. The following code:

```
img2=io.imread(imgpath)
```

opens file with 'imgpath', which can be in different format as jpeg, bmp, pngor other and store the information in the variable img2. This variable is now an array, in the current case with size 1077 x 817 x 3 unsigned integers, which means that there are three arrays with the red, green and blue values of each of the pixels.

2.2 Converting to greyscale image

In Scikit-image processing, the angle detection and several image processing functions work only with greyscale images, therefore it is necessary to convert the true color image to a greyscale image. In the example, the true color image is represented as an unsigned integers array, it need to be transferred into floats ones and then to a greyscale image by using the function 'img_as_float()' and 'rgb2gray()'. The result of this conversion is presented in Figure 3 (right).

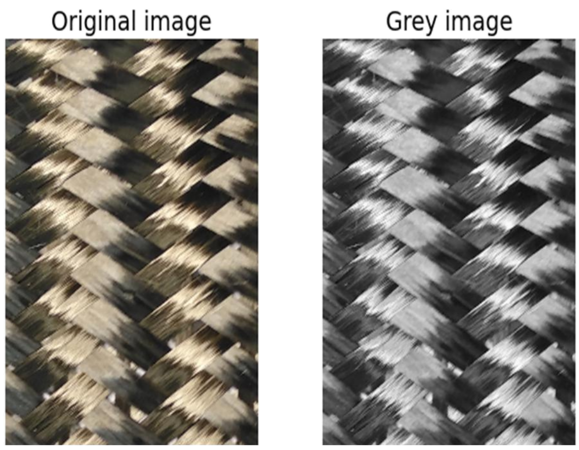

Figure 3 Image of T2.jpg – left) original true color image, right) after conversion to greyscale

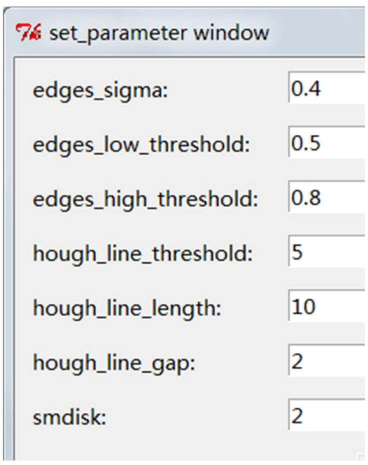

Figure 4 Parameters for the edge detection

2.3 Edge detection

For the image processing several parameters of the algorithms have to be set. As the different samples require different values, a small user interface (Figure 4) was prepared, in order different configurations to be tested quickly. The seven parameters of the image analysis procedure has to be entered, one for morphology, three for edges detection and three for hough line detection. After some experience it was found, that the edge detection works better if the image is „homogenized" – some small bright spots are removed and the small dark cracks are connected. This is done by the function 'Opening' of the Skiimage toolbox.

To find edges in the greyscale image, the 'canny' function can be used [7]. This function finds places in the image where the intensity changes rapidly. In the image those places could be the edges of the threats within the braid. The most useful edge-detection method is the 'canny' method. This method differs from the other edge-detection methods in that it detects strong and weak edges. As visible in Figure 5 (left), the main directions of the yarns can be recognized, The main commands are:

```
import skimage.morphology as sm
from skimage import feature
image = sm.opening(image1,sm.disk(int(smdisk)))
edges = feature.canny(image, sigma=float(pes),
       low_threshold=float(pelt),
       high_threshold=float(pelh))
```

2.4 Hough line detection

To get the braiding angle it is necessary to detect at least one straight line at an edge of a thread. To detect those lines the 'Hough' transformation is applied [8]. The Hough transformation creates a dual space where all possible parameters of the to-find point are entered for each point in the image that is located on an edge. After setting the threshold, line length and line gap, The 'Hough_line' function will detect the edge line and get a line list, in which the star point and end point of each line is stored as a tuple. As visible in Table 1, the main directions of the edge lines can be recognized. The main command is:

```
import skimage.transform as st
lines = st.probabilistic_hough_line(edges,
        threshold=int(pht),line_length=int
        (phl), line_gap=int(pha))
```

where „edges" is the variable with the result from the application of the canny algorithm over the figure.

3 RESULTS AND DISCUSSION

The braiding angle is the angle between the product axis and the fibers. Assuming that the image was rotate before the analysis so, that the vertical direction corresponds to the y-axis, the braiding angle can be regarded as the angle between the edge line of yarn and y-axis. Since the start point and end point is detected, the angles of all detected lines can be calculated with the equation

$$\alpha = 90° - abs\left(arctan\frac{\Delta y}{\Delta x}\right) \qquad (1)$$

This angle is calculated for each detected line and the histogram of all values is plotted (Table 2). The maximum of the histogram is taken as a braiding angle.

In the current case, nine different samples were selected for testing the algorithm. The samples was selected so, that they cover different application areas and different structures - to have a monofilament braid, ropes and multifilament structures for composites. As demonstrated (Table 2), there are several detected lines from the images, which are not parallel to the fibers. These lines are coming from shadows, different colour appearance or as well the vertical boundaries of image. But the most of the two largest bars shows the actual braiding angle, as the most of the fibers in the braid are detected as lines, oriented at plus or minus the braiding angle degree. The most difficult step for the application of the algorithm was the detection of the parameters of the edge detection algorithms. During the preparation of the manuscript was found that the algorithm is sensible against the parameters in the image detection and these have to be re-identified with several trials and errors for each new sample. The braiding angle was measured as well manually using the software ImageJ on the same images. The result of the five measurements as arithmetic mean value and the variation coefficients are given in the Table 1. Automated detected angle is presented there too, together with the relative error in % between both measurements.

As it can be seen (Table 1 and Figure 5), in the most cases (1-6) the automatic algorithm determine the braiding angle with less than 10% error. The last three samples have errors up to 20%. The histograms and the images of some typical samples (Table 2) can give explanation of these larger errors. The sample 1 in Table 2 is a structure with monofilmanent wires. The edges, extracted from this image, correspond to the yarns and the accuracy at this image is very high – it produced 0.5% error. Sample 3 is a braid produced from slightly twisted yarns. The algorithm detects there a lot of the single filaments which have different angle than the yarn itself. After playing with the edge detection parameters, still was possible to get the main edges of the yarns and have accurate result with 4.7% error, in the same way as for Figure 6 (rope of twisted linen material). In both cases, the yarns are still recognizable as objects and produce better visible edges than the single fibers or filaments. Completely different is the behaviour at the braids for composites. In such case the rovings consist of thousands of parallel filaments, which are recognized as lines. These filaments are not always exactly parallel to the roving axis and the edges of the roving are optically not easy to be detected.

Because of the large number of the single lines of the filaments, there is one very clear maximum in the histogram and all other detected lines remain with significantly lower appearance, almost not visible there. So in this case, the automatically detected angle differs significantly from the manually detected one, because the operator is able to identify the roving main line and the algorithm detect the orientation at the finer – filament level.

Table 1 Tested samples and manual and computed results

No.	Original Image	Grey Scale	Canny Edges	Probalistic Hough	Measured (Mean N=5) [°]	$V = \frac{\sigma}{\bar{x}}$ [%]	Detected [°]	Rel. Error [%]
1	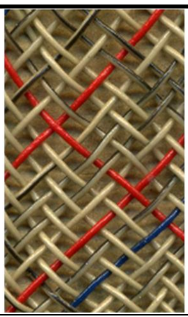	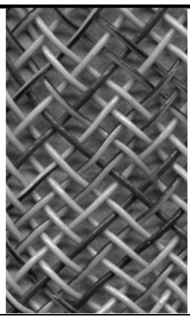		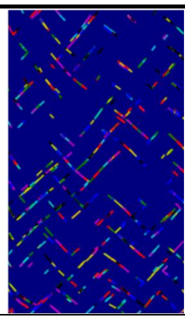	45.1	1.80	44.9	-0.5

2				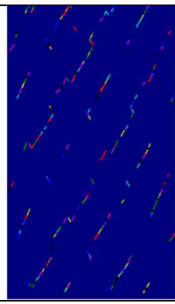	28.6	1.7	26.5	-7.3
3				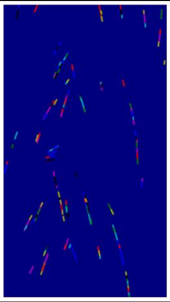	19.3	4.6	18.4	-4.7
4				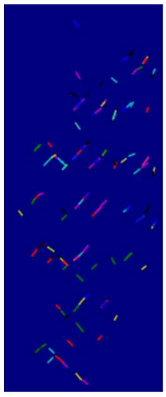	44.4	2.1	44.5	0.2
5		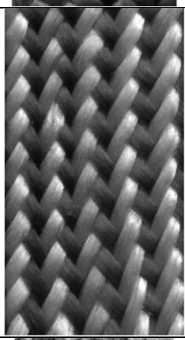		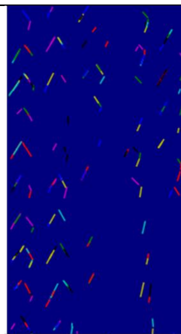	27.5	4.2	26.5	-3.9
6			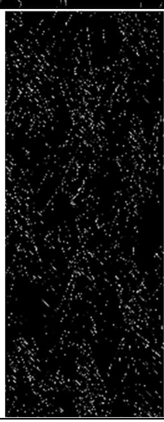	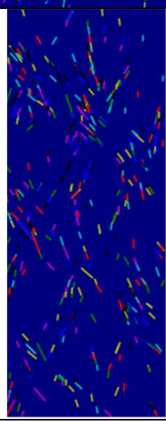	25.4	3.5	26.6	4.4

7		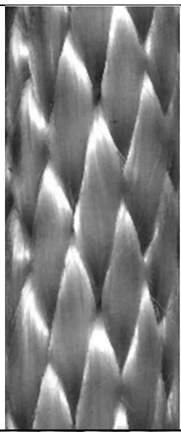		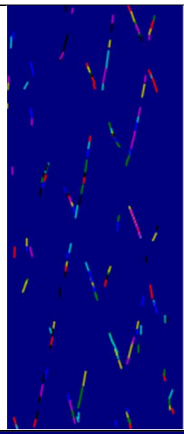	15.6	3.9	18.0	15.0
8		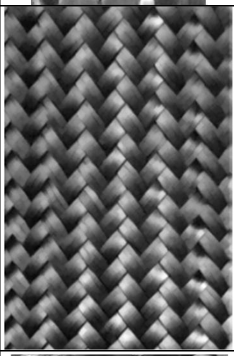	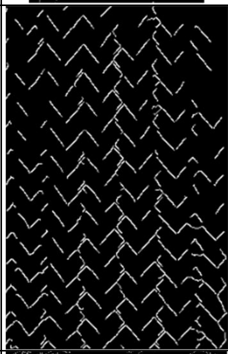	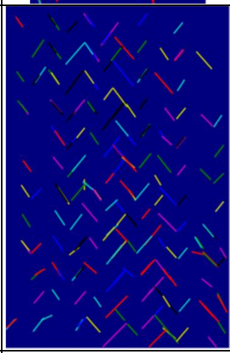	40.7	3.8	44.9	10.1
9			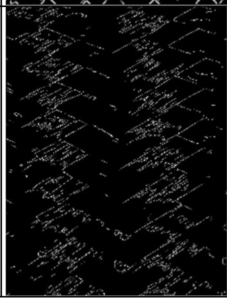	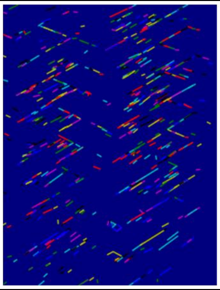	56.4	2.1	44.7	-20.7

Table 2 Automatically detected braiding angles for some samples

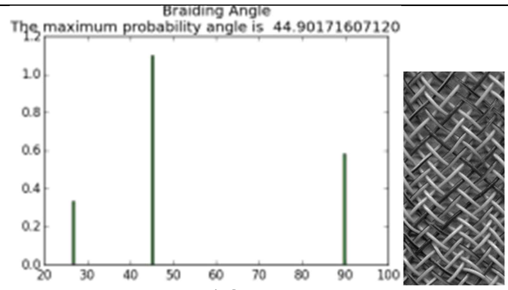

a) Sample 1

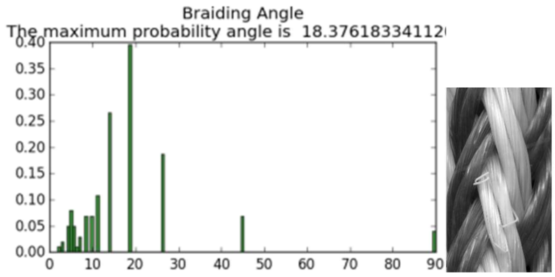

b) Sample 3

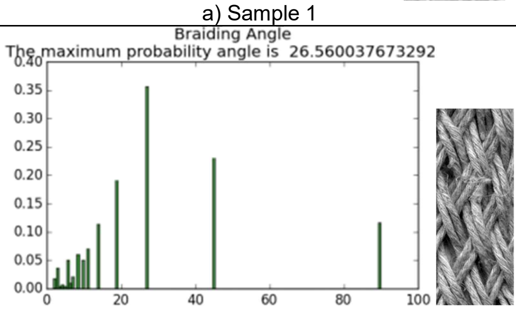

c) Sample 6

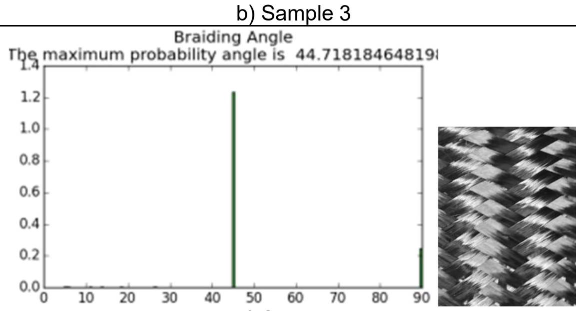

d) Sample 9

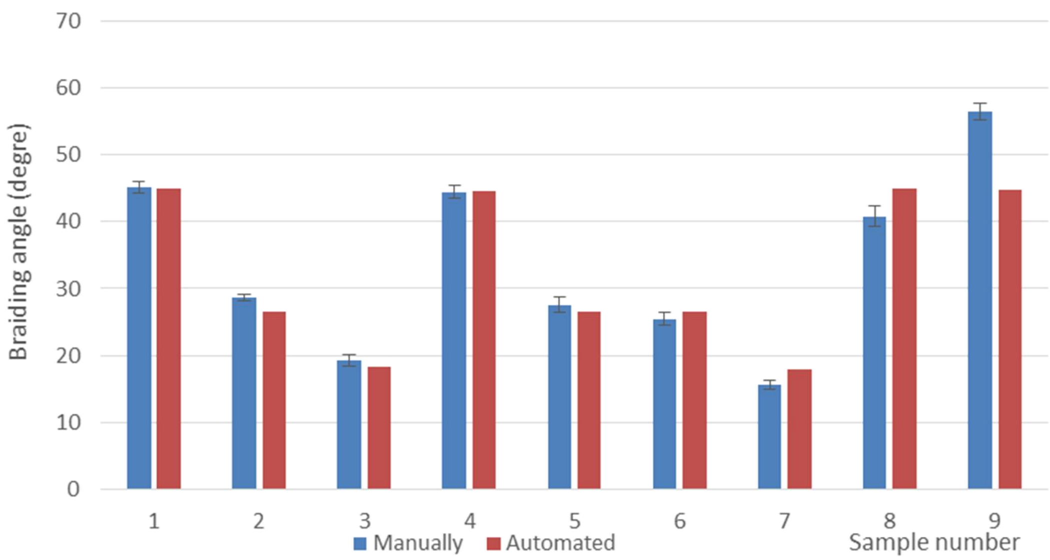

Figure 5 Comparison between the manually and automated estimated braiding angles

4 CONCLUSION

The automated program for image processing based on Python language was developed and applied for automatic detection of the braiding angle of braided products. It can be used for fast quality control of braided product and allows very good accuracy for the braid, where the yarns can be recognized optically. The algorithm can be applied for structures for composites, too, but in this case it detects the fiber orientation and not always the tow orientation. The main task for using such algorithm in the practical application seems to be the detection of the parameters of the image processing functions. Their values depend on the contrast and the brightness of the image.

5 REFERENCES

1. August Herzog, Product Catalogue, Oldenburg, 2013
2. Kyosev Y. (Ed.): Advanced in the braiding technology, Specialized Techniques and Applications, Elsevier, 2016, eBook ISBN: 9780081004265, Hardcover ISBN: 9780081009260
3. Brookstein D.S., Tsiang T.-H.: Load-deformation behavior of composite cylinders with integrally-formed braided and with machined circular holes, Journal of Composite Materials 19(5), 1985, pp. 476-487, https://doi.org/10.1177/002199838501900506
4. Kyosev Y.K.: Braiding technology for textiles: Principles, design and processes, Woodhead Publishing Series in Textiles No. 158, 1st ed, 2014, eBook ISBN: 9780857099211, Hardcover ISBN: 9780857091352, Paperback ISBN: 9780081013298
5. Python, www.python.org (2018)
6. Scikits Toolbox, https://www.scipy.org/scikits.html
7. Canny J.: A computational approach to edge detection, IEEE Transactions on Pattern Analysis and Machine Intelligence PAMI-8(6), 1986, pp. 679-698, doi: 10.1109/TPAMI.1986.4767851
8. Hough P.: Method and means for recognizing complex patterns, U.S. Patent 3069654, 18 December 1962

OIL-TREATED FIBROUS AIR FILTERS FOR AUTOMOTIVE ENGINE INTAKE APPLICATION

Ajay Kumar Maddineni and Dipayan Das

Department of Textile Technology, Indian Institute of Technology Delhi, Hauz Khas, New Delhi-110016

Abstract: *This work deals with development, characterization and performance evaluation of oil-treated fibrous air filters for automotive engine intake application. According to the classical theory of air filtration, an air filter would exhibit higher filtration efficiency when tested at higher face velocity. This is however not found true in the current research work. Here, the filtration efficiency of a cellulosic filter media was found to decrease at higher face velocities for relatively large particles. This happened apparently due to particle bounce and re-entrainment phenomenon. Nevertheless, it poses a major challenge to achieve the futuristic target of filtration efficiency with ever-increasing trend of engine downsizing and less availability of installation space for automotive engine intake air filter media. Here it was demonstrated that the particle bounce could be suppressed by oil treatment to the filter media, as a result, the filtration efficiency of the oil-treated filter media increased at higher face velocities for large particles, unlike the untreated ones. This behavior was explained in the light of theoretical and empirical models of air filtration. In case of less oil loading, the initial pressure drop across the oil-treated filter media was found to be almost the same as that across the untreated one. But, when the oil loading was high, the initial pressure drop increased tremendously. This behavior was discussed with the help of Davies equation by taking into account of the changes in diameter of oil-coated fiber and packing density due to oil treatment. Further, at lower dust loading, the oil-treated filter media exhibited lower pressure drop and lower filtration efficiency at lower face velocities, but, at higher face velocities, the same media displayed higher filtration efficiency but with a similar pressure drop. However, at higher dust loading, the same media exhibited higher filtration efficiency.*

Keywords: *Automotive engine intake air filtration, particle bounce and re-entrainment, oil-treated filter media, filtration efficiency, pressure drop, dust loading.*

1 INTRODUCTION

Engine intake air filters in automotive application were primarily used to remove the air borne dust particles to reduce the wear of moving components. Dust particles of 5-10 µm particles causes the major increase in wear over engine life time followed by 10 -20 µm [1]. Therefore, the automotive engine air filters are designed to reliably filter out those fractions of particles. Increasing emission regulations and the evolving requirements associated with engine durability, packaging environment, sophisticated engine technology, etc., are challenging the design of automotive air filter to efficiently capture the dust particles [2]. Wide variety of filter media such as polyurethane based reticulated foam, cellulose based wet laid paper, polymer based nonwoven were popularly used in automotive industry. Among the said filter media technologies, standard cellulose-based paper filter media is well known in Asia due to its performance, cost and packaging benefits. Particle penetration of such filter media is influenced by various factors such as fiber diameter, packing parameters of the fibers that result in wide pore sizes, operating conditions. A lot of efforts have been put in the past to optimize these filter media to reduce particle penetration. However, the velocity of the particles to which the media is exposed greatly affects the particle penetration. Reducing installation space in the vehicle for air filters now-a-days increases the flow velocities. It is known that with increasing flow velocity, filtration efficiency increases due to dominance of inertial impaction mechanism [3]. However the same is not true always. Increase in flow velocity increases the energy associated with the particle depending on mas-inertia relation that cause particle to bounce back and re-entrain into the fluid stream to escape through the media. This leads to an elevated risk to the engine components, associated with exposure to dust particles. These limitations are posing a challenge for the futuristic target of filtration efficiency and the air filter system design for automotive engine intake application. These new challenges motivated us to understand the particle penetration behavior of cellulosic filter media. Recently, limited studies showed the improvement of the filtration efficiency by treating the fibrous filter media with oil [4]. The present work made an attempt to investigate the impact of oil treatment on the filtration efficiency and pressure drop of automotive engine intake air filter media for different face velocities at the initial stage of filtration as well as during dust loading.

2 EXPERIMENTAL

2.1 Materials

In this study, a commercially available cellulose based filter media was used. The average fiber diameter of such filter media observed under SEM was found as 23 µm with coefficient of variation of 34%. The thickness of the fabric was measured by a digital fabric thickness tester in accordance with ASTM D5729-97 standard. The average thickness of the fabric was obtained as 0.75 mm. The basis weight of the fabric was measured by using a weighing balance as per ASTM D 6242-98 standard. The average basis weight of the fabric was determined as 181 g/m^2 with a coefficient of variation of 1.73%. Hydraulic oil with density of 0.86 g/cm^3 and viscosity ranging from 25 to 38 cSt at 40°C temperature was used to treat the cellulose filter media.

2.2 Methods

The cellulosic filter media was treated with Hydraulic oil 32 using the in-house fabricated test setup as shown in Figure 1. The oil will be sprayed in the form of fine droplets onto the filter media, using an oil atomizer. Hydraulic oil is stored in the reservoir tank and is supplied to the spraying gun. The dry filter element is hold by a mounting plate at a distance of 0.45 m from the spray gun. The mounting plate moves in lateral direction of spray gun by means of slider and piston mechanism so as to spray oil onto the filter surface as uniformly as possible. The extra oil is collected in the tray below the fixture. Defined oil quantity on 100 cm^2 of filter area is applied on the raw gas side of the pleated filter media. Iterative measurement of weighing oil element after oil treatment is performed using a weighing balance to maintain proper quantity of oil. SEM image of oil distribution on the fibers of the filter media is shown in Figure 3.

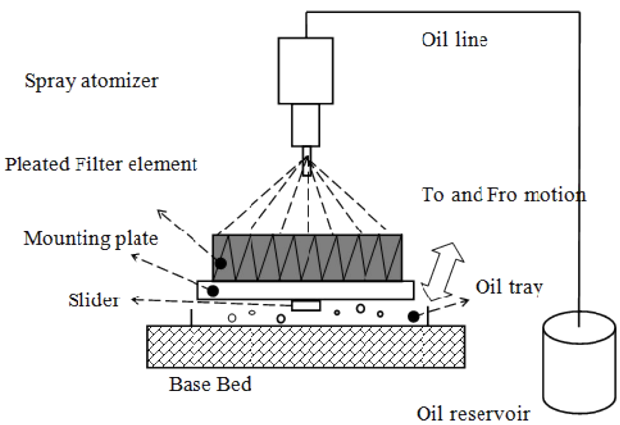

Figure 1 Chemical treatment setup

The oil treated as well as the non-treated filter media is challenged with ISO fine dust aerosol according to ISO 12103-1 was used for filtration efficiency measurements. The experimental setup for measurement of filtration efficiency is displayed in Figure 2. Test dust was dispersed by the powder dispersion generator with brush at a pressure of 2 bar. Aerosol spectrometer of Welas was used to measure particle distribution using light scattering technique. Test dust samples were attached to the particle analyzer using the iso-kinetic probe. Pressure drop was measured using the pressure taps placed across the filter media. Test dust of 0.2 g/m3 concentration was used in the current study. Particle measurements at higher concentration lead to false results. Continuous loading of the circular blank test samples using test dust and simultaneous measurement of pressure drop and particle size downstream was done.

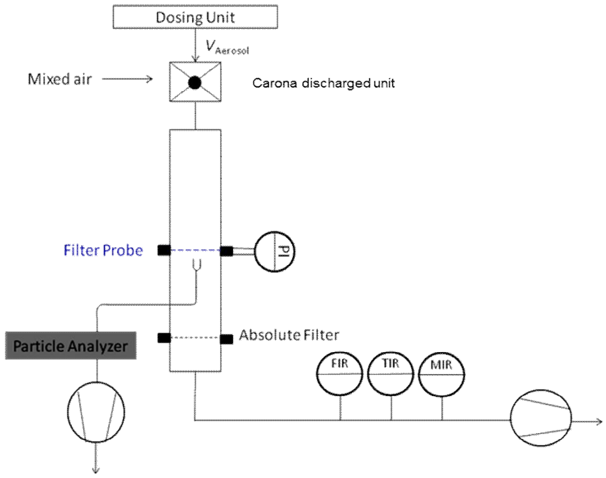

Figure 2 Experimental setup for filtration test

3 RESULTS AND DISCUSSION

The effect of face velocity on the initial pressure drop of oil-treated and untreated filter media is displayed in Figure 3. It can be observed that the untreated and the filter media treated with oil of 80 g/m^2 exhibited almost similar at all velocities tested. In contrary to this, the filter media treated with 240 g/m^2 oil displayed an increase of 5 to 9 times pressure drop as compared to the untreated filter media. This might be due to the fact that a higher quantity of oil deposited onto the filter media caused an increase of diameter of oil-coated fiber and a reduction in porosity that in turn resulted in increase of pressure drop across the media. In the following, an attempt was made to explain this scientifically using following expression [3, 5]:

$$d_{f,o} = d_f \sqrt{\left(1 + \frac{W_o}{W_f} \frac{\rho_f}{\rho_0}\right)} \quad (1)$$

$$\mu_{f,o} = \frac{W_f + W_o}{Z\left(\dfrac{g_f\rho_f + g_o\rho_0}{g_f + g_o}\right)} \tag{2}$$

$$\Delta P = \frac{64\mu_{f,o}^{1.5}\left(1+56\mu_{f,o}\right)^3 \nu U Z}{d_{f,o}^2} \tag{3}$$

where $d_{f,o}$ and d_f stand for the diameters of oil-coated and untreated fibers, respectively; W_o and W_f denote the weight of oil per unit area of the filter and weight per unit area of dry filter media, respectively; and ρ_f and ρ_o indicate the densities of fiber and oil, respectively. g_f and g_o are the mass proportions of fiber and oil, respectively, in the filter media and Z is the thickness of filter media. The diameter of oil-coated fiber and the packing density of oil-treated filter media could be substituted in the following Davies equation to determine the pressure-drop across the filter media. where ΔP denotes the pressure drop, ν indicates the viscosity of air, and Urefers to the face velocity.

It can be seen that the Davies equation using the diameter of oil-coated fiber and the packing density of the oil-treated filter media corresponded satisfactorily with the pressure drop data obtained experimentally.

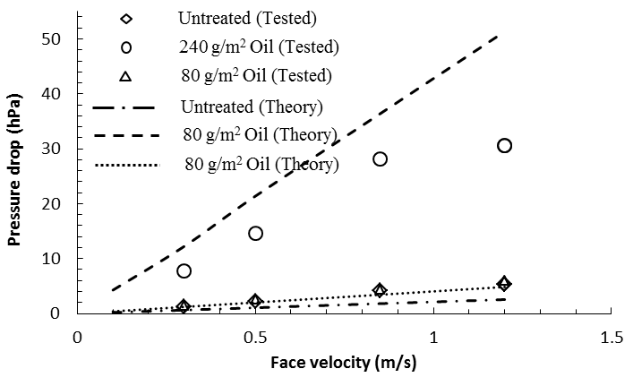

Figure 3 Initial pressure drop as a function of face velocity

Initial filtration efficiency of the untreated and oil-treated filter media at different velocities 0.1, 0.3, 0.5, 0.85 and 1.2 m/s respectively were shown in Figure 4. Particles beyond 0.5 µm particle size, the filtration efficiency increased with the increase of particle diameter as the interception and impaction mechanisms of particle capture were predominating. Filtration efficiency rose to higher than 99% for larger particles and at the face velocity of 0.1 m/s. A similar trend was observed at a face velocity of 0.3 m/s. However, the efficiency of filtering large particles at a face velocity of 0.3 m/s was less than that at 0.1 m/s. At a face velocity of 0.5 m/s, the filtration efficiency rose to 97% when the particle size was 4 µm, but decreased afterwards, however. A similar observation was found at a face velocity of 0.85 m/s velocity with significant decrease in filtration efficiency from 95 to 89% beyond the particle size of 2 µm. A further reduction in filtration efficiency was observed at 1.2 m/s when the particle size was 2 µm and beyond. It was therefore observed that the filtration efficiency decreased for larger particles at higher velocity. This finding contradicted the classical theory of air filtration. Probably, this unusual behavior was attributed to rebound of particles after colliding the filter surface and followed by subsequent re-entrainment of particles in the air streams at higher velocity. Figure 4b displays the initial filtration efficiency of the oil-treated filter media with oil loading of 80 g/m^2. The oil-treated filter media with 80 g/m^2 oil loading did not show any particle bounce for all particle sizes, regardless of the face velocities chosen. As the oil droplets present on the surface of the filter media caused the particles to adhere to the oil-coated fiber, the oil-treated filter media did not show any reduction in filtration efficiency, especially at higher face velocities and at larger particle sizes. The measured filtration efficiency of the untreated and oil treated filter media was calculated using the theoretical relations of collection efficiency.

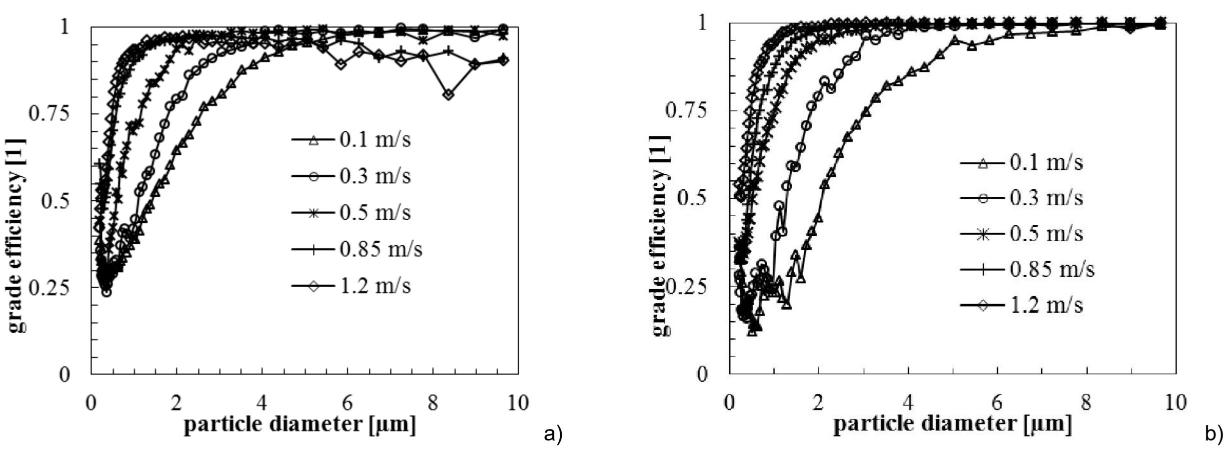

Figure 4 Measured grade efficiency at initial stage for untreated filter media (a) and oil-treated filter media with oil loading of 80 g/m^2 (b)

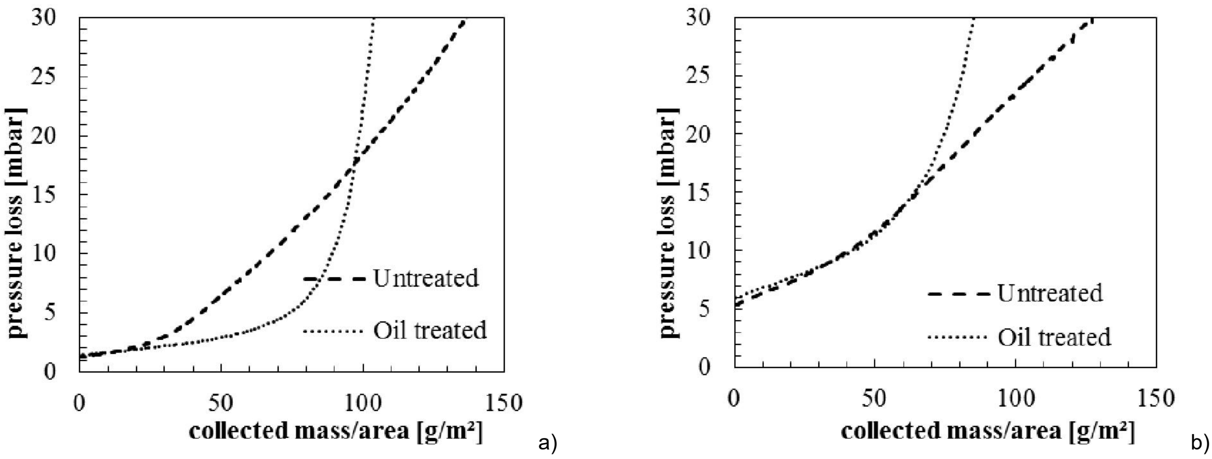

Figure 5 Evolution of pressure drop during dust loading at face velocities of 0.3 m/s (a) and 1.2 m/s (b)

The pressure drop curves of untreated and oil-treated filter media during dust loading at face velocities of 0.3 m/s, and 1.2 m/s was shown in Figure 5. At a low level of face velocity, i.e., 0.3 m/s, the untreated media exhibited slow increase of pressure drop till 30 g/m^2 of dust collection and at the end it accumulated 145 g/m^2 of dust to reach a pressure drop of 30 mbar. At the same velocity, the oil-treated filter media displayed slow increase of pressure drop till 60 g/m^2 of dust accumulation, but at the end it accumulated 100 g/m^2 of dust to reach the pressure drop of 30 mbar. The initial slow increase of pressure drop across the oil-treated filter media was due to the combined effect of depth loading and oil loading. In this stage of dust loading, the pressure curve of oil-treated filter media lay at a significantly lower position than that of the untreated one. In case of oil-treated filter media, the dust particles adhered to the oil and formed dust islands that mobilized around the fiber with the oil, creating more pore space than the untreated one. But, as the oil droplets were saturated with dust particles, surface filtration started that increased the pressure drop suddenly with very little addition of dust particles. At a very high level of face velocity, i.e., 1.2 m/s, the oil-treated and the untreated filter media exhibited similar pressure drop characteristics till the surface filtration started. At higher velocities the aerodynamic drag was dominant due to the fact that the oil droplets were saturated with the dust particles at a faster rate due to dominant inertial deposition and thus rate of pressure loss increased with dust loading.

The evolution of gravimetric filtration efficiency of untreated and oil-treated filter media at three different stages of dust loading was displayed at Figure 6. The untreated filter media showed filtration efficiency greater than 99% at a dust loaded pressure drop of 10 hPa and the same was increased with increasing pressure drop from 10 to 20 hPa at a velocity of 0.3 m/s (Figure 6a). This indicated that a dendritic growth of particles took place at the upstream side [6] and thus the increasing trend of particle capture is observed. The oil-treated filter media also exhibited increasing trend of filtration efficiency with increasing pressure drop from 10 to 20 hPa. However, the oil-treated filter media displayed lower filtration efficiency than the untreated one at pressure drops of 10 hPa and 20 hPa. This behaviour was probably due to the fact that some of the dust particles were captured by the fibres and the rest were adhered to the oil-droplets; hence the dendritic growth was not significant at this stage of filtration. At a further higher level of dust loading (equivalent to 30 hPa pressure loss), the untreated media exhibited a drop in filtration efficiency due to increased local velocities within the filter that caused the particles getting more energy and were able to penetrate the filter media. While the oil-treated media displayed an increase in filtration efficiency with increasing dust loading. Interestingly, the oil-treated filter media showed higher filtration efficiency than the untreated media at a pressure drop of 30 hPa. This might be due to increased adhesion between particles and fibers. At 1.2 m/s face velocity, the oil-treated filter media exhibited an increasing trend of filtration efficiency as the pressure drop increased. The untreated filter media showed a drop in filtration efficiency as dust loading and face velocity increased, whereas the oil-treated media displayed an increase of filtration efficiency with the increase of dust loading and face velocity. The filtration efficiency of the oil-treated filter media was related to the loading of oil by dust particles. As the oil loading was higher the increase of filtration efficiency was lower. Interestingly, the filtration efficiency of the untreated media was higher than the oil-treated media at low levels of dust loading and at lower face velocity.

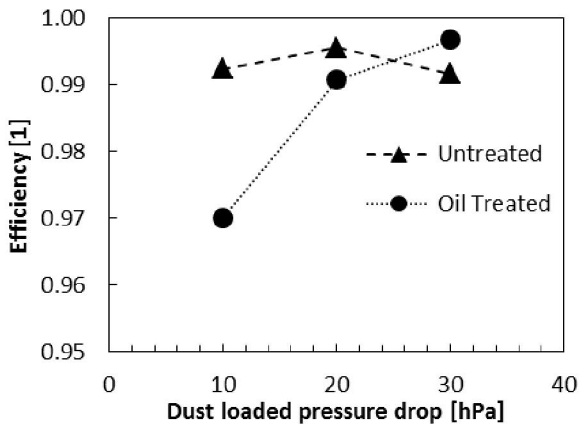

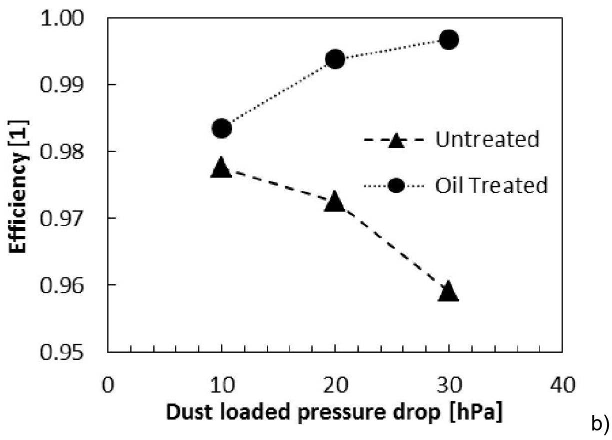

Figure 6 Evolution of filtration efficiency during dust loading at face velocities of 0.3 m/s (a) and 1.2 m/s (b)

4 CONCLUSIONS

Oil-treated and untreated cellulosic filter media were examined for pressure drop and particle filtration behaviors at the initial stage of filtration as well as during dust loading. The initial pressure drop across the oil-treated filter media was found to be almost the same as that of untreated media at a low level (80 g/m^2) of oil loading. But, when the oil loading was increased to as high as 240 g/m^2, the pressure drop was 5 to 9 times higher, depending on the face velocity, than that of the untreated media. This behavior was explained in the light of Davies equation by taking into account of the change in diameter of oil-coated fiber as well as in packing density due to oil treatment. During initial stage of filtration, the untreated filter media displayed higher filtration efficiency at higher velocity for lower particle size, but the filtration efficiency decreased for large particle size as the face velocity increased. This was attributed to particle bounce and re-entrainment phenomenon and its effect was more at higher face velocity. This behavior was explained in the light of theoretical and empirical relations. Inhibition of particle bounce using oil spraying was found to be a suitable technique, as a result, the filtration efficiency of the oil-treated filter media increased at higher face velocities for large particles, unlike the untreated ones. At lower dust loading and lower face velocities, the oil-treated filter media exhibited lower pressure drop and lower filtration efficiency. However, at higher face velocities, the oil-treated filter media displayed higher filtration efficiency but with a similar pressure drop at lower dust loading. Nevertheless, the same media exhibited higher filtration efficiency at higher dust loading.

Acknowledgements: *The financial support received from Science and Engineering Research Board of Department of Science and Technology, Govt. of India under project number SB/S3/ME/063/2015 for carrying out this work is gratefully acknowledged.*

5 REFERENCES

1. Mollenhauer K., Tschoeke H. (Eds.): Handbook of Diesel Engines, Springer, 2010, DOI 10.1007/978-3-540-89083-6
2. Maddineni A.K., Das D., Damodaran R.: Experimental and numerical study on automotive pleated air filters, SAE Technical Paper 2016-28-0100, 2016, https://doi.org/10.4271/2016-28-0100
3. Brown R.C.: Air filtration: an integrated approach to the theory and applications of fibrous filters, Pergoman press, Oxford, 1993, eBook ISBN 9780080912608
4. Müller T.K., Meyer J., Thebault E., Kasper G.: Impact of an oil coating on particle deposition and dust holding capacity of fibrous filters, Powder Technol. 253, 2014, pp. 247-255, https://doi.org/10.1016/j.powtec.2013.11.036
5. Agranovski I., (Ed.): Aerosol- Science and Technology, Wiley (Germany), 2010, ISBN: 978-3-527-32660-0
6. Oh Y.W., Jeon K.J., Jung A.I., Jung Y.W.: A simulation study on the collection of submicron particles in a unipolar charged fibre, Aerosol Sci. and Technol. 36(5), 2002, pp. 573-582, https://doi.org/10.1080/02786820252883810

PROBLEMATICS OF LARGE-SIZE BATCH WINDING OF TECHNICAL TEXTILES

Josef Žák

VÚTS, a.s. Liberec, Svárovská 619, Liberec, Czech republic
josef.zak@vuts.cz

Abstract: *When weaving technical textiles we often encounter problems that are not known from weaving ordinary textiles. This is due to the significantly different mechanical properties of the fibers forming the fabrics. At the same time, productivity pressures cause additional complications, especially in the marginal areas of weaving, whether warping or just winding the resulting product. As the resulting batch becomes larger, it becomes corrugated and consequently damages the fabric. This problem has increased in our case when weaving 3D fabric. We were therefore faced with the task of solving this problem. In the solution, we used the classical mechanics of the continuum. Due to the complexity of the problem, we had to accept some simplifications, such as the assumption of radial isotropy of the wound fabric. It turned out that the resulting relationships are quite complicated, but with the use of computing, the problem is nevertheless solvable. The result of our work is the design of the wrapping program depending on the fabric being fabricated. We have also shown that there are certain boundaries that cannot be exceeded when packing.*

Keywords: *Technical textiles, batch winding.*

1 INTRODUCTION

Currently, two different fabric winding systems are commonly used. The first, historically old and essentially original, consists in winding the fabric on a central tube, which is traditionally placed, but not necessarily, directly on the weaving loom. The tube is driven by a single drive that delivers the required tensile force in the withdrawn raw woven. In principle, it is obvious that this force acting on the circumference is transferred from the tube to the towed fabric by already packed woven. This system, therefore, does not allow the creation of large batches as shown by the experience of generations of weavers.

The second, more modern system consists in separating the fabric from its weaving and removing the woven from the fabric. The tube on which the woven is wound reposes on two rollers that are driven separately. Their circumferential velocities are controlled to produce the desired tension in the cloth withdrawn from the loom. It is clear that the tension in the withdrawn fabric acts on the circumference of the wound fabric and therefore does not affect the already packed cloth. This type of winders can be further divided into two types, namely gravity and controlled pressure. In the first case, the contact force between the valleys and the goods is given by the weight of the packing, in the latter case the compressive force is generated by the auxiliary device and can be controlled. Figure 1 gives a schema of such large-size batch winder.

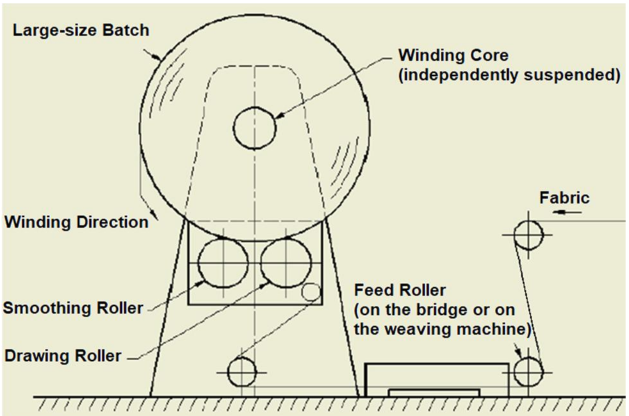

Figure 2 Scheme of large-size batch winder; courtesy of CEDIMA

2 BATCH GEOMETRY DESCRIPTION

The first problem encountered in describing a large-size batch is the description of its geometry. The batch can be considered a spiral.

Its length, depending on the outer radius, is expressed as follows:

$$L = \frac{R_2 \cdot \sqrt{t^2 + 4 \cdot \pi^2 \cdot R_2^2}}{2 \cdot t} - \frac{R_1 \cdot \sqrt{t^2 + 4 \cdot \pi^2 \cdot R_1^2}}{2 \cdot t} + \frac{t \cdot \operatorname{arcsin} h\left(\frac{2 \cdot \pi \cdot R_2}{t}\right)}{4 \cdot \pi} - \frac{t \cdot \operatorname{arcsin} h\left(\frac{2 \cdot \pi \cdot R_1}{t}\right)}{4 \cdot \pi} \tag{1}$$

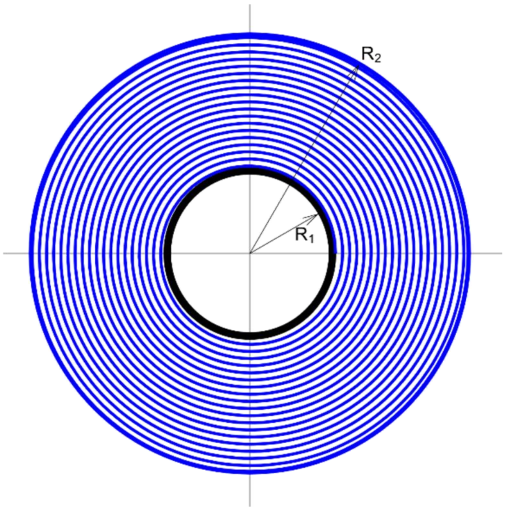

Figure 2 Schema of batch winding

Obviously, the relationship in this form is inappropriate for further calculations. An approximate relationship is therefore needed:

$$l=\frac{R_1+R_2}{2}\cdot 2\cdot\pi\cdot\frac{R_2-R_1}{t}=\frac{\pi\cdot\left(R_2^2-R_1^2\right)}{t} \tag{2}$$

Check for $t\to 0$:

$$\lim_{t\to 0}\left(L-l\right)=\lim_{t\to 0}\left(\frac{R_2\cdot\sqrt{t^2+4\cdot\pi^2\cdot R_2^2}}{2\cdot t}-\frac{R_1\cdot\sqrt{t^2+4\cdot\pi^2\cdot R_1^2}}{2\cdot t}+\frac{\operatorname{arcsinh}\left(\frac{2\cdot\pi\cdot R_2}{t}\right)\cdot t}{4\cdot\pi}-\frac{\operatorname{arcsinh}\left(\frac{2\cdot\pi\cdot R_1}{t}\right)\cdot t}{4\cdot\pi}-\frac{\pi\cdot R_2^2-\pi\cdot R_1^2}{t}\right)=0 \tag{3}$$

Thus, if we know t and l:

$$R_2=\sqrt{\frac{t\cdot l}{\pi}+R_1^2} \tag{4}$$

If we know R_2 and l:

$$t=\pi\cdot\frac{R_2^2-R_1^2}{l} \tag{5}$$

It follows from previous relationships that we have a relationship with three variables t, l and R_2, which are interdependent. To describe the velocity geometry, one of these variables should be defined as independent and the other two parameters. For other purposes and also with respect to the purpose of our work, the variable length of the packing l will be independent, the layer thickness t will be the parameter and the radius of the packing R_2 will be solved from the relations. Otherwise, we would have to continuously measure both the length of the woven fabric and the diameter (the radius) of the wrapper. A key step in the next step will therefore be to determine the thickness t.

3 FABRIC THICKNESS ESTIMATION

3.1 Plain weave fabrics

To estimate the thickness t, we use the formulation following [3]. Its assumptions are:

- double-sinusoidal cross-section shape of the thread
- 100% fabric filling (close to limit values)

The bulk filling of the cloth in plain weave and with high values of sett then moves around the value $\kappa=2/\pi$. By means of volume filling it is possible to estimate the thickness t in mm of such fabrics by means of their parameters:

$$t=\frac{\gamma}{\rho}\cdot\frac{\pi}{2} \tag{6}$$

Estimating the thickness of a cloth in a non-plain weave binding (e.g. twill or satin) can be done in an analogous manner, but the relevant models have not yet been prepared. Similarly, no analysis has been performed so far and no model of leno binding has been developed. For any measurement as the basis for optimizing the winding of such fabrics, it would be necessary to measure the actual wrapping.

3.2 3D fabrics

The main motivation of our work is to master 3D fabrics, more accurately the so-called distance fabric. It consists of two fabrics, for example in plain weave, interconnected by a set of threads.

The thickness of the binding yarns layer must also be included in the calculation of the thickness of the 3D fabric. Their number per unit area is given by their warp density and their pitch in the direction of warp. Their weight (weight per unit area in g/m^2) is given by:

$$\gamma_3=n\cdot l_3\cdot\frac{j_3}{10^6}=\frac{1}{100}\cdot d_3\cdot j_3\cdot\frac{l_3}{r} \tag{7}$$

Thickness of layer of binding yarns then is:

$$t_3=\frac{\gamma_3}{\rho_3}\cdot\frac{1}{\kappa_3} \tag{8}$$

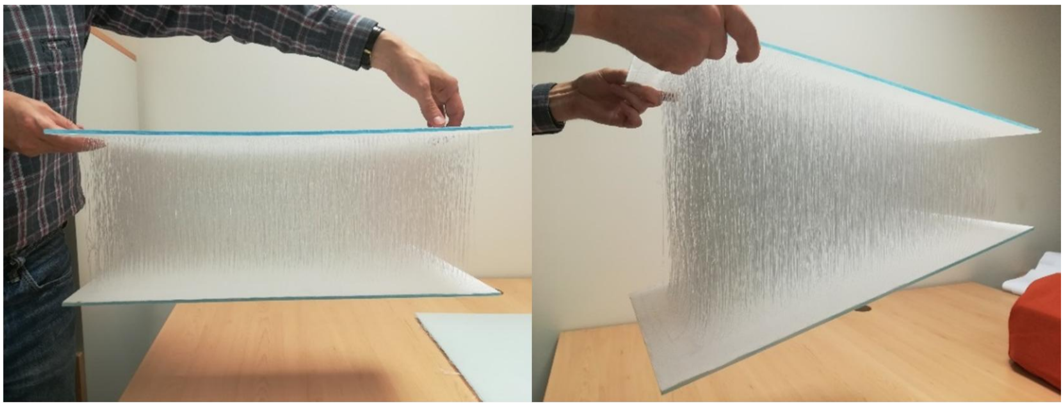

Figure 3 Examples of 3D fabrics

The fill value κ_3 should be determined experimentally, depending, for example, on the twist of the yarns or on the quality of the loop forming. The total weight of the 3D fabric is, of course, the sum of the weights of the surface fabrics and the weight of the staple yarns. The overall thickness is also determined in a similar manner.

4 THEORY

The following chapter presents a procedure for calculating the mechanical behavior of the batch.

4.1 Basic concepts

In our work, we came out of the idea of rotational symmetry of the batch. It is then possible to proceed as follows:

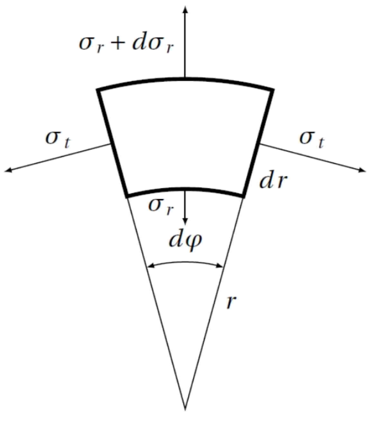

Figure 4 Balance of forces acting on an element

Equilibrium of forces in the radial direction yields as follows:

$$\frac{d}{dr}\left(r\cdot\sigma_r\right)-\sigma_t=0 \tag{9}$$

Assuming radial isotropy of the batch we get following constitutional laws:

$$\begin{aligned}\sigma_r &= K\cdot\left(\varepsilon_r+\mu\cdot\varepsilon_t\right)\\ \sigma_t &= K\cdot\left(\varepsilon_t+\mu\cdot\varepsilon_r\right)+f\left(r\right)\end{aligned} \tag{10}$$

where K is stiffness and μ another Lamé's coefficient (it can be proved that they are meaningless in the case of radial isotropy and assuming state of planar deformations). Then *f(r)* is the force per width reported on unity of radius.

Using deformation restrictions we obtain for the expression of deformation:

$$\begin{aligned}\varepsilon_t &= \frac{u}{r}\\ \varepsilon_r &= \frac{du}{dr}\end{aligned} \tag{11}$$

By expressing constitutional laws and putting them into the equation of radial equilibrium we get fundamental equation:

$$\frac{d}{dr}\left(\frac{1}{r}\cdot\frac{d}{dr}\left(r\cdot u\right)\right)=f\left(r\right) \tag{12}$$

Its solution is easy by double integrating its right side if the *f(r)* is “reasonably” simple. During this integration we will get 2 unknown constants of integration. In order to obtain their values we must provide two boundary conditions. The first one is obvious:

$$u\left(R_1\right)=0 \tag{13}$$

which yields the non-deformability of the central tube.

The second one comes from the fact that the radial stress (or radial pressure) vanishes on the outer radius:

$$\sigma_r\left(R_2\right)=0 \tag{14}$$

4.2 Practical use of mathematical model

For sake of simplicity of this presentation we will assume the polynomial form of the right side *f(r)*. Even then the resulting formulae are in form of a complex rational function. Figure 5 represents the behavior of the tangential stress in the batch for two standard shapes of tension (in function of *r*) as used in praxis.

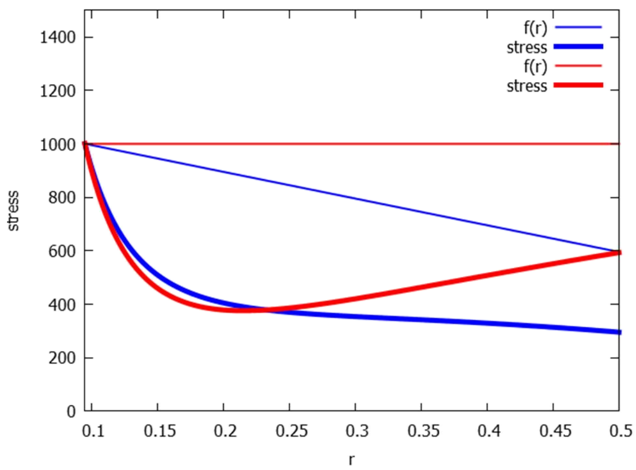

Figure 5 Tension of woven and resulting tangential stress in the batch

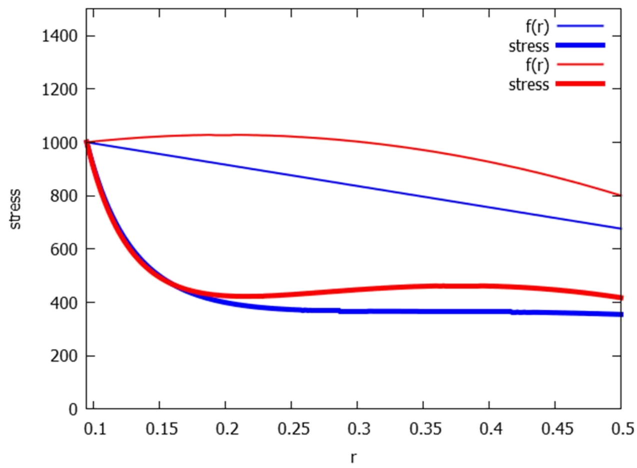

Figure 6 Optimized tension of woven and resulting tangential stress in the batch

It is obvious that such a variation of the cloth tension with the radius of batch has non-negligible effect on the shape of the tangential stress in the wound woven. Variation of the contact press is correspondingly important.

As the control system of winder allows entry of up to 5 point curve along the wound length of woven (not the radius of batch, there no device to measure it), we tried to shape the tension curve using a linear and a quadratic function (Figure 6).

It is known that “best” batches are those with little variation of the stress along the length of the woven (this stress is regularly checked in fabric factory using a special device). Evidently there is a function *f(r)* that allows the creation of large-size batch with a near-constant stress inside, at least along the majority of the wound length of cloth.

5 EXPERIMENT

To verify this hypothesis, the following method was chosen: Several wires are gradually inserted into the batch in the weft direction during wrapping. The force that can be moved by these wires (moving them in the weft direction to one or the other side) is directly proportional to the contact pressure between the layers of the packing between which the wire is inserted. Assuming that the properties of both the fabric and individual wires are constant, both in the width direction of the fabric, both the length of the wire and the direction of the warp (i.e. the inserted wires are identical and the fabric sett do not change, nor changes of lubrication of the fabric, i.e. a constant coefficient of friction between the fabric and the wire can be assumed), it is possible to determine the relation of this force depending on the position of the respective wire to the radius on which the said wire is located. By this method it is possible to verify the contact pressure distribution along the radius of the packing.

The value of the coefficient of friction must be known to determine its absolute values. This can be determined either by a direct measurement by wire tweaking the fabric or by measuring the above-mentioned force immediately after wrapping the respective wire where the contact tension can be determined directly from the fabrics tension when packed. Unfortunately, both methods are burdened by a relatively large measurement error.

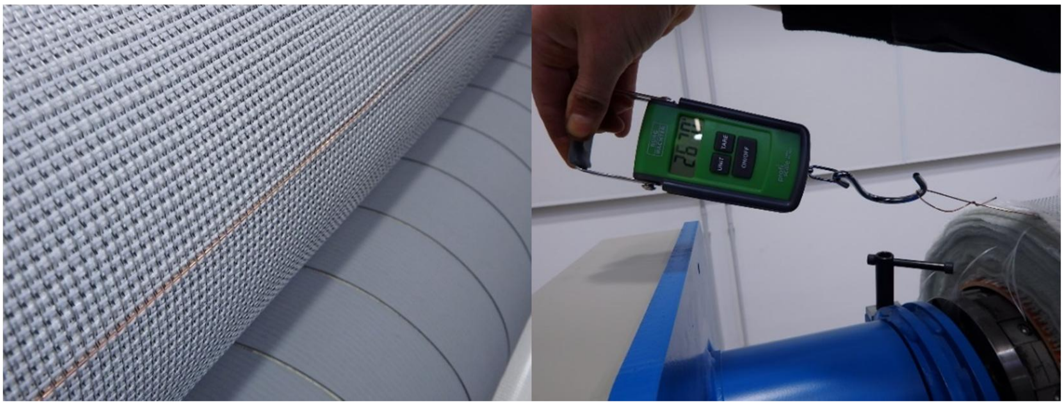

Figure 7 Arrangement of measuring wire and load cell

Another option would be differential measurement, i.e. the comparison of the measured values on individual wires), which are gradually located at the same depth below the surface of the packing. So we get sets of pairs [r_i, T_{iTheor}] and [r_i, T_{iExp}], assuming $f=const$ it will be possible to put through a regression line whose slope will be directly proportional to f. However, this method has not yet been elaborated in more detail.

6 CONCLUSION

While we have developed a plausible mathematical model its credibility is to be verified. Presently an experimental campaign is prepared in cooperation with a fabric factory. Once this model is verified we should be able to predict behavior of any batch depending on the conditions of the winding.

In future a possible extension of the model for non-isotropic material could be found. Anyway the problems with the determination of the orthotropic moduli of the batch should be solved before.

Another way for a future development leads to find a reverse function $f(\sigma(l)=const)$ which should allow the loom operator to program in advance the best fitting tension function for any type of batch. Unfortunately the $f(r)$ is rather complex and its reverse function may not exist.

Acknowledgement: *This work is prepared in cooperation with St. Gobain ADFORS Litomyšl, using CEDIMA large-size batch winder.*

7 REFERENCES

1. Höschl C.: Flexibility and strength II (Pružnost a pevnost II), in Czech, (1st edition), VŠST in Liberec, Faculty of Mechanical Engineering. Liberec, 1992
2. CEDIMA Meziměstí s.r.o.: Basic Installation, Operating and Maintenance Instructions (2006 edition), Meziměstí
3. Dvořák J., Karel P., Žák J.: Study of Interactions between weaving process and weaving machine systems, VÚTS, a.s., 2018

INSTRUCTIONS FOR AUTHORS

The journal ,,**Vlákna a textil**" (**Fibres and Textiles**) is the scientific and professional journal with a view to technology of fibres and textiles, with emphasis to chemical and natural fibres, processes of fibre spinning, finishing and dyeing, to fibrous and textile engineering and oriented polymer films. The original contributions and works of background researches, new physical-analytical methods and papers concerning the development of fibres, textiles and the marketing of these materials as well as review papers are published in the journal.

Manuscript

The original research papers are required to be written in English language with summary. The advertisements will be published in a language according to the mutual agreement.

The first page of the manuscript has to contain:

The title of the article (16 pt bold, capital letters, centred)

The full *first name* (s) and also *surnames* of all authors (11 pt, bold, centred).

The complete address of the working place of the authors, e-mail of authors (9 pt, italic, centred)

Abstract (9 pt, italic)

Key words (9 pt, italic)

The manuscript has to be written in A4 standard form, in **Arial, 10 pt**.

The text should be in ***double-column format*** *(width 8.1 cm)* ***in single line spacing***.

Page margins: up and down 2.5 cm; left and right 2.0 cm.

Do not number the pages and do not use footnotes. Do not use business letterhead.

Figures, tables, schemes and photos (centered) should be numbered by Arabic numerals and titled over the table and under the figure or picture.

Photos and schemes have to be sufficiently contrastive and insert in text as pictures.

Figures, tables, schemes and photos, please, send in separate file.

Mathematical formulae should be centred on line and numbered consecutively on the right margin.

Physical and technical properties have to be quantified in SI units, names and abbreviations of the chemical materials have to be stated according to the IUPAC standards.

References in the text have to be in square brackets and literature cited at the end of the text. References (9 pt), have to contain names of all authors.

[1] Surname N., Surname N.: Name of paper or Chapter, In Name of Book, Publisher, Place of Publication, YYYY, pp. xxx-yyy

[2] Surname N., Surname N.: Name of paper, Name of Journal Vol. (No.), YYYY, pp. xxx-yyy

[3] Surname N., Surname, N.: Title of conference paper, Proceedings of xxx xxx, conference location, Month and Year, Publisher, City, Surname N. (Ed.), YYYY, pp. xxx-yyy

[4] Surname N., Surname N.: Name of Paper, Available from http://www.exact-address-of-site, Accessed: YYYY-MM-DD

The final template of manuscript is available on **http://www.vat.ft.tul.cz**

Authors are kindly requested to deliver the paper (in Word form) to be published together with information about at least 3 recommended reviewers from institutions others than the parent (name, e-mail, institution, department) by e-mail: marcela.hricova@stuba.sk

After successful review procedure there is charged fee (article processing charge) of EUR 100. All articles after review process are freely available online and this fee helps to cover the costs of taking a manuscript and turning it into a finished article.

Address of the Editor Office:

Marcela Hricová

Faculty of Chemical and Food Technology,

Slovak University of Technology in Bratislava

Radlinskeho 9

812 37 Bratislava,

Slovakia

ADFORS

People are our strength

2 production plants - in Litomyšl and Hodonice

more than **2000** employees

turnover **7.8 bn CZK**

120 k tons of glass fibre per year

6 brands of unique glass fibre production

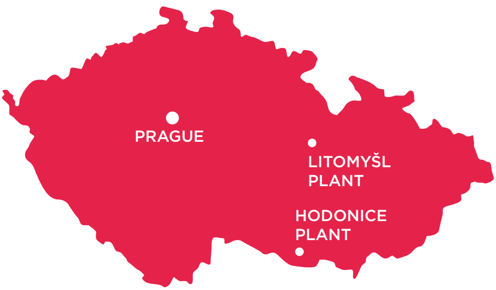

PEOPLE ARE OUR STRENGTH SO THEY ARE OUR FIRST PRIORITY.

Thanks to this approach, we already have been certified as a Top Employer for the last few years.

top EMPLOYER CZECH REPUBLIC 2018
CERTIFIED EXCELLENCE IN EMPLOYEE CONDITIONS

We are still growing and investing in both our employees and our technology too.

Working for us is very fulfilling. Come and join us!

CONTACTS

HEADQUARTERS AND LITOMYŠL PLANT

SAINT-GOBAIN
ADFORS CZ s.r.o.
Sokolovská 106
570 01 Litomyšl

+420 461 651 111

HODONICE PLANT

SAINT-GOBAIN
ADFORS CZ s.r.o.
Zahradní 256
671 25 Hodonice

+420 515 207 111

HR department
kariera.adfors@saint-gobain.com

www.adfors.cz

SAINT-GOBAIN

ADFORS
People are our strength

2 production plants - in Litomyšl and Hodonice

more than **2000** employees

turnover **7.8 bn CZK**

120 k tons of glass fibre per year

6 brands of unique glass fibre production

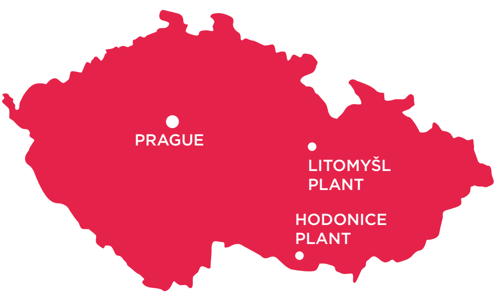

PEOPLE ARE OUR STRENGTH SO THEY ARE OUR FIRST PRIORITY.

Thanks to this approach, we already have been certified as a Top Employer for the last few years.

top EMPLOYER CZECH REPUBLIC 2018
CERTIFIED EXCELLENCE IN EMPLOYEE CONDITIONS

We are still growing and investing in both our employees and our technology too.

Working for us is very fulfilling. Come and join us!

CONTACTS

HEADQUARTERS AND LITOMYŠL PLANT

SAINT-GOBAIN
ADFORS CZ s.r.o.
Sokolovská 106
570 01 Litomyšl
+420 461 651 111

HODONICE PLANT

SAINT-GOBAIN
ADFORS CZ s.r.o.
Zahradní 256
671 25 Hodonice
+420 515 207 111

HR department
kariera.adfors@saint-gobain.com
www.adfors.cz

SAINT-GOBAIN

STAP a.s. – Narrow Fabrics Manufacturer from Czech Republic

Our products are tailored to meet exacting specifications established by a number of NATO military forces. STAP a.s. is a major webbing manufacturer of military webbings, bindings and elastics to meet specifications in both IRR webbings and non-IRR webbings.

We are one of the few webbing suppliers who can offer our own in-house dying facilities to colour match to forces exacting shade requirements.

Our Multi Colour Camo printed webbing (up to 5 colours) is widely used on a variety of PLCE (Personal Load Carrying Equipment), MTP Webbing Systems & Pouches, Molle Webbing along our latest IRR Camo printed binding, designed to be used in conjunction with The Multi-Terrain Pattern (MTP) camouflage print.

We can offer bespoke custom printed webbing to match your military camouflage textile pattern.

Special treatments can be applied to the webbing straps including anti-bacterial, rotproof, water-repellent and flame-retardant finishes.

Webbings are cut to length and heat-sealed using our automatic machines and we are also able to offer a cutting and holing service using our ultrasonic facility.

Here we are able to create a wide range of made-up units, sewn webbing straps also with buckles.

We can also offer wide range of comercial products, like webbings, elastics, binding tapes, zippers, woven labels, braids, jacquard ribbons…

www.stap.cz